N°: 41535

THESE DE DOCTORAT

Functionalization of Geotextiles by Physical Methods for Heavy Metal Ions Remediation

---

Présentée et soutenue publiquement à

L'Université Lille 1

pour obtenir le grade de

DOCTEUR

Spécialité : Molécule et Matière Condensée

par

Marianne VANDENBOSSCHE

Ingénieur ENSCL

Thèse dirigée par

Pr. Michel Traisnel et Dr. Mathilde Casetta

Soutenue le 28 octobre 2014 devant la commission d'Examen composée de :

Dir. Recherche CNRS S. Pellet-Rostaing	ICSM	Rapporteur
Pr. D. Hegemann	EMPA	Rapporteur
Pr. F. Bohr	Université de Reims	Examinateur
Dr. M. Jimenez	Université Lille 1	Examinateur
Pr. M. Traisnel	Université Lille 1	Directeur
Dr. M. Casetta	Université Lille 1	Co-encadrant

Acknowledgements

This manuscript concerns my PhD work that was carried out in the laboratory UMET headed by Prof. Alexandre Legris in the team “Ingénierie des Systèmes Polymères” managed by DR. Jean-Marc Lefebvre, as well as Prof. Bourbigot and Prof. Traisnel for welcoming and giving me the opportunity to work on this interesting project.

I also would like to acknowledge Prof. Michel Traisnel, Dr. Mathilde Casetta and Dr. Maude Jimenez for the supervision of my work during these three years. They bring me some advices in order to guide my work, and also, they bring me moral support in some difficult periods. I also want to thank them for their patience and their time spent to correct my work.

I would like to acknowledge DR Stéphane Pellet-Rostaing and Prof. Dirk Hegemann for having accepted to take of their time and to bring their expertise as examiners to assess this manuscript and Prof. Frédéric Bohr for having accepted to be examinator during the PhD defense.

As my PhD work is included in the DEPOLTEX project, I would like to thank the Up-Tex Competitiveness Cluster for their support and all the DEPOLTEX partners for collaboration and discussion. Moreover, I would like to thank Pr. Serge Bourbigot, present at the origin of the project, for the advices he provides me.

I would like to thank Prof. Dominique Derozier for allowing me to use the KrF excimer laser during my PhD and also for all the laser physics skills and knowledge he taught me. I also would like to thank Dr. Sébastien Canneaux for teaching me the use of Gaussian09, and for his guidance and help concerning the computational study presented in this manuscript.

I also would like to acknowledge DR Herve Vezin and Mrs Nadia Touati for the EPR analyses they made and their support in the interpretation of the results. That part was not easy for me as I did not know this method before. I would like to thank them for their patience and time spent to explain me the principles.

I would like to thank Dr. Séverine Bellayer for the SEM analyses, Dr. Arnaud Beaurain for the XPS analyses and Dr. Nicolas Nuns for the ToF-SIMS analyses. I also would like to thank Mrs Catherine Candelier, Mr. Patrick Daubias and Mr. Maxence Vandewalle for the use of flame atomic absorption spectroscopy, Fourier transform infrared spectroscopy and fluorescence X respectively.

I would like to acknowledge the support of FEDER (Fonds Européen de Développement Régional), Nord-Pas-de-Calais region, and FUI (Fonds Unique Interministériel) for funding this work.

I also would like to acknowledge all the persons working in the laboratory during my PhD for their warm welcome and for all the discussions: Anil, Andréa, Antoine, Bastien, Benjamin, Bertrand, Brigitte, Carmen, Clémence, Charaf, Elisabeth, Fabienne, Fouad, Frank-Estimé, Gaëlle, Ghassan, Gwenaelle, Hassan, Jérémie, Marion, Maryska, Mathieu, Nicolas L, Nicolas R., Pauline, Peng, Pierre, Renaud, Sophie, and Trang. I also would like to thank my trainees Yann and Amandine.

Finally, I would like to thank my husband, my family and my friends for their invaluable support.

Table of contents

Figure captions

Scheme captions

Table captions

Abbreviations

AA: Acrylic acid

Cys: Cysteine

EDC: N-(3-Dimethylaminopropyl)-N'-ethylcarbodiimide

FTIR/ATR: Fourier transformed infrared spectrometry with attenuated total reflectance

MTs: Metallothioneins

MTM: Mass transfer model (kinetics)

PCs: Phytochelatins

PET: Poly(ethylene terephthalate)

PET-c-AA: Poly(ethylene terephthalate) fabrics coated with acrylic acid

PFO: Pseudo first order (kinetic model)

PP: Polypropylene

PP-g-AA: Acrylic acid grafted polypropylene fabrics

PSO: Pseudo second order (kinetic model)

SEM: Scanning electron microscopy

SRM: Surface reaction model (kinetics)

Tyr: Tyrosine

XPS: X-ray photoelectron spectrometry

General Introduction

Metallic and organic pollutants in sediments can cause physico-chemical modifications of the contaminated areas, and thus lead to environmental and human health issues. Indeed, very toxic pollutants can be found in marine sediments: organic pollutants like tributyltin, polychlorinated biphenyl (PCBs), polycyclic aromatic hydrocarbons (PAHs), BTEX (benzene, toluene, ethylbenzene and xylene); and metallic pollutants like arsenic, cadmium, chromium, copper, lead, mercury, nickel, and zinc. An accumulation of these pollutants can be observed all over the food chain (fish, ducks and other wildlife), and human beings are concerned as well [1]. The issue of sediments pollution is one of the most important research topics of the 21st century.

Heavy metals are naturally present in the environment, but their concentration can increase according to some geologic events or, above all, human activities. Thus, heavy metals concentrate in soil and particularly at the soil surface. These metals can get away by surface run-off which erodes soils and allows transporting particles to rivers, seas and oceans. As a consequence, heavy metals contaminate fluvial and marine sediments and sludge. These contaminated sediments are dredged and, most of the time, are immersed in seas a few kilometers away from the coast. But sometimes, this practice is prohibited due to the concentration of heavy metals.

Nowadays, the highly contaminated sediments are placed in storage centers, but this practice is expensive and a new issue is raised, i.e. the saturation of these sites. Moreover, the treatment of these sediments could allow upgrading them in agriculture or civil engineering (road construction, landscape hill), which would also fit with the sustainable development politics. To treat the contaminated sediments, the idea further exposed in this PhD thesis manuscript is to develop a low cost functionalized material having a high efficiency to adsorb trace metals. The trace metals sequestered during the process could then be recycled in order to be reused for other purposes.

This PhD thesis is part of the DEPOLTEX Project (DEPOLlution through the use of TEXtile structures). Industrial partners (IDRA Environnement, BAUDELET Environnement, PGI France SAS, DYLCO, AFITEX, NEO ECO) and academic partners (Armines, ENSAIT, IFTH and UMET) collaborate together in order to develop a new process based on the use of functionalized geotextiles for the removing of mobile trace metals from marine and fluvial dredged sediments. Indeed, sediments are considered hazardous if the leachate contains contaminants. Three classes can be distinguished depending on the amount of trace elements (mg/kg dry matter (DM)) in the leachate (Table 1) for a liquid/solid ratio of 10 L/kg. If the

amount of trace elements in the sediments does not exceed the limit values of class III, the sediment is considered inert; if the amount of trace elements is more important but does not exceed the limit values of class II, the sediment is considered safe; and finally if the leachate exceeds the limit values of class II, the sediment is considered class I. Storage centers must receive authorizations to treat the different classes of sediments. In addition to these authorizations, some prefectural decree can modify the amount of trace elements for each class.

Table 1: Authorized maximum amount of trace elements in leachate for each class of waste [2, 3]

mg/kg DM	Class III / Inert	Class II / Safe	Class I / Unsafe
Arsenic (As)	0.5	2	25
Cadmium (Cd)	0.04	1	5
Chromium (Cr)	0.5	10	70
Copper (Cu)	2	50	100
Mercury (Hg)	0.01	0.2	2
Nickel (Ni)	0.4	10	40
Lead (Pb)	0.5	10	50
Zinc (Zn)	4	50	200

During the leaching process, mobile pollutants are extracted from sediments by the action of the percolating water (scheme 1). In this process, a part of the pollutants remains attached to the sediments due to: (i) occlusion in amorphous materials [4], (ii) adsorption at clays surfaces [5, 6] or on iron/manganese oxyhydroxides [7], or (iii) complexation with organic matter, notably humic [8, 9] and fulvic acids [10]. Thus, the trace metals immobilized on sediments are considered as stabilized pollutants. The mobile pollutants, such as trace metal ions, are more dangerous as they are bioavailable, and can be absorbed easily by living organisms.

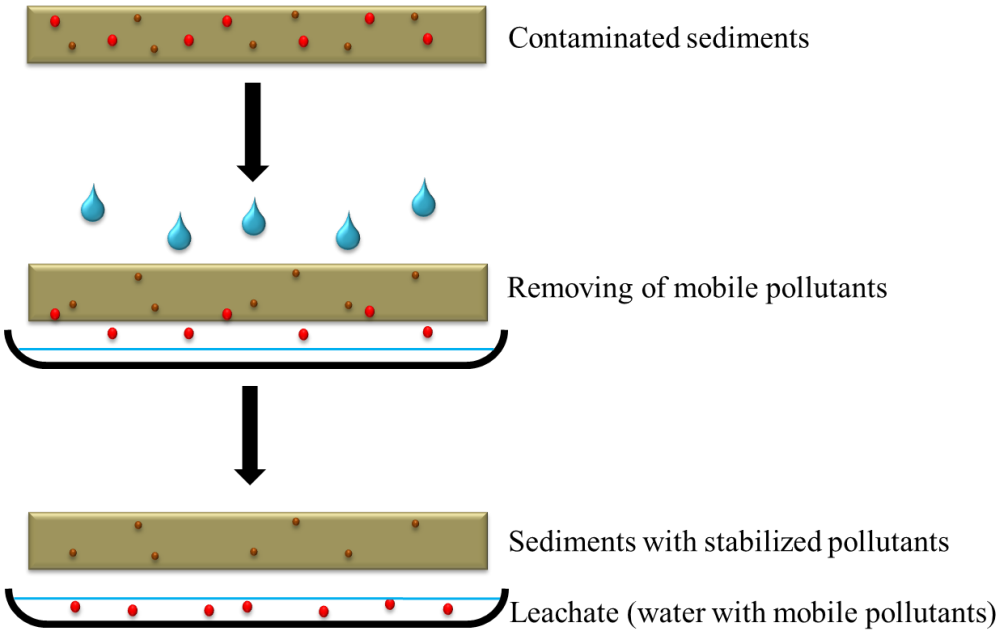

Scheme 1: Leaching process leading to the separation of mobile pollutants (●) from sediments, the pollutants remaining in sediments being considered as stabilized pollutants (●)

The objective of my PhD work, in the DEPOLTEX project, consisted in the development of biomolecules-grafted-textiles, through physical methods, allowing to reduce the amount of trace metal ions in leachate below the tolerance threshold. In this study, geotextiles were selected as they have a permeable structure allowing the drainage and filtration of wastewater.

Chemical methods are traditionally used to graft molecules on textiles [11-13]. Physical processing methods were however considered for the functionalization step because of (i) the quick grafting of molecules, (ii) the possibility to avoid using toxic solvents and (iii) the potential transposition of these methods at industrial scale.

A number of physical methods were already used and described in the literature for the grafting of molecules on synthetic textiles or polymeric films [12-15] such as electron beam [16], UV radiation [17, 18], LASER [19], low pressure cold plasma [20, 21] and atmospheric plasma [22-24] processes. In this project, plasma process was chosen at first as it is an emerging technique for the treatment of textiles, and as it allows modifying the surface chemistry and topography without affecting the bulk properties of the fibers [25]. Indeed, in 2002, Höcker wrote that: "*plasma technology performed under atmospheric pressure or under reduced pressure leads to a variety of processes to modify fiber or textile materials to fulfill additional highly desirable requirements. It is to be expected that this technology (…) in the near future will conquer textile industry as well*" [26]. The increasing use of plasma

processes for the treatment of textiles since 2000 has been reported by the Textile Institute of Manchester [27]. This tendency (figure 1) can be explained by the efficiency of plasma technology to treat textiles as it is an environmentally-friendly manner to bring new functional groups, and thus new functional properties to textiles such as hydrophilization, hydrophobization, adhesion capacity etc., for various applications such as clothing, filtration, automotive industry, architecture, medical engineering, biotechnology [28, 29].

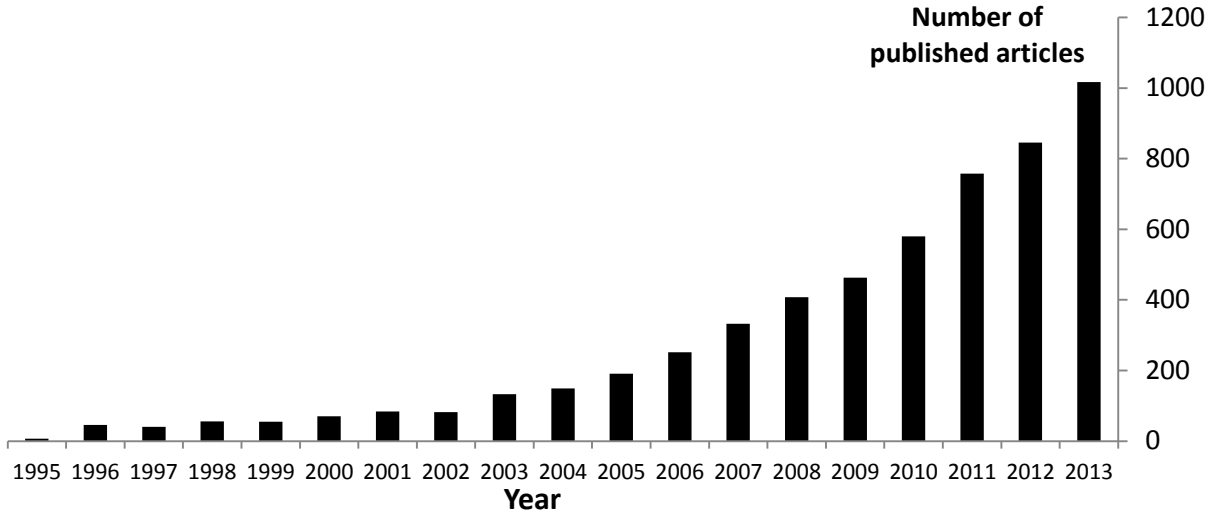

Figure 1: Statistical data related to the number of publications dealing with plasma treatments on textiles from 1995 to 2013 (on Scopus; keywords: plasma process and textile; all fields)

As plasma processes are "conquering" the textile industry, they were first considered for the grafting of biomolecules onto geotextiles. However, direct grafting of biomolecules is not possible, even using cold plasma treatment, without losing the main chemical groups involved in the remediation process. Thus, it was first necessary to graft a "spacer", i.e. a monomer such as acrylic acid [30, 31] or maleic anhydride [32] in order to bring carboxylic acid groups at the surface of the fibers. Then, biomolecules can be immobilized by chemical coupling onto the carboxylic acid groups while keeping their chelation properties.

LASER process can also be used to functionalize geotextiles. Indeed, excimer LASERs present some advantages such as (1) the recyclability of the gas used to create the LASER (which is not possible with plasma), and (2) the speed of processing. Nowadays, LASERs are mainly used in the automotive industry, but this process can also be applied in the textile industry. Thus, both plasma and LASER processes can be used to graft molecules on textiles. However, the choice of the molecules which will be immobilized onto the textile is crucial regarding the functionalized textile efficiency. Indeed, a specific decontamination property of the textile is expected: the ability to complex heavy metals in fluvial or marine sediments (aqueous media).

Many studies were carried out in the depollution of heavy metals from aqueous media using synthetic chemical compounds: poly(dimethylaminoethyl methacrylate – cross linked pregelled starch graft copolymers), or poly(DMAEM-CPS), used to chelate copper, cadmium, mercury or lead [33], poly(2-hydroxyethyl methacrylate-n-vinyl imidazole), or poly(HEMA-VIM), used to sequester copper, lead, zinc and cadmium [34]. Some natural polymers, generally polysaccharides like cellulose and alginate, are able to complex copper, lead and zinc [35]. The most well-known natural polymers generally used in the trapping of trace metals are lignin, alginate, cellulose, starch, cyclodextrins, pectins, chitosan and chitin [36, 37]. But, other natural molecules are able to complex trace metals: polypeptides and proteins which play a major role in living cells, like heavy metals detoxification. These polypeptides such as glutathione [38], phytochelatins (PCs) [39, 40] and metallothioneins (MTs) [41, 42], are made up of amino acids and are natural trace metals traps. Cysteine, the only amino acid containing a thiol group in the side chain, is the binding site of these peptides. The metal ions are coordinated through mercaptide bonds, in arrangements typical of metal-thiolate clusters [43]. Thus, cysteine was chosen to be grafted at the surface of textiles to decontaminate sediments from heavy metals.

Another amino acid, tyrosine, was also used in this work as the presence of an aromatic ring on the side chain can be interesting for the complexation of trace metals, and also for the interactions with some aromatic pollutants. Indeed, some studies were carried out in order to determine the chemical groups of tyrosine involved in the complexation with trace metals. A crystallographic study showed that there was a weak interaction between the π-electron system of the phenolic ring and the Cu(II) ion [44]. Recently, the capacity of aromatics to chelate heavy metals was extensively studied, and more precisely the cation-π interactions [45-47]. Fundamental gas-phase studies, both experimental and theoretical, allowed proving that the cation-π interaction is among the strongest non-covalent binding forces [45, 47].

This manuscript summarizes the work carried out for 3 years concerning the grafting of cysteine and tyrosine on geotextiles for the sequestration of trace metals in aqueous media.

The first chapter of this manuscript is an overview concerning the ability of natural molecules to sequester trace metal ions in aqueous media. In this chapter, chitosan efficiency is reported as this biomolecule is well-known in the environmental field. Then, the great potential of amino acids, especially cysteine and tyrosine, is highlighted. Finally, a classification of the efficiency of different chemical functional groups towards trace metals

adsorption has been done taking into account their reactivity and the pH conditions in the sediments.

The second chapter describes the methodologies used to graft acrylic acid onto poly(ethylene terephthalate) (PET) and polypropylene (PP) fabrics according to two different physical processes: radiofrequency low pressure cold plasma and KrF excimer laser. The characterizations of the functionalized samples are also presented in this chapter.

The third chapter of this manuscript details the immobilization of two biomolecules (cysteine and tyrosine) onto acrylic acid-functionalized fabrics and the characterizations of the functionalized textiles obtained. A protocol was developed in order to determine the sorption efficiency of the functionalized material. A comparison between the different textiles obtained is presented in order to ensure a good selection for further work at industrial scale.

The fourth and last chapter is focused on the adsorption mechanisms of trace metal ions on the functionalized surfaces. More precisely, a computational study was carried out in order to better understand the interactions occurring at the surface of the fibers and the complexes formed between heavy metals and biomolecules.

This dissertation is based on the papers listed below. Thus, the details concerning the experimental techniques are already given in Appendix 2 and will not be described in the manuscript.

- M. Vandenbossche, M. Jimenez, M. Casetta, S. Bellayer, A. Beaurain, S. Bourbigot, M.Traisnel, Chitosan-grafted nonwoven geotextile for heavy metal sorption in sediments, *Reactive & Functional Polymers*, **2013**, 73, pp. 53-59.
- M. Vandenbossche, M. Casetta, M. Jimenez, S. Bellayer, M. Traisnel, Cysteine-grafted Nonwoven Geotextile: A New and Efficient Material for Heavy Metals Sorption – Part A, *Journal of Environmental Management*, **2014**, 132, pp. 107-112.
- M. Vandenbossche, H. Vezin, N. Touati, M. Casetta, M. Jimenez, M. Traisnel, Cysteine-grafted Nonwoven Geotextile: A New and Efficient Material for Heavy Metals Sorption – Part B, *Journal of Environmental Management*, **2014**, 143, pp. 99-105.
- M. Vandenbossche, A. Dehaese, M. Casetta, M. Jimenez, M. Traisnel, Tyrosine: an Efficient Natural Molecule for Copper Remediation, *Green Materials*, **2014** *(in press)* DOI: 10.1680/gmat.14.00006
- M. Vandenbossche, M. Jimenez, M. Casetta, M. Traisnel, Remediation of Heavy Metals by Biomolecules - A Review, *Critical Reviews in Environmental Science and Technology*, **2014** *(accepted)*
- M. Vandenbossche, D. Derozier, M. Casetta, M. Jimenez, S. Bellayer, M. Traisnel, KrF Laser: an Innovative Method to Functionalize Textiles for the Remediation of Polluted Media, *Applied Surface Science*, **2014** *(submitted the 22nd of May)*

Chapter I
Natural molecules for heavy metal ions remediation

I.1. Introduction

Trace metals are present in the environment due to industrial activity, and environmental disasters sometimes occur. The most relevant catastrophe took place in Minnamata bay, Japan: the polluted effluents contained trace metals, mainly methylmercury, and the aquatic organisms and also the fisherman's community were severely affected. However, trace metals are not necessarily toxic, it depends on their bioavailability and solubility in aqueous media. The higher the solubility of the trace metal, the higher its toxicity as it can be absorbed by living organisms.

In this chapter, the mobility and speciation of trace metals will thus be first considered. As most of the soluble trace metals are toxic, the sequestration of these ones is essential and allows the separation of these soluble pollutants from water. Some synthetic molecules or inorganic structures are able to sequester trace metal ions, such as the well-known zeolites [48] and Ethylene Diamine Tetraacetic Acid (EDTA) [49]. Some categories of biomolecules can also sequester trace metal ions and in this PhD thesis, the use of natural molecules will be mainly considered for various reasons: (i) these molecules are natural and consequently they are non-toxic for the environment; (ii) these molecules are well-known in the chelation of trace metals and are present in the detoxifying process of several cells; (iii) the price of these molecules is not so expensive compared to other sorbents like activated carbon. Thus, an overview concerning the ability of natural molecules, or biomolecules, to sequester trace metal ions will be given.

The mobility and speciation of trace metals can change according to the surrounding environment. Indeed, there are some factors, such as pH and redox potential, able to modify the oxidation degree of trace metals leading to more soluble and potentially toxic compounds. Under ionic form, trace metals may be more toxic for living organisms. It was observed that some cells possess their own trace metals detoxification system: some biomolecules, such as, glutathione, phytochelatins (PCs) and metallothioneins (MTs) are involved in the sequestration of trace metal ions. These natural ions traps are made up of amino acids. Thus, these biomolecules can be used for the removal of trace metal ions from wastewater, because of the presence of some reactive amino acids (cysteine, lysine, histidine) [50]. Indeed, PCs and MTs contain high percentage of cysteine, possessing the thiol groups primarily responsible of metal binding [51]. According to these observations, amino acids, such as cysteine, can be used as metal binding alternatives to natural polysaccharides, and also polypeptides.

The first section of this chapter concerns first the mobility and the speciation of trace metals in soil and sediments, and the conditions for their mobility and speciation will be given. Then, three amino acids presenting good potential for the adsorption of trace metal ions are presented: cysteine, tyrosine and histidine. Some studies were carried out to show the efficiency of these amino acids to sequester trace metal ions, such as copper, and also to explain the good efficiency of amino acids in trace metal ions sequestration.

The second section of this chapter details all the chemical functional groups and atoms present in biomolecules and involved in the trace metal sorption mechanisms. Since the 20th century, some theories (i.e. HSAB (Hard and Soft, Acids and Bases) principle of Parr and Pearson [52, 53], the Irving-Williams series of stability constants [54, 55], and the empirical rules explaining the different coordination geometries of transition metals in the experimentally determined molecular structures [56]) have been developed in order to explain the affinity between some chemical functional groups/atoms and trace metal ions. These theories are reported and compared with recent X-ray absorption spectroscopy (XAS) studies, which are used to determine the geometry of the biomolecule/metal complexes.

This chapter is based on the following paper:

M. Vandenbossche, M. Jimenez, M. Casetta, M. Traisnel, Remediation of Heavy Metals by Biomolecules - A Review, *Critical Reviews in Environmental Science and Technology*, **2014** *(accepted)*

I.2. Mobility and speciation of trace metals in sediments

1.2.1. Factors and conditions for the mobility

Heavy metals are more or less soluble in soil or sediments: some parameters, such as pH and redox potential, have an important influence on the mobility of trace metals. The most important factor is the pH. Indeed, the lower the pH, the higher the mobility of the trace metals. This phenomenon is observed because of either the solubilization of the metal or the destruction of the retention phase. In the same way, the higher the pH, the lower the mobility of trace metals because of the formation of insoluble complexes. The French legal framework order from 08/01/1998, relative to the technical requirements that can be used for sludge spreading on agricultural soils, sets the minimum of pH 6 for sludge, except for liming sludge which pH is about 5.

Heavy metals can be soluble or insoluble according to their oxidation degree. Indeed, this parameter, and thus presence of dissolved oxygen and other oxidizing agents like nitrates, iron or manganese oxides and sulfates, can impact the duration of heavy metals presence in

the soil. The decrease or the absence of dissolved oxidizing agent compounds and the decrease of bioavailability is called anoxia. Climatic events can lead to this phenomenon. Indeed, when there are heavy rains, soil is saturated with water, and a low amount of oxygen is dissolved in this water. Human activities can also have an impact on the redox potential of the soil: irrigation for agricultural purposes, settling occurring after repeated passages of tractors, and addition of biodegradable substances leading to the increase of micro-organisms activity and then to the increase of the consummation of oxygen that affects the aeration degree of soils. An important factor is the mobility of iron and manganese: under reduced form, iron and manganese are mobile, but not under oxidized form [57]. Moreover, iron and manganese oxides are able to sequester trace metals, and thus to immobilize them in the soil. For example, manganese oxide is able to keep lead in the soil. To summarize, the influence of pH and of redox potential on the mobility of some trace metals is given in table 2.

Table 2: Relative mobility of trace metals as a function of pH and redox potential [58]

Relative mobility	**Hydrogen potential**		**Redox potential**	
	Neutral or basic	Acid	Oxidant	Reducer
High	-	Cd, Zn	-	-
Medium	-	Cr, Cu, Pb	Cd, Cu, Zn	-
Low	Cd, Pb, Zn	-	Pb	Zn
Very low	Cr, Cu	-	Cr	Cd, Cr, Cu, Pb

The temperature and soil humidity play an indirect role in the mobility of trace metals. Indeed, if the temperature is around 37°C with a humidity rate at 50%, there will be a biological activity in the soil which leads to biodegradation, and thus, to the formation of acidic compounds: pH will decrease and the mobility of trace metals will increase. Temperature can also make trace metals more soluble, and consequently, the trace metals can be absorbed by plants.

Some kinds of soils can retain more trace metals than others, which is a phenomenon due to the soil composition: for example clays, humic and fulvic acids [59], or some minerals can interact with heavy metals. An immobilization of trace metals in the soil can occur when they are trapped by organic compounds coming from substances like fertilizers or pesticides that are added in the soil. But biodegradation phenomena occur in the soil, and organic compounds are consumed: thus, trace metals are released in the soil, oxygen rate decreases because of the biodegradation process, and a chemical reduction occurs in the soil leading to the solubilization and the remobilization of trace metals.

1.2.2. Chemical speciation of trace metals

According to the IUPAC definition, speciation is the "distribution of an element amongst defined chemical species in a system" [60]. This term is generally used to describe all forms of an element, in this case all the complexes formed with one given trace metal. Thus, depending on the speciation, the metal is more or less bioavailable and more or less mobile in soils and waters [61-63]. Examples of speciation of some heavy metals can be given but each location on Earth is unique and speciation of trace elements will not be the same everywhere. In this work, general principles of speciation will be given, copper presented as a model heavy metal mostly because of its high amount in Dunkirk sediments.

Copper interacts mainly with chalcogens, and preferably with sulfur. Copper II cation is more reactive than copper II in a complex, and thus its bioavailability and its toxicity are more important. Generally, in soils and waters, copper is complexed with organic and inorganic ligands [64]. As a consequence to the speciation of copper, the total amount of copper is the same, but there are less copper cations, so less toxic copper. This observation can be illustrated by a study carried out by Serpaud (figure 2). Indeed, the amount of copper complexed with acetic and phosphoric acids was evaluated and compared to the amount of free copper cations, as a function of pH.

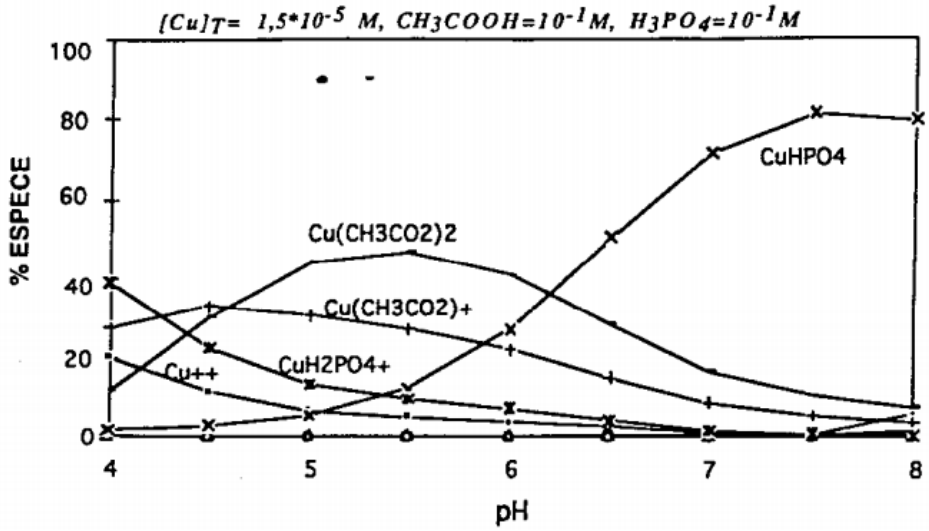

Figure 2: Speciation diagram of Copper as a function of pH [59]

Chemical speciation of heavy metals depends not only on the pH but also on the redox potential [64]. Figure 3 is presented in order to illustrate the variability of copper speciation: this study was carried out on soils from contaminated sites affected by Cu mining, Cu-based fungicides, and Cu smelting in China [65]: soils S1 to S5 were taken from agricultural soils near an abandoned mine, in Nanjing City, Jiangsu Province; soils S6 to S11 were taken from

orchards treated with Cu-based fungicides in Rizhao City, Shandong Province; and soils S12 to S17 were taken from Guixi City, Jiangxi Province which was polluted by solid waste deposition from an adjacent Cu smelting factory [65].

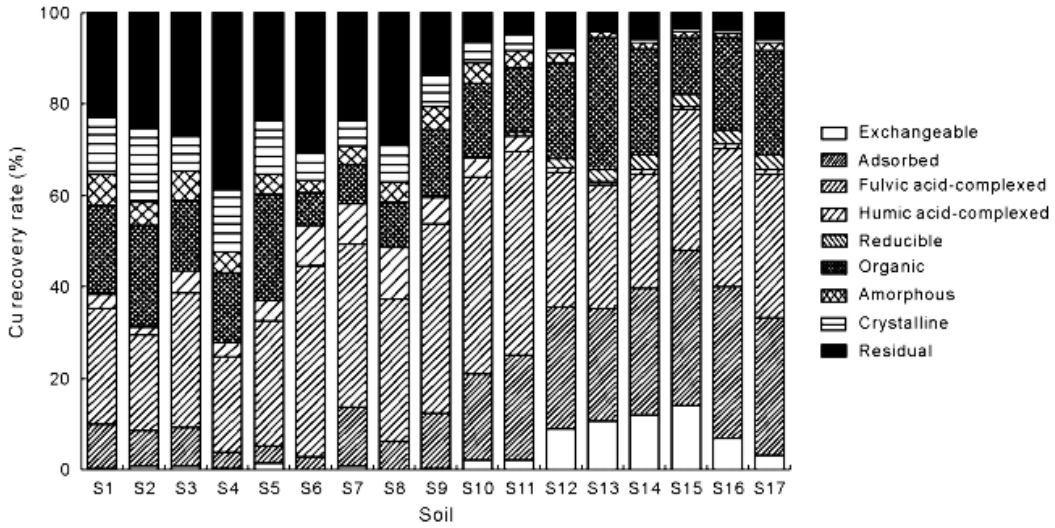

Figure 3: Example of the chemical speciation of copper in 3 kinds of soils in China [65]

All the possibilities have not been given for copper in figures 2 and 3. A lot of possibilities exist for copper and other trace metals, and all the cases are summarized in scheme 2. This scheme shows that there is a very small amount of toxic trace metals in the soil, as the bioavailable trace metals are, most of the time, absorbed by living organisms. Moreover, as some living organisms are able to absorb trace metals and as some of them have also a detoxification system, then this PhD work was focused on biomolecules present in living organisms and able to sequester trace metals.

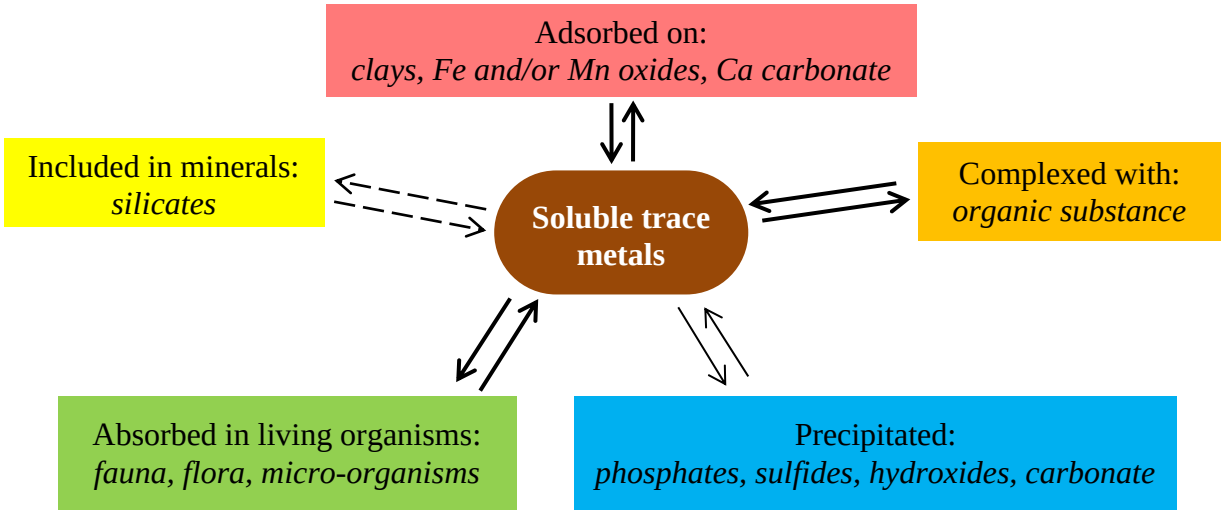

Scheme 2: Assessment of the speciation of trace metals in the soil [58]

I.3. Amino acids: cysteine, tyrosine and histidine

As the species targeted in this study are trace metal cations, an exhaustive bibliographic study was carried out in order to identify the biomolecules able to sequester these pollutants. The article entitled "Remediation of Heavy Metals by Biomolecules - A Review" gathers information on many potential biomolecules. It was observed that amino acids are ideal building blocks for metal chelation systems because of their high potential and their small size: it could be possible to immobilize a significant amount of amino acids at the surface of a textile, and thus, possible to increase the efficiency of the functionalized material towards trace metals decontamination. In this chapter, special interest for some amino acids is highlighted: cysteine, tyrosine and histidine are presented to show their specificity and ability to sequester trace metal ions.

I.3.1. Cysteine

Cysteine (figure 4), the only amino acid containing a thiol group on the side chain, is the binding site on some important peptides (MTs and PCs) for cells detoxification, as explained previously. The metal ions are coordinated through mercaptide bonds, in arrangements typical of metal-thiolate clusters in metallothioneins [43, 66, 67]. Thus, cysteine can interact with metals thanks to carboxylic acid, amine and/or thiol groups [68, 69]. The discovery of the so-called zinc fingers in the early 1980s shows that thiol group of cysteine (with imidazole group of histidine) is important in the coordination between proteins and metal, i.e. zinc in that case [70]. Thus, cysteine is an interesting molecule in the trace metals complexation, but surprisingly there are few studies on this amino acid in remediation processes in spite of its high capacity to chelate trace metals.

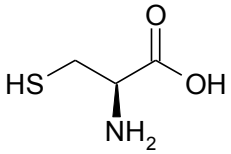

Figure 4: Representation of L-cysteine

Some studies concerning remediation processes were carried out using L-cysteine. Indeed, poly-L-cysteine was prepared from L-cysteine in order to chelate metal ions such as Hg(II), Cd(II), Pb(II), Ni(II) and Cu(II) [71-74]. However, biohomopolymers are prohibitively expensive and difficult to produce at large scale. To overcome these problems, some scientists used monomeric amino acids as well as polypeptides covalently attached to a substrate, like for example, glassy carbon microspheres [75, 76], graphite powder [77], or bentonite [78].

Glassy carbon spherical powder (10–20 mm diameter) modified with cysteine methyl ester (CysOMe-GC) was developed for heavy metals remediation in water. This is an inexpensive novel material for the rapid removal of large quantities of toxic trace metal ions such as Cd(II) and Cu(II) from aqueous media [75, 76]. It was demonstrated that CysOMe-GC powder is a powerful ‘‘catch-all’’ material for the removal of some heavy metal ions: 0.78 mmol of Cd^{2+} were adsorbed per gram of CysOMe-GC [75] and 0.49 mmol of Cu^{2+} per gram of CysOMe-GC [76]. A better sorption efficiency was observed for poly-L-cysteine grafted carbon graphite (PCcarbon): 1.22 mmol of Cd^{2+} were adsorbed per gram of PCcarbon [77]. The great potential of cysteine in heavy metal remediation was also proven by Merrifield *et al.*, more precisely concerning the removal of mercury [79]. Indeed, spherical beads of cysteine-grafted-chitosan were able to adsorb approximately 8.0 mmol of Hg per gram of dry beads at pH 7 [79]. In another study, cysteine was adsorbed on bentonite in order to sequester Cd(II) and Pb(II). One gram of this material could adsorb 0.503 mmol of Pb^{2+} and 0.525 mmol of Cd^{2+} in a 7.0 mmol/L artificially polluted solution at pH 4-5 and 25°C [78].

To summarize, cysteine is a very interesting amino acid, very effective in the trapping and the removal of heavy metal ions from polluted aqueous media. Moreover, this biomolecule is not expensive and is selective for heavy metals.

I.3.2. Phenylalanine, tyrosine and tryptophane

Phenylalanine, tyrosine, and tryptophane (figure 5) are amino acids containing aromatic group in the side chain. The capacity of aromatics to sequester trace metals was extensively studied, and more precisely the cation-π interactions [45-47, 80-82]. Indeed, benzene has a substantial permanent quadrupole moment [83]. Topologically, quadrupoles are equivalent to d orbitals, and the quadrupole, especially in benzene, is topologically equivalent to a dz^2 orbital. Thus, there is a permanent, nonspherical charge distribution in benzene, with regions of negative and positive relative charges [45, 80].

Fundamental gas-phase studies, both experimental and theoretical, established the cation-π interaction to be among the strongest noncovalent binding forces [45, 47], and a simple electrostatic model can fit major binding trends. However, phenylalanine is less studied than the others. Phenylalanine only has an aromatic ring in the side chain whereas tyrosine and tryptophane also have other reactive chemical groups: the π-site along with the oxygen lone-pair site on the phenol side chain of tyrosine, and two π-sites along with the nitrogen lone-pair site on the indole side chain of tryptophane [47]. These differences in the side chains composition lead to clear differences concerning the amino acid reactivity towards

divalent metal ions. Indeed, by computational studies using Ni^{2+}, Cu^{2+} and Zn^{2+} as divalent metal ions, the following order was observed: tryptophan > tyrosine > phenylalanine [82]. The reactivity of these aromatic amino acids is affected by the chemical nature of their side chain: phenylalanine has a benzyl group, tyrosine a phenol group, and tryptophan an indole group.

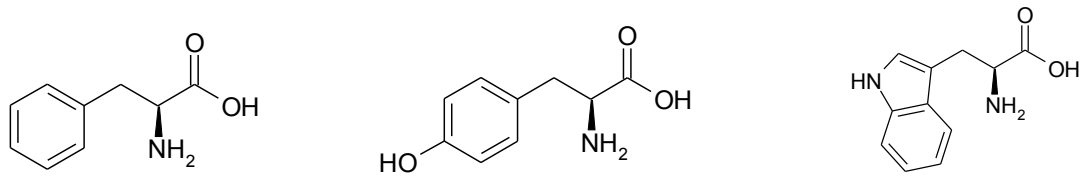

(a) (b) (c)

Figure 5: Representation of (a) L-phenylalanine, (b) L-tyrosine and (c) L-tryptophane

Hu *et al.* [46] proposed various possible conformations of tyrosine to chelate metal ions on peptides. They simulated different structures of metal ions chelated on tyrosine: the structures in which the metal ions are bound to the aromatic ring and to the adjacent amide nitrogen are the most probable ones. Moreover, these should be stable structures compared to when metal ions are bound to the oxygen and the nitrogen from the amide bonds. Therefore, tyrosine is proposed to coordinate to the metal ion primarily via its aromatic ring (figure 6). The involvement of the hydroxyl group in the metal chelation, however, cannot be excluded [46]. A more recent computational study was carried out in order to model the role of the cation-π interaction in the formation of the L-tyrosine•Zn^{2+} complex. The most stable complex was found to be the same as the one observed by Hu *et al.*: Zn^{2+} coordinates preferably with the aromatic ring of the phenol group and the nitrogen of the amine group [82]. Calculations were also carried out using the zwitterionic form: divalent cations essentially interact with the oxygen of the carboxylate groups [82].

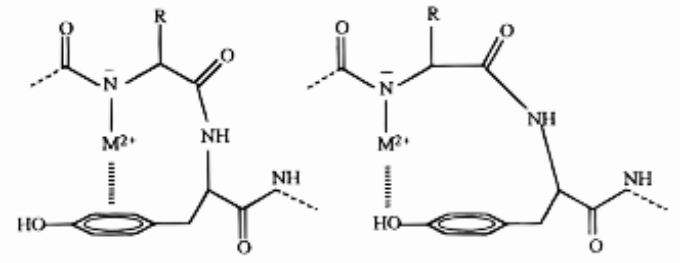

Figure 6: Possible interactions between divalent heavy metals and phenol group [46, 47]

I.3.3. Histidine

Histidine (figure 7) is the only amino acid containing an imidazole group on the side chain. Imidazole is a highly polar group made up of a planar 5-membered ring. Moreover, imidazole is amphoteric: it can be both an acid and a base. Among amino acids, histidine is

one of the strongest metal coordinating ligands and it plays an important role in the binding of metal ions by proteins [84]. Indeed, histidine, like cysteine, is well-known in the chelation of zinc in the "zinc-fingers": zinc is chelated thanks to two thiol groups from cysteine molecules and thanks to two imidazole groups from histidine molecules. Furthermore, free histidines can act as tridentate ligands to sequester heavy metals, leading to the formation of N,O,N-chelates [85] thanks to the three binding sites, namely the carboxylate oxygen ($O_{carboxyl}$), the imidazole imido nitrogen (N_{im}) and the amino nitrogen (N_{am}) (figure 8). On the contrary, when histidine is included in a protein, the binding with metal ions generally occurs with the imidazole nitrogen [86]. The formation of copper-histidine complexes (and more generally of copper-amino acids complexes) decreases the copper toxicity because the complexes are less toxic than copper alone [87].

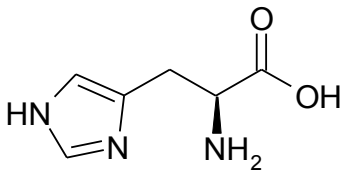

Figure 7: Representation of L-histidine

Recent studies were carried out concerning the use of histidine in water depollution [88]. A chromium(III)-methacryloylhistidine (MAH/Cr(III)) complex monomer was first synthesized and the Cr(III) ion imprinted ethyleneglycoldimethacrylate-methacryloylhistidine (Poly(EDMA-MAH/Cr(III))) was polymerized. Cr(III) ions were removed from the Cr(III)-imprinted polymer and a new material was obtained for the complexation of Cr(III). At pH=6.0, 25°C and 100 mg/L Cr(III) in the artificially polluted solution, 69.28 mg of chromium were adsorbed per gram of polymer in 30 minutes. Moreover, this material is selective: a study was carried out with Ni(II), Co(II) and Cr(VI) as imprinted ions and evidence of selectivity was given as the amount of Cr (III) adsorbed on Cr(III)-imprinted polymers is higher than that of the other studied ions [88].

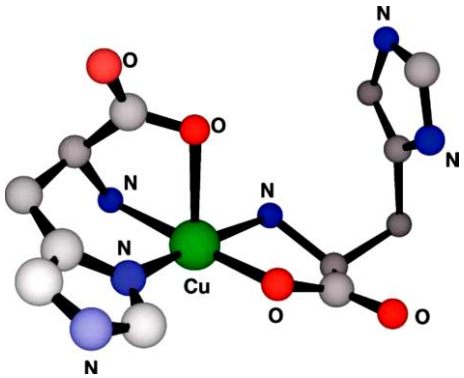

Figure 8: Representation of the N,O,N-chelates with copper and hisidine ($Cu(His)_2$) [89]

Cysteine, tyrosine and histidine are able to sequester trace metal ions thanks to some chemical groups (figures 6 and 8). Thus, it seems interesting to focus more on the sorption mechanisms and mainly on the interaction between copper and chemical groups.

I.4. Sorption mechanisms

I.4.1. Chemical groups involved in the sorption mechanisms

Biosorbents, such as amino acids, able to sequester trace metals under cation form, contain appropriate chemical active groups within their structures [90]. Many chemical groups can interact with trace elements, but some of these are more efficient. In polysaccharides, some recurring chemical groups are present like hydroxyl groups that can be found in all polysaccharides (cellulose, chitin/chitosan, alginate, and pectin for example). However, this chemical group is not the most efficient. Indeed, the amine group (in chitosan for example) [91], and the carboxyl group (in alginate) [92] are well-known for their efficiency to sequester trace metals. The imidazole group is also able to chelate trace metals, and studies were carried out using copper as trace metal [89, 93]. The intrinsic ability of the previously mentioned chemical groups for trace metals binding can be modified depending on the pH conditions. Indeed, with the pH increase, the main binding chemical groups (table 3) are under anionic form, facilitating the metal cations uptake.

Table 3: Main binding chemical groups for trace metals [90]

Binding group	Structural formula	pKa	Potential structure in sediments (pH 8.2)
Hydroxyl	—OH	**9.5-13**	—OH
Thiol	—SH	**8.3-10.8**	—SH
Amine (primary)	—NH_2	**8-11**	—NH_2
Carboxylic acid		**1.7-4.7**	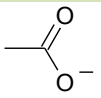
Sulfonate	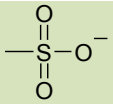	**1.3**	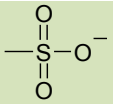
Imidazole	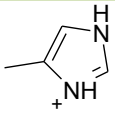	**6.0**	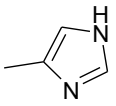
Amide	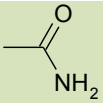	**15.1**	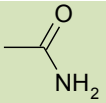
Phosphonate	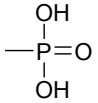	**0.9-2.1** **6.1-6.8**	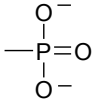
Phosphodiester		**1.5**	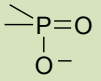

I.4.2. Atoms involved in the sorption mechanisms

As observed previously, active chemical groups are involved in the metal binding: hydroxyl, amine and carboxylic acid groups. In polypeptides, and more precisely in amino acids, these functional groups play the same chelating role, but structures are more complex. The particular interest for amino acid molecules in the remediation field is due to the presence of both amine and carboxylic groups at the end of the side chains, together with functional groups which can also play an important role in the complexation of heavy metals (e.g. imidazole group of histidine containing nitrogen, phenol group of tyrosine containing oxygen, and thiol group of cysteine containing sulfur). In the case of an aromatic ring, the cation-π interaction plays an important role. Thus, in the different biomolecules, the most important chemical groups are: the hydroxyl, carboxylic, sulfonate, amine, amide, imidazole, phosphonate and phosphodiester groups [90]. In these chemical groups, only few common non-metallic atoms, i.e. sulfur, nitrogen and oxygen, are able to trap heavy metals.

Many studies based on qualitative or semi-quantitative theories or principles try to explain the factors influencing the specificity of metal ion uptake. The most frequently used theories are: HSAB (Hard and Soft, Acids and Bases) principle of Parr and Pearson [52, 53]; the Irving-Williams series of stability constants [54, 55]; the empirical rules explaining the different coordination geometries of transition metals in the experimentally determined molecular structures [56].

HSAB principle is widely used in chemistry to explain the reactivity of some compounds or molecules and particularly to explain the selective reaction between a functional group, an ion or a molecule with another. Lewis acids and bases are divided into two categories: the polarizable species are called “soft”; and the nonpolarizable ones are called “hard”. Hard acids and bases can be described as small radii atoms, with a high oxidation degree and a high electronegativity, whereas soft acids and bases are characterized by large radii atoms, with a low oxidation degree and a low electronegativity. According to Pearson, hard acids bind strongly to hard bases and soft acids bind strongly to soft bases [52]. However, the HSAB theory can hardly explain the reactivity with borderline acids and bases like Cu^{2+} which is considered as a borderline acid (table 4). Moreover the reactivity of organic compounds is not well described. Therefore, approaches based on thermodynamic and kinetic control have been developed [94].

Table 4: Classification of some hard and soft acids and bases [95]

Hard acids	Borderline acids	Soft Acids
H^+, Na^+, K^+ ,Mg^{2+}, Ca^{2+} , Ba^{2+}, Cr^{3+}, Mn^{2+}	Fe^{2+}, Co^{2+}, Ni^{2+} , Cu^{2+}, Zn^{2+}, Pb^{2+}	Cu^+, Cd^{2+}, Hg^{2+}, RHg^+, $Hg2^{2+}$
Hard bases	Borderline bases	Soft bases
HO^-, RO^-, $RCOO^-$, RNH_2	SO_3^-	HS^-, RS^-, C6H6

According to Sigel and McCormick, oxygen, nitrogen and sulfur are the donor atoms of greatest biological interest [54] as they are, for example, present in some active sites of metal ion dependent enzymes. A stability scale was established: oxygen donor ligands are the less discriminating atoms towards metal ions, nitrogen donors are intermediate, and sulfur donors are the most discriminating ones [55]. This property can be correlated with the electronegativity of each atom: an electronegative element, such as Oxygen ($\chi = 3.44$), cannot give easily its electrons to heavy metals. Nitrogen ($\chi = 3.04$) is slightly more efficient than Oxygen, and the most efficient is Sulfur ($\chi = 2.58$). But, regardless of the atom, a stability order was observed for complexes formed between ligands and some divalent metal ions, and it corresponds to the Irving-Williams series [54]: $Mn^{2+} < Fe^{2+} < Co^{2+} < Ni^{2+} < Cu^{2+} > Zn^{2+}$.

The sorption of trace metals in MTs has been particularly studied and it was shown that oxygen, sulfur and nitrogen are involved in the chelation of metals, with coordination geometries depending generally on the considered trace metal (figure 9). It was demonstrated that an octahedral arrangement was formed for Co^{2+} and Ni^{2+} ions, a square planar coordination was commonly observed for Cu^{2+} whereas a tetrahedral arrangement and a linear coordination were usually obtained for Zn^{2+} and Hg^{2+} respectively [96, 97]. In the case of cadmium, either tetrahedral arrangement or octahedral arrangement was equally reported. These preferential coordination geometries were determined using two sources of experimental data: Protein Data Bank and Cambridge Structural Database.

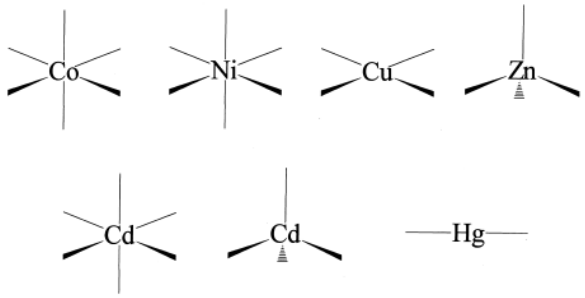

Figure 9: Preferred coordination chemistry of some divalent trace metals [96]

Thus, the efficiency of O, S and N atoms not only depends on their ability to interact with a trace metal, but is also related to the chemical group they are inserted in, as a specific coordination geometry can be formed around the trace element. Moreover, the spatial accessibility to chemical functional groups able to sequester trace metals is crucial, as it could be observed in figure 10. Indeed, ligand-ligand interactions in metal-amino acid complexes was proved by Yamauchi *et al.*: weak interactions involving the side chain groups of amino acids are closely related to the formation of complexes, favored by attractive intramolecular ligand-ligand interactions [98].

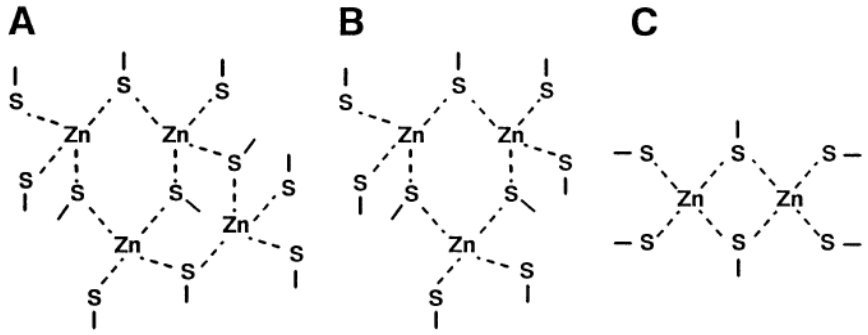

Figure 10: Representation of main clusters formed with metallothioneins in the trapping of zinc (A) α-domain, (B) β-domain and (C) γ-domain [41]

The geometry of the complexes presented in this section were not verified. Nowadays, as described in next section, the X-ray absorption spectroscopy can be used to determine and/or verify the structure of the metal/biomolecules complexes.

I.4.3. Experimental studies for the determination of the structure of metal/biomolecule complexes

X-ray absorption spectroscopy (XAS) can provide information on the local structure of the elements at sub-atomic spatial resolution. XAS includes both X-ray absorption near edge structure (XANES) and extended X-ray absorption fine structure (EXAFS). These two methods are complementary as XANES provides information about the oxidation state and molecular geometry, and EXAFS gives structural information about metal site bindings such as the type of neighboring atoms, coordination number and bond distances [99, 100]. Thus, these analytical techniques are particularly adapted to determine the structure of metal/biomolecule complexes.

Amino acids are often considered as bidentate chelating agents because of their carboxylic and amine functional groups. The simplest amino acid, i.e. glycine, was observed to complex Cu(II) thanks to these two functional groups and Carrera *et al.* determined the distance between the atom and the trace metal thanks to EXAFS studies: Cu-N and Cu-O are

respectively 2.000 Å long and 1.955 Å long [101]. All amino acids, except glycine, possess another functional group on the side chain that can be involved in the complexation of some metals. For example, zinc was observed to be chelated by cysteine under a tetrahedral geometry (confirming the conclusions of Rulíšek and Vondrášek), thanks to the thiol and amine groups: the distances observed between zinc and sulfur or nitrogen were Zn-S 2.259 Å and Zn-N 2.099 Å [102]. These conclusions are helpful not only to prove the ability of these functional groups to complex metals, but also to make the assumption that the stability scale observed by Martin is in accordance with the distance between the metal and the "interacting atom": Metal-O < Metal-N < Metal-S.

The high bond distance observed between a metal ion and the thiol group of cysteine was verified recently [103]. It was also observed in that study that the pH and the ligand concentration play a significant role in the complex structure. For example, a study carried out at pH 7.5 with mercury and N-acetylcysteine (H_2NAC) with two ligands for one mercury ion leads to a linear complex $Hg(NAC)_2^{2-}$ where Hg is coordinated to two sulfur atoms with a bond Hg-S distance of 2.33 Å. The same experiment carried out with three ligands for one mercury ion gives not only the linear complex previously observed but also another trigonal complex $Hg(NAC)_3^{4-}$ with a Hg-S bond distance of 2.42 Å. Then, with five ligands for one mercury ion, a small amount of tetrathiolate complex $Hg(NAC)_4^{6-}$ (with a Hg-S bond distance of 2.52 Å) can also be observed in addition to the two previously mentioned complexes. At pH 10.5, H_2NAC is completely deprotonated to NAC^{2-} which promotes the formation of both $Hg(NAC)_3^{4-}$ and $Hg(NAC)_4^{6-}$. Indeed, from four ligands for one mercury ion and above, the proportion of the linear complex $Hg(NAC)_2^{2-}$ is negligible at pH=10.5: up to 9% contrary to a maximum of 72% at pH 7.5 [103]. When a small amount of cysteine at alkaline pH is considered, the $Hg(N,S\text{-}Cys)_2^{2-}$ complex is obtained with a Hg-S bond distance of 2.34 Å. At a mole ratio Cys/Hg = 4, it is possible to observe a $Hg(S\text{-}Cys)_3^{4-}$ trigonal complex with a bond distance of 2.44 Å, and above Cys/Hg = 5, the $Hg(S\text{-}Cys)_4^{6-}$ tetrathiolate complex with a bond distance of 2.52 Å can be observed [104].

Many studies were carried out concerning metal/histidine complexes as histidine plays an important chelating role in living organisms. For instance, it reduces the bioavailability of toxic metals used as active components in several drugs [102]. Moreover, metal/histidine complexes allow to transport copper in the human blood [86]. Thus, a better understanding of the formation of metal/histidine complexes is necessary to determine the trace metals sorption mechanism.

Histidine possesses various heteroatoms which can interact with metals, as described previously (1.3.3): oxygen from the carboxylic group (O_c), nitrogen from the amine group (N_{am}) and the two nitrogens from the imidazole ring (N_{im}). Thus, there are four potential sites for metal coordination. But, Mesu *et al.* reported that metal binding via the deprotonated imidazole ring could not be considered as the pKa value (pKa = 14) of this form is very high [105]. Thus, three sites, namely O_c, N_{am} and N_{im}, can be involved in the coordination to heavy metals, which might result in mono-, bi- or tridentate binding forms.

A bidentate binding form is generally observed: two histidine molecules bind to one trace metal. In the case of Zn(histidine)$_2$, a tetrahedral geometry was observed [102], confirming the favored tetrahedral coordination of Zn reported by Rulíšek and Vondrášek. In that structure, Zn ion was coordinated with 4 N, with a Zn-N distance of 2.032 Å. Contrary to Zn(histidine)$_2$, a square planar geometry was identified for Cu(histidine)$_2$ with 2 N and 2 O bindings with copper, with a Cu-N distance of 1.974 Å and a Cu-O distance of 2.033 Å. The presence of two other oxygen atoms located at 2.48 Å from copper ions was also reported [102].

This study allowed a better understanding of the binding complexation but the pH conditions were not mentioned while pH is an important and influencing parameter in the complex formation [105, 106]. Then, three coordination modes were considered for histidine/copper complex (2:1) in order to determine the influence of pH: *glycine-glycine* coordination type (gly-gly) corresponding to an aminocarboxylate complex, where only O_c and N_{am} of histidine are involved in copper binding; *glycine-histamine* coordination type (gly-him) corresponding to the binding of copper with O_c and N_{am} from the first histidine, and with N_{im} and N_{am} from the other one; *histamine-histamine* coordination type (him-him) where only N_{im} and N_{am} bind to copper in a square planar arrangement [101].

At pH = 4, a gly-gly coordination mode was observed [105, 106], despite the higher pKa value of the imine group compared to the amine group, *i.e.* pKa(N_{im}) = 18.6 (determined in DMSO) whereas pKa(N_{am}) = 9.1. This observation was attributed either to an energetically more stable geometry or to a reduced inductive effect on N_{im} [105]. In the case of copper binding, the average distance between heteroatoms and copper is 1.95 Å [106]. From pH 4.5 to 5, the gly-him coordination mode is observed, with an average distance of 1.96 Å between heteroatoms and copper, and above pH = 5.0, the him-him coordination mode is predominant and the average distance between heteroatoms and copper is 1.98 Å [106]. These conclusions are consistent with the result of another study on the Cu(histidine)$_2$ complex at pH 7.3: a

square planar geometry was observed with a Cu-N distance of 1.99 Å [101]. Thus, the pH increase is correlated with the increase of the distance between heteroatoms (nitrogen and oxygen) and copper. Moreover, this pH increase leads to a change in the spatial arrangement: the O_c atom moves from the equatorial plane to the axial position giving a new geometry structure. At pH 4.8, a five-coordinate complex is observed under a distorted square pyramidal geometry with bidentate and tridentate L-histidine ligands [106]; at pH 7.3, an octahedral configuration coordinated by N_{am} and N_{im} atoms of histidine in a square planar arrangement is obtained and this configuration is coordinated by O_c atoms of carboxylic groups in the axial positions [86, 105].

Finally, an interesting study was carried out concerning the configuration of L-histidine with Mn^{2+}, Co^{2+}, Ni^{2+}, Cu^{2+}, and Zn^{2+} at pH 6.0 with a metal/L-histidine molar ratio of 1:2 [107]. In these conditions, the metal(histidine)$_2$ complex was in the him-him coordination mode in accordance with the previously mentioned studies. As oxygen and nitrogen atoms are very difficult to distinguish by EXAFS due to similar scattering abilities, only oxygen was considered as coordination atom in the first shell around metal ions for the EXAFS fitting process. The different complexes obtained have distorted octahedral configurations and the distances between oxygen and metal ions vary according to the following order: Mn (2.17 Å) < Co (2.12 Å) < Ni (2.06 Å) < Cu (1.97 Å) > Zn (2.04 Å). This classification is consistent with the Irving-Williams series which states that the complex stability should increase when the bond distance between oxygen and metal decreases.

Thus, pH and ligand concentration are two key parameters that must be known precisely before analyzing the complexes by XAS. However, these two parameters have not been taken into account by Rulíšek and Vondrášek. Some studies were in accordance with their observation [101, 102], but more recently, the study of the influence of pH and ligand concentration led to complexes structures different from those expected by Rulíšek and Vondrášek [103, 105-107].

I.5. Conclusion

The most toxic trace metals present in the sediments and aqueous media are the soluble trace metal ions. Some well-known biomolecules are able to sequester trace metal ions, such as cellulose, chitosan, alginate, cyclodextrin, etc. In this chapter, the interest was focused on some small polyfunctional biomolecules, i.e. amino acids, as they contain amine and carboxylic acid functional groups that can sequester trace metal ions. Moreover, except

for glycine, all amino acids also contain a functional group on the side chain: for instance, thiol group for cysteine, phenol group for tyrosine, and imidazole group for histidine. The ability of these biomolecules to sequester trace metal ions was also proved by some XAS studies, showing a first coordination shell of amino acid heteroatoms, such as nitrogen, oxygen and sulfur, around the considered metal ion.

Thus, these amino acids show a great potential for the sequestration of trace metal ions. However, as most amino acids are soluble, it is difficult to separate these biomolecules from aqueous medium. Thus, the idea consists in immobilizing biomolecules onto supporting materials to facilitate the removal of heavy metals from the aqueous medium. In this way, textiles or geotextiles are interesting porous materials for remediation purpose: biomolecules will be grafted onto geotextiles to ensure good remediation efficiency. This process requires a first functionalization step consisting in the grafting of acrylic acid, used as a spacer, to bring carboxylic acid groups at the surface of the fibers. Then, biomolecules will be immobilized by chemical coupling with these carboxylic acid groups.

The next chapter describes the development and the optimization of the acrylic acid grafting onto fibers using plasma or laser processes.

Chapter II

Development and optimization of acrylic acid grafting

II.1. Introduction

Physical methods, such as cold plasma and excimer laser processes, were selected to graft molecules onto textiles. However, direct grafting of biomolecules onto synthetic textile structures using plasma or laser processes is not possible because: there is not a sufficient density of functional groups generated at the surface of the fibers to allow the grafting with molecules, and moreover, biomolecules can be fragmented during the plasma treatment, leading to a loss of remediation properties. Therefore, the solution is the graft-polymerization of a functional monomer such as acrylic acid (AA) [21, 108-110] or N-vinyl-2-pyrrolidone [111] or maleic anhydride [32] onto the activated surface, a strategy that leads to a coating rich in functional groups available for further chemical modifications. In this study, acrylic acid was selected as a spacer as: it can be grafted and polymerized using low pressure cold plasma process, and it can lead to the formation of a functional film at the surface of fibers [20, 108-110, 112, 113]. Thus, acrylic acid must be first graft-polymerized onto PP and PET, and then the immobilization of biomolecules can be carried out by chemical coupling. In this chapter, the development and optimization of acrylic acid and polyacrylic acid grafting onto fabrics by physical methods (radiofrequency low pressure cold plasma, and KrF excimer laser) will be explained.

The first section of this chapter details the grafting of acrylic acid onto polypropylene nonwoven (PP) by radiofrequency plasma process. The protocol was already developed and optimized in the laboratory [20]. Thus, this section mainly deals with the chemical modifications occurring at the surface of the fibers during the plasma treatment. Then, the surface of the fibers was characterized using Scanning Electron Microscopy (SEM), Fourier Transform InfraRed with Attenuated Total Reflectance (FTIR/ATR) and X-ray Photoelectron Spectroscopy (XPS).

The second section of this chapter deals with the coating of acrylic acid onto poly(ethylene terephthalate) knitted fabrics (PET) by KrF excimer laser. The protocol was developed and optimized using the experimental design technique. The surface characterization was carried out as for plasma functionalized PP: SEM, FTIR/ATR and XPS were used. As acrylic acid can already adsorb metal ions, some studies were carried out in order to determine the sorption efficiency of the acrylic acid-coated PET. Finally, it was observed that this process can be applied on all types of PET textile structures.

This chapter is based on the following papers:

M. Vandenbossche, M. Jimenez, M. Casetta, S. Bellayer, A. Beaurain, S. Bourbigot, M.Traisnel, Chitosan-grafted nonwoven geotextile for heavy metal sorption in sediments, *Reactive & Functional Polymers*, **2013**, 73, pp. 53-59.

M. Vandenbossche, D. Derozier, M. Casetta, M. Jimenez, S. Bellayer, M. Traisnel, KrF Laser: an Innovative Method to Functionalize Textiles for the Remediation of Polluted Media, *Applied Surface Science (Submitted the 22nd of may)*

II.2.Acrylic acid grafting onto PP by radiofrequency cold plasma process

The radiofrequency low pressure cold plasma process (appendix 1) is interesting because it allows the modification of the surface properties without altering the bulk characteristics, and also, it avoids the use of toxic solvent and can minimize the use of water. This grafting process requires several steps: (i) the activation of PP to increase its wettability; (ii) the impregnation of the activated PP in an acrylic acid solution using a roll-padder; (iii) the polymerization of acrylic acid onto PP; (iv) the washing and the drying of the acrylic acid-grafted-polypropylene nonwoven (PP-g-AA).

To evaluate the efficiency of the acrylic acid grafting, the sample has been weighed before plasma activation (W_i in mg) and after the acrylic acid grafting step, more precisely after the washing and drying steps (W_f in mg). It allowed the calculation of the grafting rate, using the following equation:

$$\% = 100 \times (W_f - W_i) / W_i \qquad \text{Eq. (1)}$$

First of all, the acrylic acid grafting onto fabrics will be presented. Then, the surface characterizations will be detailed in order to give the evidence of the grafting. Finally, the grafting mechanisms, obtained from published literature and compared to surface analyses, are presented.

II.2.1. Polypropylene nonwoven wettability improvement

PP is a hydrophobic inert material. As a consequence, it is not possible to graft a molecule onto the raw PP material and it is necessary to create active functional groups on its surface before immobilizing any molecule. For this purpose, irradiation techniques, especially low pressure cold plasma treatments, are used to create radicals upon the surface of polypropylene which is allowed by the use of argon leading to the etching of the surface. The post-plasma oxidation of the surface improves the surface wettability (figure 11).

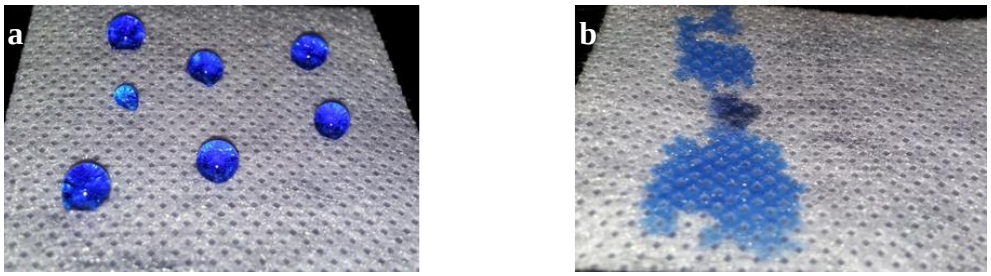

Figure 11: Polypropylene nonwoven textile (a) before and (b) after plasma activation

The increase of wettability can be explained by the creation of new chemical groups at the surface of PP fibers. Indeed, X-Ray Photoelectron Spectroscopy (XPS) was used to determine the evolution of the atomic concentration percentage at the surface of the fibers (before and after plasma treatment), and also to identify the new functional groups created at the surface of the virgin PP (table 5). After argon plasma activation, the amount of carbon has decreased from 97.4% to 87.8% whereas the amount of oxygen has increased from 2.6% to 12.2%, which is in accordance with the post-plasma oxidation. This information is essential, but not sufficient: the oxygen atom must be included in some functional groups. Thus, the C1s peak has to be decomposed in order to determine the new functional groups at the surface of PP fibers (figure 12).

Table 5: Atomic quantification by XPS of various elements at the surface of PP

Samples	C1s	O1s	N1s	(O1s)/(C1s)	(N1s)/(C1s)
Virgin PP	97.4%	2.6%	0%	2.7	0
Activated PP	87.8%	12.2%	0%	13.9	0
PP-g-AA	82.1%	17.9%	0%	21.8	0

C1s peak of virgin polypropylene is quite asymmetric (figure 12a), which can be explained by the manufacturing process of fibers that can lead to a slight oxidation of the surface of the fibers. This fact can also explain the small amount of oxygen observed in virgin PP (table 5). The C1s peak of the activated PP can be decomposed into five peaks (figure 12b): one peak at 285.0 eV (fwm = 1.2 eV), corresponding to C-C bonds; one peak at 285.8 eV (fwhm = 1.2 eV), corresponding to the C-O bonds; one peak at 286.9 eV (fwhm = 1.2 eV), corresponding to C=O or O-C-O chemical groups; one peak at 288.2 eV (fwhm = 1.2 eV), corresponding to the ester O-C=O group; and one peak at 289.4 eV (fwhm = 1.2 eV), corresponding to the acid O-C=O groups.

As a conclusion, the plasma treatment brings new chemical groups at the surface of the fibers leading to hydrophilic properties of the PP fibers. Thus, the PP nonwoven is activated, and then, grafting of acrylic acid is possible.

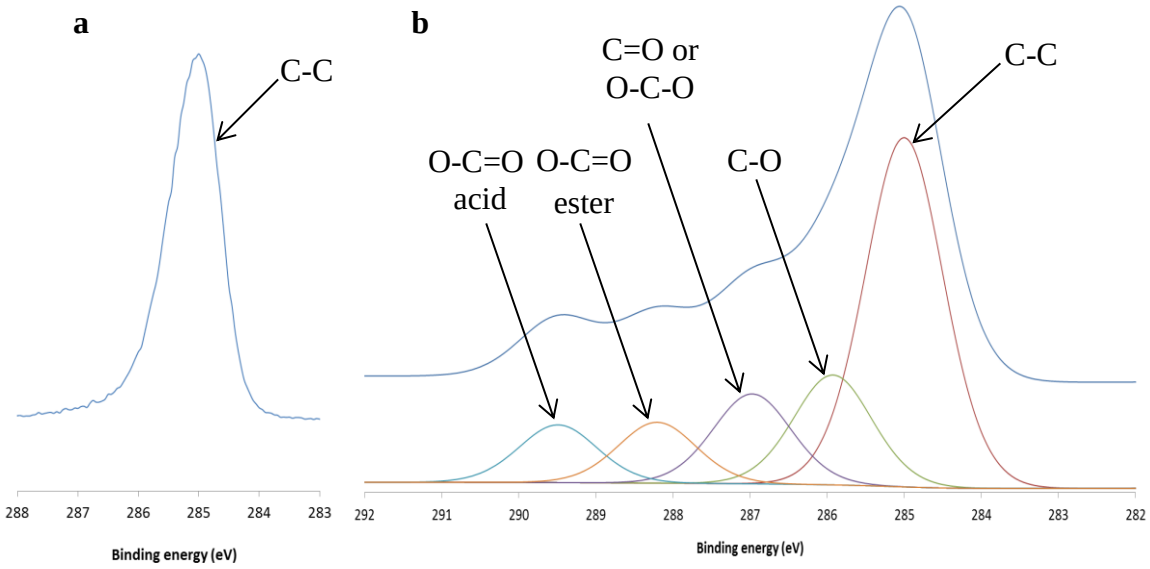

Figure 12: XPS high resolution C1s spectra of (a) virgin PP and (b) activated PP

II.2.2. Acrylic acid grafting onto activated polypropylene nonwoven

After PP activation, the grafting of acrylic acid is possible. Textiles are first impregnated with acrylic acid using a roll-padder, and then, a plasma treatment is carried out in order to polymerize acrylic acid. The covalent grafting of acrylic acid onto PP has to be verified as the next step of the functionalization process is the immobilization of biomolecules. Indeed, if acrylic acid is not covalently grafted onto PP, it represents a hazard as it can be released in the environment.

PP fabrics were analyzed by scanning electron microscopy (SEM, appendix 2) in order to observe the new morphology of fibers after plasma treatment. A homogeneous coating covers the fibers as it can be observed in figure 13. For INTN50 (PP at 50g/m²) and INTN100 (PP at 100 g/m²), 2% and 3%-weight gain were obtained respectively. But these visual results cannot allow determining the nature of this coating. Thus, complementary analyses were carried out in order to verify the nature of the coating.

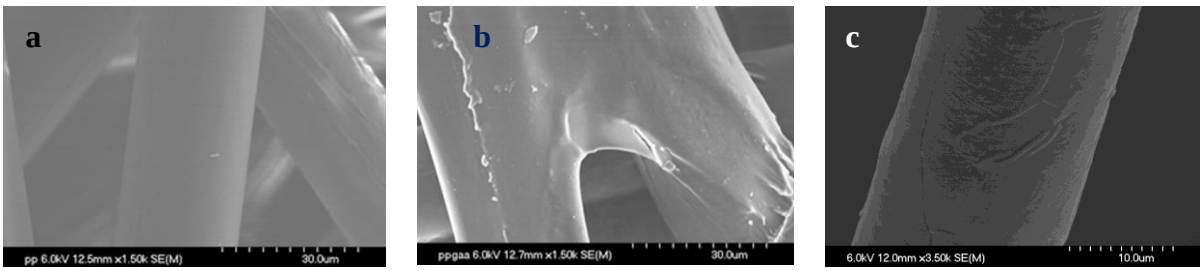

Figure 13: SEM images (a) virgin PP, (b) PP-g-AA at a magnification of 1.50 k and (c) PP-g-AA at a magnification of 3.50 k

FTIR/ATR (appendix 2) can be used to detect the presence of characteristic chemical groups at the geotextile surface, and thus, to determine the nature of the coating. Evidence of the presence of acrylic acid is given figure 14 as a new peak is obtained for PP-g-AA that was not observed with virgin PP: an asymmetric elongation peak is obtained at 1716 cm^{-1}, assigned to the carboxylic acid groups. However, this observation is not sufficient to conclude that acrylic acid is really grafted onto PP. Thus, other studies were carried out by X-ray photoelectron spectrometry in order to verify the covalent grafting of acrylic acid.

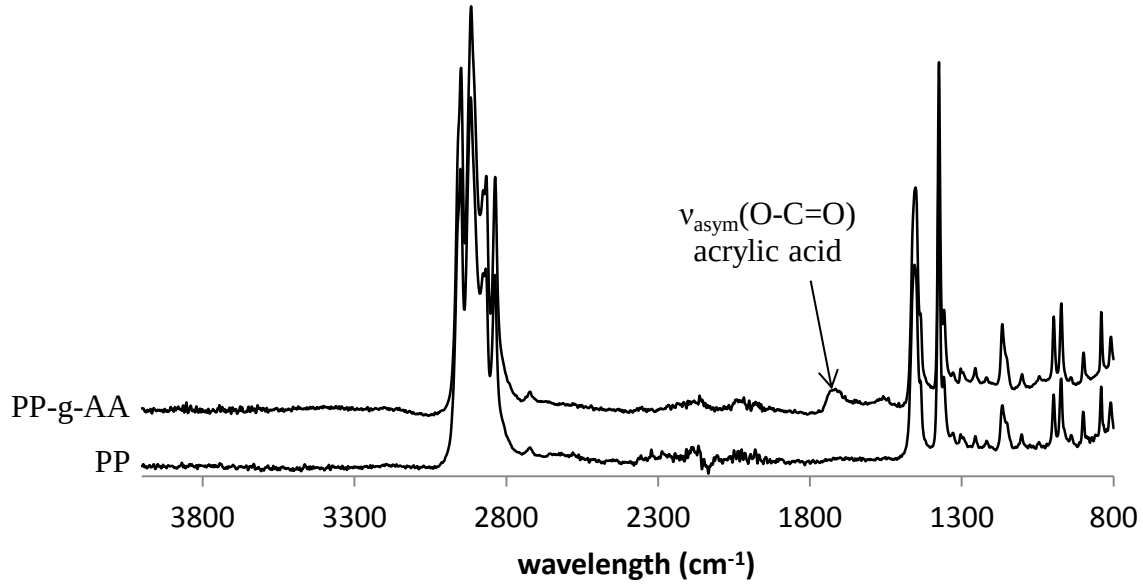

Figure 14: FTIR–ATR spectra of the virgin PP and PP-g-AA

XPS analyses (appendix 2) can provide information on the amount of carbon and oxygen at the surface of the fibers after the graft-polymerization of acrylic acid. The activated PP contained 87.8% carbon and 12.2% oxygen. After the immersion and plasma treatment steps, the functionalized textiles contained 82.1% carbon and 17.9% oxygen (table 5). Thus, this treatment step increases the amount of oxygen at the expense of the amount of carbon, which can be explained by the new functional groups created at the surface of the fibers, especially carboxylic acid groups.

The decomposition of the C1s peak is necessary in order to verify the covalent grafting of acrylic acid. Indeed, the C1s peak can be divided into 3 peaks: one peak at 289.3 eV (fwhm = 1.3) due to the contribution of acrylic acid and polyacrylic acid (O-C=O); one peak at 286.5 eV (fwhm = 1.3) corresponding to the ether group, explaining the grafting of acrylic acid on PP [112]; and one peak at 285.0 eV (fwhm = 1.3) corresponding to C-C bonds of acrylic and polyacrylic acids and PP (figure 15).

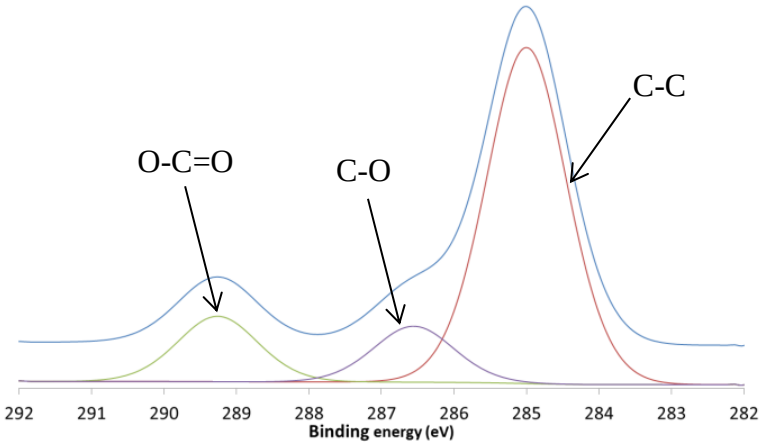

Figure 15: XPS high resolution C1s spectra of PP-g-AA

Thus, acrylic and polyacrylic acids are proven to be covalently grafted onto PP, and a thin functional film is observed at the surface of the fibers. The carboxylic acid groups of acrylic acid can then be used for the immobilization of biomolecules able to sequester trace metal ions.

II.2.3. Functionalization mechanisms

The treatment of polymeric substrates using plasma creates an important amount of radicals at the surface of the material [112]. Argon plasma under low pressure conditions favors the etching of the material's surface, allowing the creation of some radicals. When the activated material is exposed to dry and clean air, the radicals react with oxygen giving functional groups such as: hydroperoxide (R-C-O-O-H), peroxide (R-C-O-O-R'), hydroxide (R-O-H), carbonyl (R-C(=O)-R') and carboxylic acid (R-C(=O)-O-H) groups.

According to XPS results, new chemical groups were generated after argon plasma treatment, confirming Gancarz study [112]. Moreover, the formation of ester groups could be explained by recombination mechanisms: during the post-plasma oxidation, the creation of some carboxylic acid groups occurs that may react with other radicals at the surface of the fibers, leading to the formation of ester groups. To summarize, the important functional groups created during the textile activation by argon plasma process and then during the post-plasma oxidation are given in scheme 3.

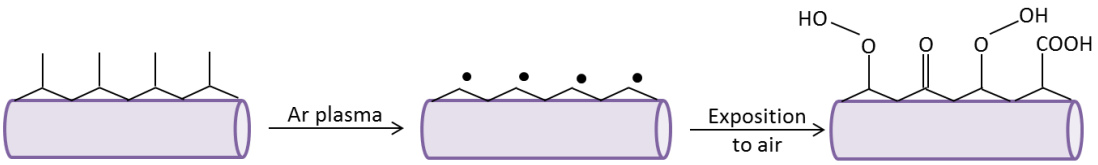

Scheme 3: Mechanisms during the PP fiber activation

Then, during the impregnation step of the activated textile into the acrylic acid solution, peroxide groups can react with vinyl monomers of acrylic acid and create a new covalent bond through a redox reaction, leading to the grafting of the vinyl monomer [112]. For instance, the vinyl group of acrylic acid can react with the hydroperoxide groups at the surface of the fibers, leading to the formation of an ether group involved in the covalent grafting of acrylic acid onto the surface of the fibers (scheme 4). Thus, the covalent grafting of acrylic acid is proven by the presence of an ether group and confirmed using XPS analysis.

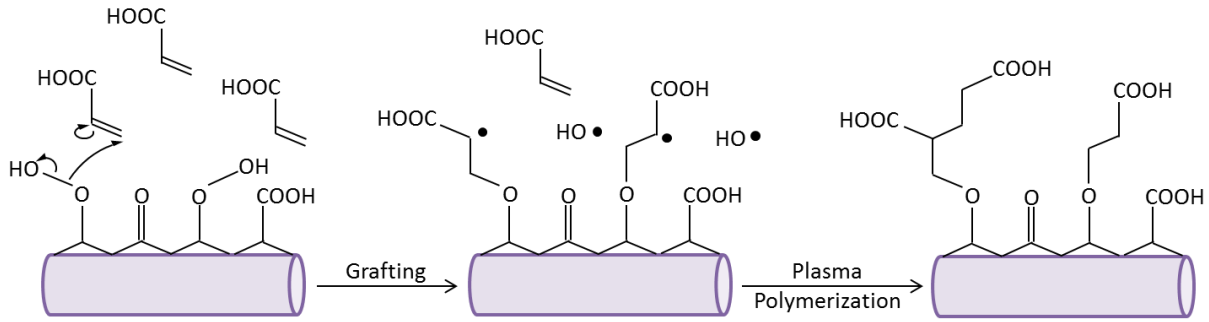

Scheme 4: Mechanisms during grafting and polymerization of acrylic acid onto PP fiber

Once impregnation in the acrylic acid solution, PP fibers are treated under low pressure cold plasma (with argon flow) leading to the polymerization of the monomer, and then, to the formation of a thin film of acrylic and polyacrylic acid. Thus, fibers are covered with a coating enriched with carboxylic acid groups. These functional groups are very interesting as they can be used for further immobilization of biomolecules through chemical coupling.

II.3.Acrylic acid grafting onto PET by excimer laser process

Excimer laser (appendix 1) is an interesting process that can be used for the coating of acrylic acid onto PET fabrics because: (i) the textile does not need any activation step before immersion; (ii) the polymerization of acrylic acid can be carried out at atmospheric pressure; and (iii) this functionalization method is very easy to transfer at industrial scale.

II.3.1. Development and optimization of the acrylic acid coating

II.3.1.1. Preliminary laser tests

Before starting the optimization of the excimer laser treatment allowing the coating of PET with acrylic acid, it is necessary to adjust the limits of each experimental parameter. A rapid evaluation of the influence of the fluency and of the number of pulses was done. First, seven fluencies were tested at 300 pulses: 5, 10, 20, 30, 40, 50 and 60 mJ/cm². A linear relationship between fluency and weight gain of the samples was obtained. Then, various

numbers of pulses were tested at 30 mJ/cm²: 100, 200, 300, 400, 500 and 1000 pulses. A linear relationship was observed between the weight gain and the number of pulses: the weight gain increases with the number of pulses until 500 pulses and then remains quite stable. But, at high fluency or high number of pulses, there is a risk to damage the fibers (figure 16a). From about 40 mJ/cm², the fibers are deteriorated and even if a high weight gain is obtained, acrylic acid does not cover regularly the fibers surface (figure 16b). Thus, a maximal energy of 30 mJ/cm² was considered for the optimizing step.

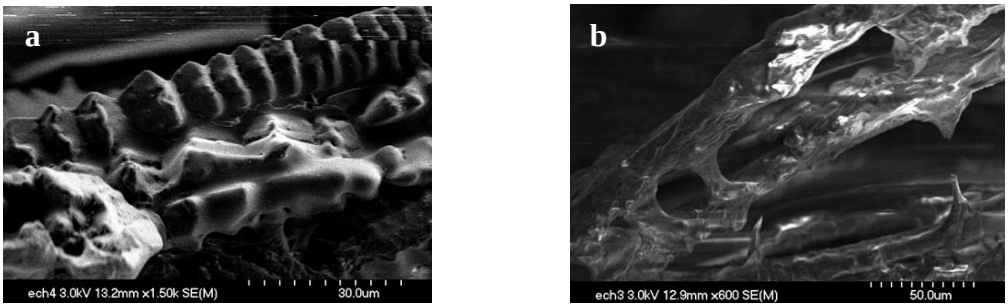

Figure 16: Images by SEM of acrylic acid impregnated fibers irradiated by KrF laser at 58 mJ/cm² and 738 pulses: (a) damaged fibers and (b) large amount of acrylic acid

II.3.1.2. Optimization of the coating of acrylic acid onto PET

As the preliminary studies showed the influence of fluency and number of pulses on the weight gain, an experimental design was carried out to optimize the acrylic acid coating on PET knitted fabrics by varying 2 parameters (table 6): the fluency (U_1) and the number of pulses (U_2). A central composite design (CCD) was used and the weight gain was considered as the response (Y).

Table 6: Coded and real values of experimental parameters used for the CCD

Coded variable	Parameter	Levels				
		-α	-1	0	+1	+α
X_1	**U_1** fluency (mJ/cm²)	9	12	20	28	31
X_2	**U_2** number of pulses	220	300	500	700	780

The determination coefficients associated to the mathematical model were determined and show that the regression model fits the experimental data correctly. In fact, R^2 value is 96.8%, indicating that only 3.2% of the total variation is not explained by the model. The value of the adjusted determination coefficient is also high (R^2adjusted = 92.7%), showing a high significance of the model. The weight gain is well predicted by the model as the coefficient of prediction Q^2 is 77.9%.

The second-order polynomial equation associated to the response Y is:

$$Y = 1.60 + 0.52\ X1 + 0.88\ X2 - 0.13\ X12 + 0.19\ X22 + 0.20\ X1X2 \quad \text{Eq. (2)}$$

This model allows plotting the evolution of the predicted weight gain as a function of the fluency and the number of pulses (figure 17). It is observed that the higher the fluency and number of pulses, the higher the weight gain. However, the aspect of the fibers has also to be taken into account as the laser treatment can deteriorate the fibers. A microscopic analysis of the samples obtained with the experimental design showed that for a high fluency and a high number of pulses, the acrylic acid coating is not homogeneous and the fibers are damaged. Particularly, a slight yellowing of the knitted fabric can be noticed for a number of pulses higher than 700. To determine the optimal conditions for the laser treatment, a maximum value of 700 pulses was thus considered. Then, it was also decided to adjust the value of the fluency to avoid the degradation of the fibers. A weight gain of 3 w.-% was considered as a good result for the acrylic acid coating. The response surface predicts a 3 w.-% weight gain using a fluency of 24 mJ/cm² and 700 pulses (figure 17). Thus an experiment was carried out in these conditions and a weight gain of 3.2 ± 0.3 w.-% was obtained, allowing validating the model.

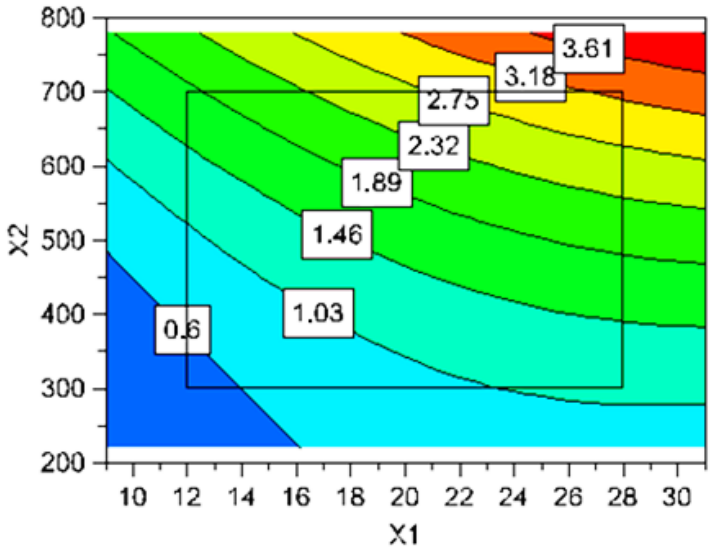

Figure 17: Contour plot showing the evolution of the weight gain as a function of fluency (X_1) and number of pulses (X_2)

This process is easily transferable at industrial scale, especially as it is possible to accelerate the process speed by increasing the size of the treated area. In this study, the removal of the cylindrical lens of the laser apparatus allowed irradiating larger areas, up to 40 x 11.5 mm², compared to 40 x 3.5 mm² for the previous experiments. However, in order not to modify the total fluency of irradiation and to obtain the same weight gain, a fluency of

24 mJ/cm² and 700 pulses (celerity of 0.150 mm/s) were applied for the largest treated surface. In these conditions, a similar acrylic acid coating was obtained compared to the optimized acrylic acid-coated-polypropylene nonwoven (PET-c-AA) sample, and this new protocol was thus considered for the following characterizations and remediation tests.

II.3.2. Characterization of the PET-c-AA

SEM analyses (appendix 2) were carried out on the treated fibers to determine the morphology of the acrylic acid coating compared to the virgin PET fibers. Virgin PET fibers (figure 18a) are smooth with a non-circular section. When irradiated with the excimer laser (figure 18b), virgin PET fibers show thin stripes on the exposed side. After laser irradiation, acrylic acid impregnated PET fibers present various types of structures but only on the area irradiated by the excimer laser: small balls regularly distributed along the fibers (figure 18d) or waves (figure 18c, 18e and 18f). Thanks to SEM observations, the following conclusion can be made: only the area exposed to the excimer laser beam is functionalized with acrylic acid. Consequently, if one part of a fiber is hidden by another fiber, then the hidden part cannot be functionalized.

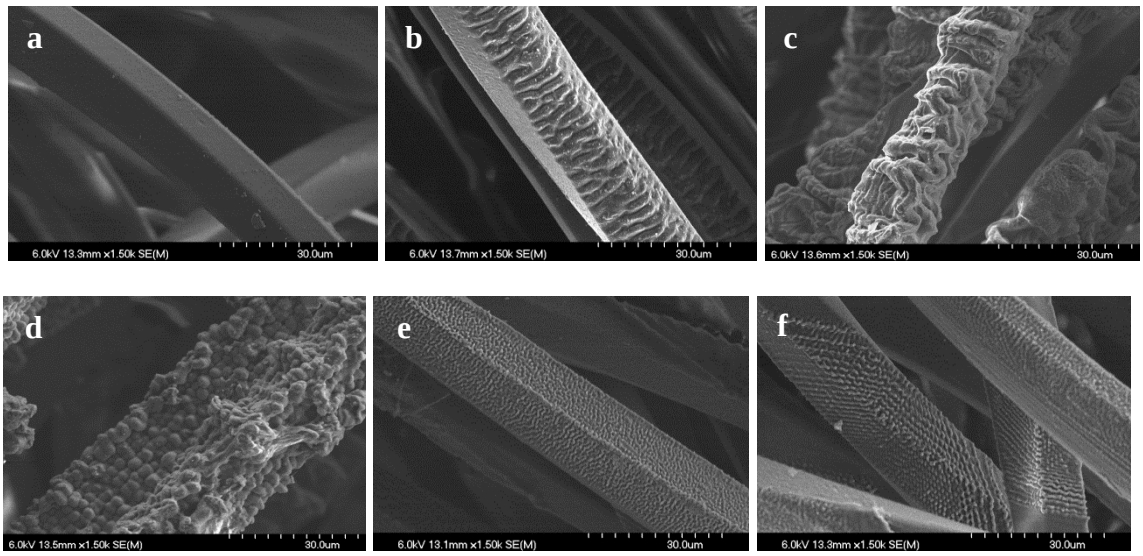

Figure 18: Images by SEM of (a) virgin PET, (b) irradiated virgin PET, and (c, d, e, f) different morphologies obtained for acrylic-acid-impregnated PET irradiated with laser

FTIR-ATR was used to identify the chemical groups at the surface of PET fibers before the treatment, after the degradation due to excimer laser, and also to confirm the presence of acrylic acid at the surface of the textile (figure 19). Some characteristic peaks of PET can be observed: the peak of asymmetric elongation of the aromatic ester (O-)C=O at 1713 cm^{-1}; the peak of asymmetric elongation of the (O=)C-O-C at 1242 cm^{-1}; the peaks of

symmetric elongation of the (O=)C-O-C at 1118 cm^{-1} for the amorphous structure and 1095 cm^{-1} for the crystalline structure; and the peak of the out-of-plane deformation of the para-substituted aromatic ring at 722 cm^{-1}. Concerning the acrylic acid impregnated PET irradiated with laser, a loss of intensity for the important peak of PET is observed. Moreover, the peak at about 1713 cm^{-1} is larger.

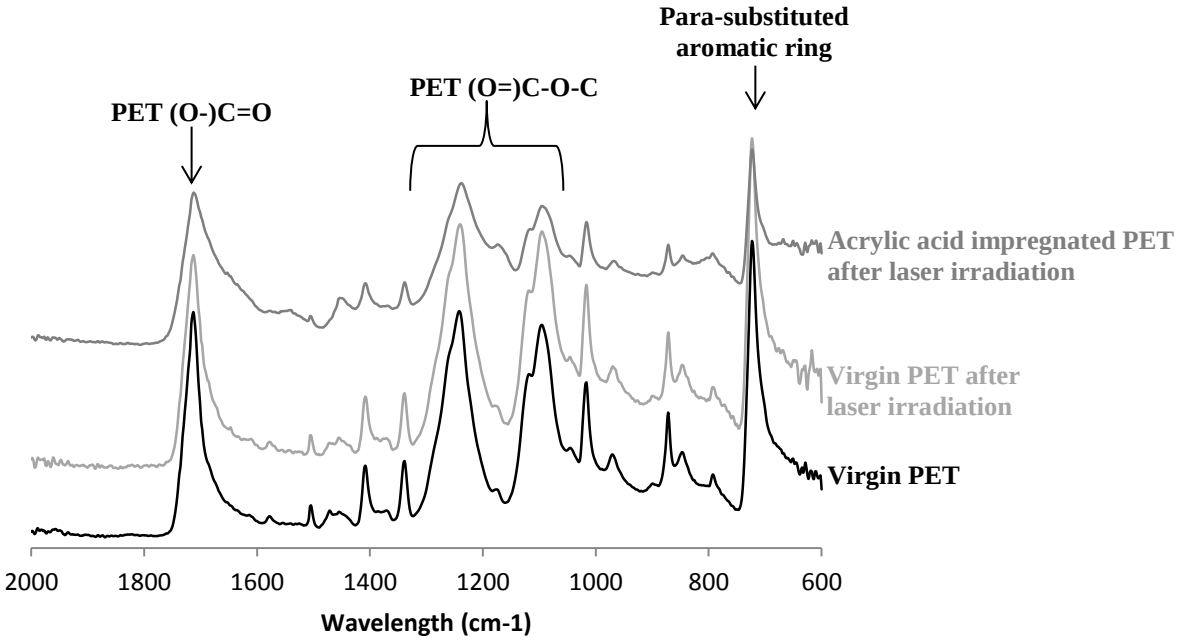

Figure 19: FTIR/ATR spectra of virgin polyethylene terephthalate (PET), virgin PET irradiated with an excimer LASER, and acrylic acid impregnated PET irradiated with an excimer laser

As it is not easy to observe the differences between the spectra (figure 19), subtractions were carried out. To ensure a good subtraction process between these spectra, two peaks were considered as reference: at 1407 cm^{-1} and at 1339 cm^{-1} attributed to the vibration of the aromatic ring. The result of the subtraction between the spectra of virgin PET irradiated with LASER and the spectra of the untreated virgin PET give a piece of information (figure 20). Indeed, an important loss is observed at about 1713 cm^{-1}. Thus, less aromatic esters are present after an irradiation with an excimer laser. This phenomenon could be explained by a decarboxylation [114] or a decarbonylation [115] of PET, phenomenon induced by laser irradiation.

If the sample is impregnated with acrylic acid before the laser irradiation, the loss of intensity at about 1713 cm^{-1} is less important and two new peaks are observed: at 1693 cm^{-1} an important peak corresponding to carbonyl groups. These carbonyl groups can be formed thanks to a recombination of acrylic acid when irradiated with laser. As a conclusion, the impregnation of the textile with acrylic acid protects in a certain way the fibers because

they are not directly irradiated with excimer laser: acrylic acid interacts with the excimer laser to form new radicals that can interact with acrylic acid or fibers.

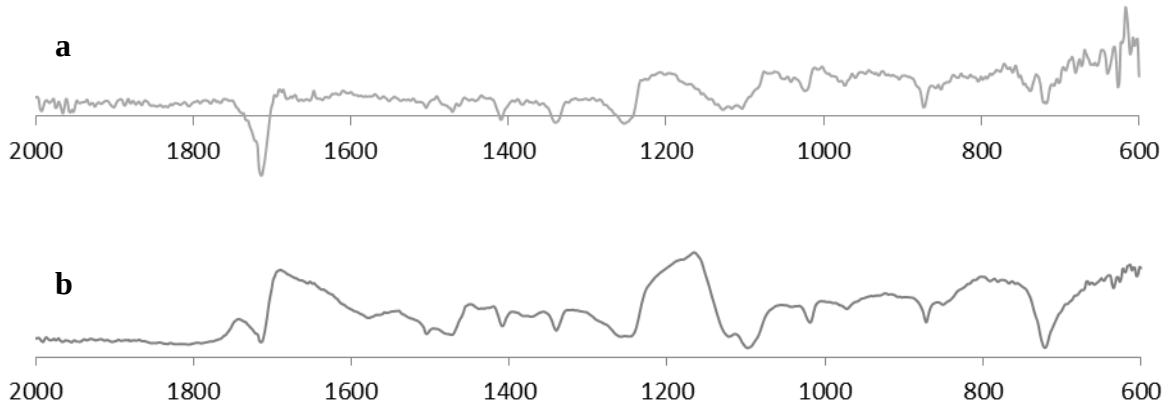

Figure 20: FTIR/ATR subtraction spectra (a) virgin PET after laser irradiation minus virgin PET and (b) acrylic acid impregnated PET after laser irradiation minus virgin PET

Then, XPS analyses (appendix 2) were carried out on virgin PET and on acrylic acid-impregnated PET after laser irradiation in order to determine the atomic percentage of carbon and oxygen at the surface of the fibers, and to identify the bonds created during the excimer laser treatment on acrylic-acid-impregnated PET. Evolutions of the atomic percentages of carbon and oxygen are given in table 7.

Table 7: Atomic quantification by XPS of various elements at the surface of the textiles

Samples	C1s	O1s	N1s	(O1s)/(C1s)	(N1s)/(C1s)
Virgin PET	79.0%	21.0%	0%	26.6	0
PET laser	81.2%	18.9%	0%	23.3	0
PET + AA laser	77.3%	21.1%	1.6%	27.3	2.1

Virgin PET contains about 79% carbon and 21% oxygen. The same sample, irradiated with an excimer laser, contains about 81% carbon and 19% oxygen. Thus, the irradiation process leads to a decrease of the (O1s)/(C1s) ratio. This phenomenon could be explained by a decarboxylation [114] and/or decarbonylation process [115]. After impregnation with acrylic acid and then irradiation with laser, PET contains about 77% carbon, 21% oxygen and 2% nitrogen. A small amount of nitrogen was detected with XPS only for this third sample. It may be supposed that the fiber surface becomes so reactive after laser irradiation that it might react with nitrogen from the ambient air. Concerning the oxygen percentage, it is the same as the one obtained for virgin PET. But, as the acrylic acid coating should lead to an increase in the number of oxygen atoms, there is also a loss of oxygen due to the laser irradiation process.

Decomposition of the C1s peak of each sample was carried out in order to identify the main chemical bonds at the surface of PET fibers (figure 21). The virgin PET curve can be decomposed into 4 peaks (fwhm = 1.3, figure 21a): the most important one is the aromatic C=C peak at 284.0 eV; then, the C-C peak at 285.0 eV; the C-O peak at 285.8 eV; and the aromatic ester peak (O-C=O) at 288.1 eV. Concerning the irradiated virgin PET (figure 21b), 5 peaks (fwhm = 1.3) are obtained: the first 4 peaks are similar to those observed for the non irradiated sample but an additional peak is obtained at 289.4 eV corresponding to the O-C=O bonds of an acid group. Thus, laser irradiation on virgin PET leads to a break of chemical bonds, mainly observed for the aromatic ester group. Indeed, the percentage of aromatic C=C is quite the same in virgin PET (59.8%) as in irradiated PET (58.6%). An increase is observed for the C-C peak (from 14.1% for PET to 20.8% for irradiated PET) which can be related to the loss of oxygen in the sample due to the laser irradiation process (decarbonylation and/or decarboxylation processes mentioned previously). This phenomenon also explains the important decrease of the C-O peak (from 15.2 to 8.1%), and the slight decrease of the O-C=O ester peak (from 10.8 to 9.6%). The decomposition of the C1s peak of the acrylic acid-impregnated PET irradiated with laser gives information on the surface composition (figure 21c): the aromatic C=C is observed at 283.9 eV (fwhm = 1.3); the C-C peak at 285.0 eV (fwhm = 1.3); the C-O peak at 286.0 eV (fwhm = 1.3); the O-C=O for an ester group at 288.2 eV (fwhm = 1.3); and the O-C=O for an acid group at 289.5 eV (fwhm = 1.3). But, there is also a new peak at 287.2 eV which could correspond to C=O of carbonyl or O-C-O of acetal/cetal group. The percentage of aromatic C=C bonds is lower than before (only 41%) as the PET structure is less accessible to the X-ray source due to the covering of fibers with acrylic acid. On the contrary, there is an increase of the C-C bonds percentage as there is not only the contribution of PET but also that of acrylic acid. The C-O percentage increases compared to virgin PET or irradiated virgin PET (16.7% versus 8.1 and 15.2% respectively). The O-C=O ester percentage is not so far from the previous results (8.4%), whereas the O-C=O acid percentage is slightly higher (3.9% compared to 2.9% for the irradiated virgin PET). In this work, the covalent grafting of acrylic acid is thus impossible to prove. It was however observed that the coating is durable as there is no change of the final sample weight and no change of the surface morphology after a 1-hour washing in ultrasonic bath.

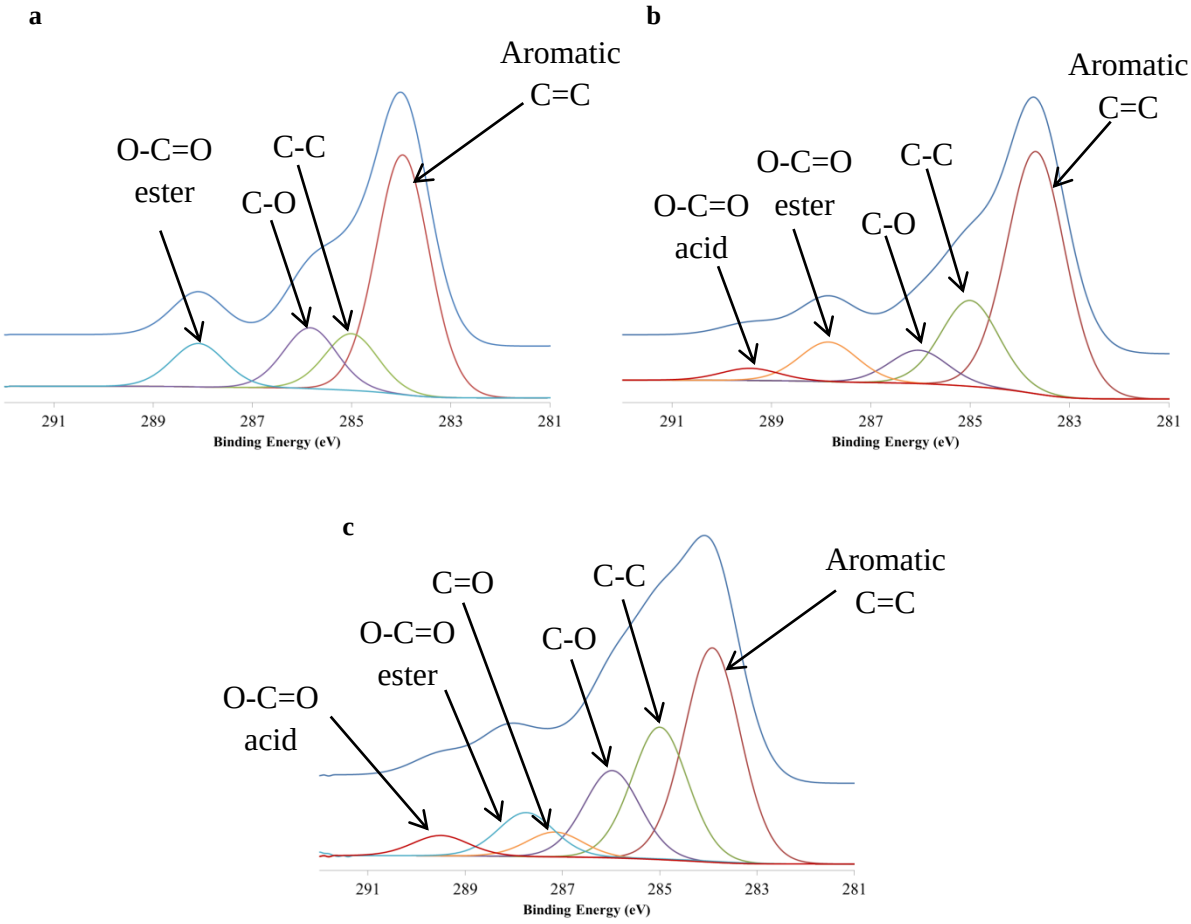

Figure 21: XPS high resolution C1s spectra of (a) virgin PET (b) virgin PET after laser irradiation and (c) acrylic acid impregnated PET after laser irradiation

II.3.3. Determination of the mechanisms

In this work, fibers were first impregnated with acrylic acid, and then irradiated with the excimer laser. The polymerization of acrylic acid is initiated by some radicals formed at the surface of the fibers by photon dissociation [115]. Moreover, the cleavage of some bonds is photoinduced due to the excimer laser irradiation. During the treatment of the fabrics, it is considered that a part of the photon energy, i.e. 1 eV, goes toward further increasing the potential of the material surface [116]. Thus, as a KrF excimer laser is at 248 nm, and consequently, as the photon energy is at about 5 eV, a maximum of 4 eV can be used for the bond cleavage. Thus, only two bonds can be considered in this part as they need an energy lower than 4 eV to be cleaved: the C-O and the C-C bonds (figure 22).

It is thus possible to predict the compounds created at the surface of the fabric during the laser treatment of virgin PET and impregnated PET. Figure 23 gives information on the decomposition of PET fibers induced by the excimer laser treatment. The degradation of PET corresponds mainly to a Norrish type II mechanism, which leads to the break of two molecular chains: C-C and C-O bonds.

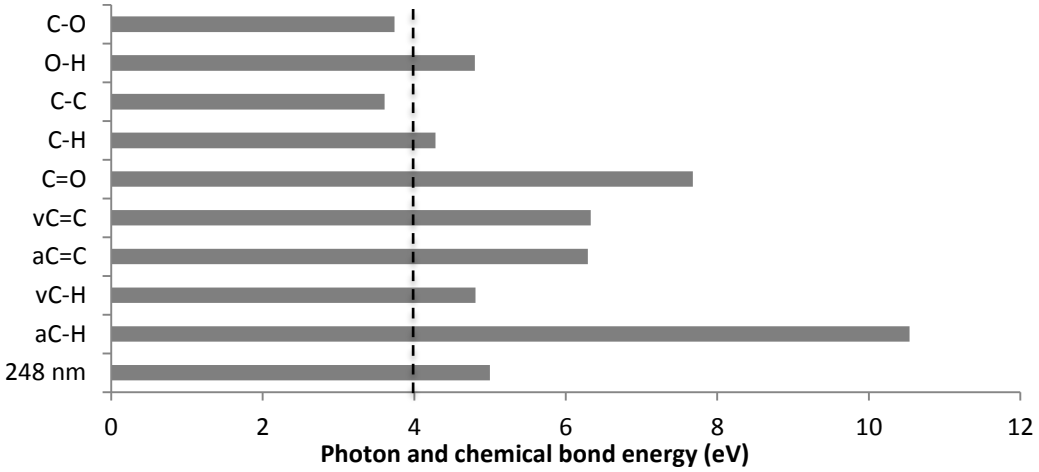

Figure 22: Energy of a 248 nm excimer laser and of the main chemical bonds in acrylic acid and PET (with "a" abbreviation for aromatic and "v" abbreviation for vinyl)

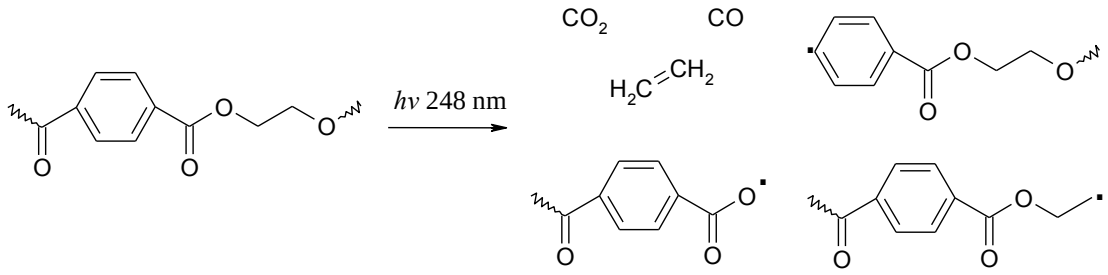

Figure 23: Mechanism of PET degradation induced by KrF excimer laser treatment [115]

Acrylic acid is also present at the surface of the fibers. Under the laser beam, acrylic acid could also undergo a degradation corresponding to a Norrish type II mechanism (figure 24). From this observation, there is the possibility of a recombination leading to the formation of carbonyl group. This assumption is in accordance with the results obtained by FTIR and XPS. But, as there is an increase of the acidic groups in O1s XPS result in the case of irradiated acrylic-acid-impregnated PET sample, it is also possible that acrylic acid is not totally damaged. Moreover, excimer laser irradiates the sample surface under a pulsed mode alternating excitation and relaxation periods at the surfaced of the fabrics. During the relaxation period, radicals formed during the previous period can interact with the surface to create new bonds. Acrylic acid can also polymerize thanks to a radical polymerization mechanism that can be induced by the laser beam at 248 nm.

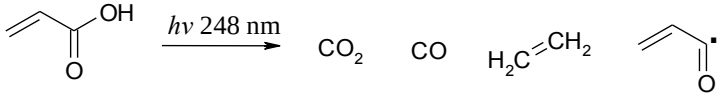

Figure 24: Assumed mechanism of acrylic acid degradation induced by KrF excimer laser treatment

The most important phenomenon that occurs during laser irradiation is the crosslinking, through the formation of an oxygen bridge between the ester group of PET and

the acid groups of acrylic acid [117]. Indeed, the negatively charged acidic oxygen atom can react with the positively charged ester carbon atom (figure 25). In this case, the acrylic acid is grafted through an anhydride bond.

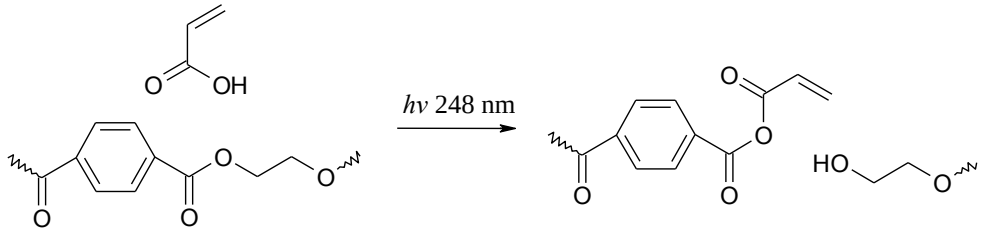

Figure 25: Potential crosslinking of acrylic acid and PET under 248 nm laser beam [117]

II.4. Conclusions

In this work, two different methods were used for the functionalization of PP and/or PET fabrics with acrylic acid: the radiofrequency low pressure cold plasma and the excimer laser processes. The morphologies of the coatings obtained are really different: by plasma process, a thin film of polyacrylic and acrylic acids covers the fibers, whereas by excimer laser, some waves can be observed at the surface of the fibers. Moreover, chemical analyses show the great potential of the use of plasma technology. In fact, acrylic acid is proven to be covalently grafted onto the fibers, and carboxylic acid functional groups are available at the surface of the fibers. On the contrary, the laser treatment leads to a durable coating, even if the covalent grafting was not proven. Moreover, some recombination reactions occur during the treatment, leading to the loss of carboxylic acid groups at the surface of the fibers. It would be interesting to make some tests with another laser (for instance, quadruple YAG) to try to obtain a good coating without any recombination. As a conclusion to this chapter, only the functionalized fabrics prepared with the radiofrequency cold plasma process will be considered for the biomolecule immobilization.

The following chapter details the immobilization of biomolecules, i.e. cysteine and tyrosine, onto PP-g-AA, and also, the evaluation of the performance of the PP-g-AA-biomolecules to adsorb trace metals.

Chapter III

Biomolecules immobilization for trace metal ions sorption

III.1. Introduction

In this chapter, the biomolecules immobilization onto PP-g-AA is presented, as well as the performance evaluation of the PP-g-AA-biomolecules to adsorb trace metal ions. According to the HSAB theory, thiol groups and aromatic rings, which are soft bases, favor the complexation of some trace metal ions such as Cu^{+}, Cd^{2+}, Hg^{2+}, Hg_2^{2+} (soft acids), and also Fe^{2+}, Co^{2+}, Ni^{2+}, Cu^{2+}, Zn^{2+}, Pb^{2+} (borderline acids). These two functional groups are particularly interesting as they can reduce the formation of complexes with Na^{+}, K^{+}, Mg^{2+}, Ca^{2+}, Ba^{2+}, Cr^{3+} and Mn^{2+} (hard acids). As demonstrated in the first chapter, amino acids are interesting polyfunctional biomolecules able to sequester trace metal ions. Thus, 2 amino-acids, cysteine and tyrosine, were selected as they contain respectively a thiol and a phenol group in the side chain.

The first section of this chapter concerns the optimization of the grafting of amino acids onto PP fibers. Cysteine grafting was optimized using experimental design. The grafting of tyrosine onto PP was also carried out, but at higher temperature than for cysteine to speed up the grafting step in view to upscale the process. The covalent grafting of cysteine and tyrosine was verified using SEM, FTIR/ATR and XPS studies.

The second section of this chapter concerns the evaluation of the efficiency of these new materials. Functionalized samples were immersed in solutions containing trace metals, and then, the amount of trace metals adsorbed was evaluated. Thanks to this protocol, it was possible to compare the remediation efficiency of PP-g-AA-cysteine and PP-g-AA-tyrosine. The best material was selected and further studies were carried out with leachate from the sediments of Dunkirk harbor.

This chapter is based on the following papers:

M. Vandenbossche, M. Casetta, M. Jimenez, S. Bellayer, M. Traisnel, Cysteine-grafted Nonwoven Geotextile: A New and Efficient Material for Heavy Metals Sorption – Part A, *Journal of Environmental Management*, **2014**, 132, pp. 107-112.

M. Vandenbossche, H. Vezin, N. Touati, M. Casetta, M. Jimenez, M. Traisnel, Cysteine-grafted Nonwoven Geotextile: A New and Efficient Material for Heavy Metals Sorption – Part B, *Journal of Environmental Management*, **2014**, 143, pp. 99-105.

M. Vandenbossche, A. Dehaese, M. Casetta, M. Jimenez, M. Traisnel, Tyrosine: an Efficient Natural Molecule for Copper Remediation, *Green Materials*, **2014** *(in press)*

III.2. Optimization of the immobilization step of biomolecules

III.2.1. Principle

Selected biomolecules should be covalently grafted onto PP-g-AA to obtain good sorption properties. This step is allowed by a specific chemical coupling using a carbodiimide. Indeed, carbodiimides are generally used to make carboxylic acid group more reactive and thus to improve the chemical coupling between this functional group and amine groups. In this work, the N-(3-Dimethylaminopropyl)-N'-ethylcarbodiimide hydrochloride or EDC was used for the chemical coupling between the amine group of amino acids and carboxylic acid groups at the surface of the PP-g-AA (scheme 5).

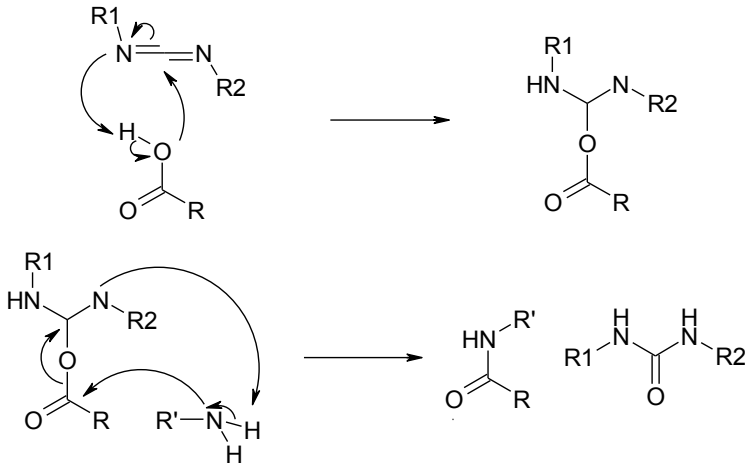

Scheme 5: Mechanism of the coupling between carboxylic acid and amine functions using a carbodiimide

III.2.2. Cysteine immobilization

Prior to the experimental design, a rapid evaluation of the influence of cysteine concentration and immersion time in the cysteine containing bath has been realized in order to adjust the limits of each parameter.

First, the influence of cysteine concentration was evaluated with an immersion time fixed at 24 hours. Four cysteine concentrations were tested: 0.075 mol/L, 0.15 mol/L, 0.30 mol/L and 0.45 mol/L and the grafting rates respectively obtained were 1.5 wt.-%, 2.7 wt.-%, 3.0 wt.-% and 3.3 wt.-%. The grafting rate seems to increase when the initial cysteine concentration increases.

Then, the influence of the immersion time was evaluated with a cysteine concentration fixed at 0.15 mol/L. Three immersion times were tested: 4 h, 24 h, and 72 h. The following grafting rates were respectively obtained: 0.5 wt.-%, 2.7 wt.-%, and 8.3 wt.-%. It was observed that for 72 h of immersion, a cysteine homopolymerisation phenomenon occured.

As a consequence, the maximum immersion time used in the experimental design was chosen around 35 h.

As the preliminary studies showed the influence of cysteine concentration and immersion time on the grafting rate, an experimental design was set up in order to improve cysteine immobilization on PP-g-AA. All PP samples were first grafted with acrylic acid using the protocol described in section II.2, and were then chemically activated thanks to EDC (1 g of EDC in 100 mL distilled water, for 1 h at 4°C). Table 8 details the experimental conditions applied to the 10 experiments and also the experimental results obtained for the response.

Table 8: Central Composite Design (CCD) in coded values with the corresponding experimental grafting rate

Experiments	X1	X2	U1	U2	Cysteine grafting rate (Y (wt.-%))
1	+1	+1	0.30	32	2.1 ± 0.8
2	+1	-1	0.30	16	1.9 ± 0.4
3	-1	+1	0.15	32	2.1 ± 0.9
4	-1	-1	0.15	16	0.9 ± 0.3
5	-α	0	0.12	24	1.1 ± 0.7
6	+α	0	0.33	24	3.8 ± 0.9
7	0	-α	0.225	12.66	1.6 ± 0.8
8	0	+α	0.225	35.33	3 ± 1
9	0	0	0.225	24	2.9 ± 0.9
10	0	0	0.225	24	3.2 ± 0.4

The determination coefficients obtained for the response show that the regression model fits the experimental data correctly. In fact, R^2 value is 98%, indicating that 2% of the total variation is not explained by the model. The value of the adjusted determination coefficient is also high ($R^2_{Adjusted}$ = 94.6%), showing a high significance of the model. The grafting is also well predicted by the model as the coefficient of prediction Q^2 is 77%.

The second-order polynomial equation associated to the response is:

$$y = 3.05 + 0.2202\ X_1 + 0.4225\ X_2 - 0.25\ X_1X_2 - 0.8617\ X_1^2 - 0.3962\ X_2^2 \qquad \text{Eq. (3)}$$

This model allows plotting the evolution of the predicted grafting rate as a function of cysteine concentration and immersion time (figure 26). Thus, the sample must be immersed in a solution containing 0.229 mol/L of cysteine for 28 hours to reach the best grafting rate, namely 3.16 wt.-%. A new experiment was realized using the optimal conditions determined thanks to the experimental design. An experimental grafting rate of 3.2 ± 0.5 wt.-% close to the predicted one was obtained, thus validating the experimental design procedure. This grafting rate corresponds to 0.033 mmol of cysteine grafted onto PP-g-AA.

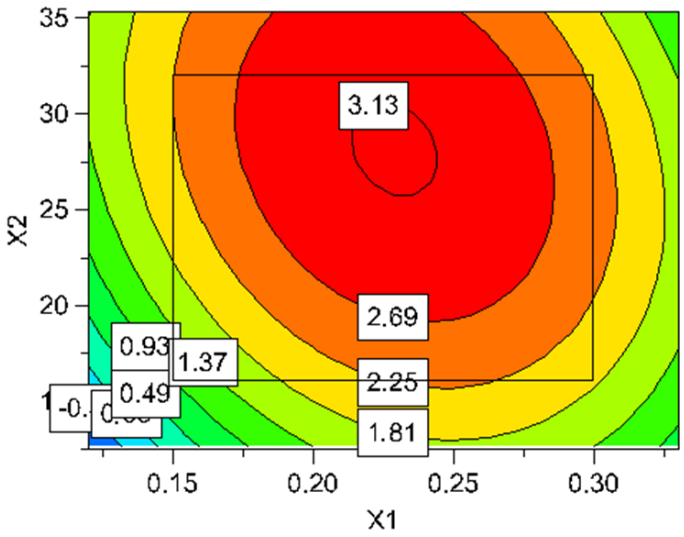

Figure 26: Contour plot showing the evolution of the cysteine grafting a function of cysteine concentration (X1) and immersion time (X2)

III.2.3. Tyrosine immobilization

The same protocol was used to optimize the tyrosine grafting. However, as the optimal protocol developed for the cysteine immobilization is too long to be transferred at industrial scale, it is necessary to speed up the functionalization process. That is why, in addition to the previously studied experimental parameters, i.e. the biomolecule concentration and the immersion time, the influence of temperature on the tyrosine immobilization was also evaluated.

First, PP-g-AA samples were immersed for 1 h at 4°C in a solution containing EDC (1g in 100 mL distilled water). Then, samples were immersed in the solution containing tyrosine. In order to evaluate the influence of temperature, the experimental conditions were kept constant: 0.110 ± 0.007 mol/L tyrosine in 100 mL distilled water, pH was adjusted at 9.5 using a 1 mol/L NaOH solution, and the samples were immersed in this solution for 24 h. Two temperatures were tested, namely 20°C and 50°C, and the grafting rate was shown to depend on the temperature: at 50°C, 4.9 ± 1.2 wt.-% tyrosine were grafted instead of 2.2 ± 0.4 wt.-% at 20°C.

In order to evaluate the influence of the immersion time on the tyrosine grafting, the tyrosine concentration, the pH and the temperature were kept constant (0.110 ± 0.007 mol/L, pH 9.5 and 50°C respectively) and different immersion times were tested: 1 h, 4 h, 8 h, and 24 h. The grafting rate was observed to vary as a function of the immersion time: respectively 2.4 ± 0.2 wt.-%, 3.6 ± 0.4 wt.-%, 6.2 ± 1.3 wt.-%, 4.9 ± 1.2 wt.-% of tyrosine were grafted onto PP-g-AA fibers. Taking into account the important standard deviation obtained for the experiments with 8 h and 24 h of immersion, the results can be considered as comparable. Thus, the experiments give more relevant results for smaller immersion times. Moreover, a compromise has to be found between the tyrosine grafting rate and the immersion time if an application of the process at industrial scale is considered. Thus, an immersion time of 1 h was chosen as it gave an acceptable grafting rate.

Finally, the influence of the tyrosine concentration was evaluated using two different solutions: one at 0.055 mol/L and the other one at 0.110 mol/L of tyrosine. The pH of the 100 mL-solution was adjusted at 9.5 with 1 mol/L NaOH solution, and the immersion was carried out for 1 h at 50°C. Obtained results were quite similar as the amount of dissolved tyrosine is the same: 2.8 ± 0.2 wt.-% and 2.4 ± 0.6 wt.-% for initial tyrosine concentrations of 0.055 mol/L and 0.110 mol/L respectively.

As a conclusion, the selected protocol was the following one: PP-g-AA samples were first chemically activated in an EDC containing solution at 4°C for 1 h, and then, chemically activated PP-g-AA sample were immersed in a solution containing 0.055 mol/L of tyrosine, adjusted at pH 9.5 with 1 mol/L NaOH, at 50°C and for 1 h. Finally, textiles were washed for 1 h with distilled water in an ultrasonic bath. The samples were dried under vacuum leading to the PP-g-AA-Tyrosine material. In that conditions, 0.039 mmol of tyrosine were grafted.

III.2.4. Surface characterization of PP-g-AA-cysteine and PP-g-AA-tyrosine

The grafting of acrylic acid onto PP was already described and verified in the chapter II. This section is focused on the confirmation of the covalent grafting of cysteine and tyrosine onto PP-g-AA (appendix 2). First, SEM was carried out on fibers after cysteine or tyrosine grafting.

The morphology of optimized PP-g-AA-cysteine and PP-g-AA-tyrosine samples can be observed on figure 27. The coating obtained after cysteine grafting (figure 27a) is smooth and looks like a film which regularly covers PP-g-AA. On the contrary, the coating obtained after tyrosine grafting (figure 27b) is quite regular and rough. Further analyses are necessary

in order to determine the chemical nature of these coatings: FTIR/ATR and XPS analyses are useful techniques to determine the functional groups present at the surface of the coated fibers.

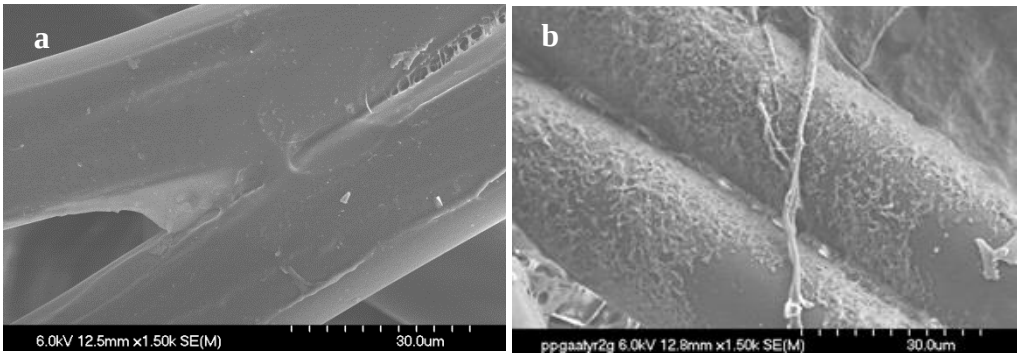

Figure 27: SEM Images of the optimized (a) PP-g-AA-cysteine and (b) PP-g-AA-tyrosine.

FTIR-ATR analyses were carried out on PP-g-AA-cysteine and PP-g-AA-tyrosine samples (figures 28 and 29 respectively). The presence of acrylic acid was evidenced by the peak of asymmetric elongation of the carboxylic group at 1715 cm^{-1} as it was already observed in chapter II. The grafting of cysteine was shown by two different peaks: scissoring deformation of the N-H of the amide group at 1566 cm^{-1} and asymmetric elongation of the carboxylic group of cysteine at 1640 cm^{-1} [118]. The presence of the peak of amide scissoring deformation evidences the grafting of cysteine on PP-g-AA: a coupling reaction between the carboxylic group of acrylic acid and the amine group of cysteine occurred.

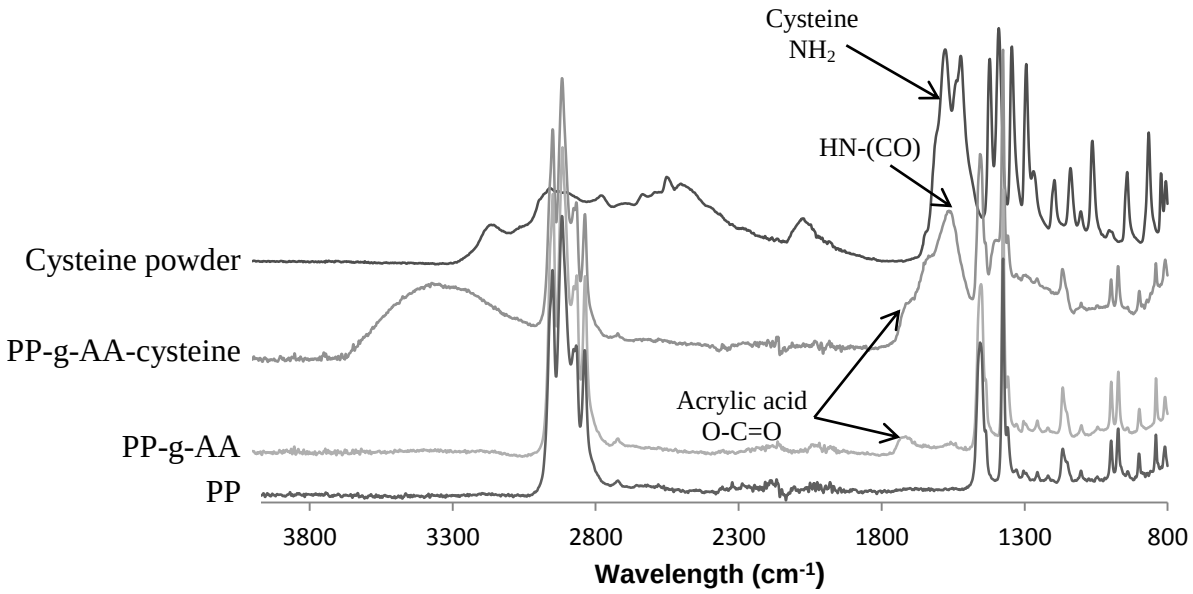

Figure 28: FTIR-ATR spectra of the virgin PP, PP-g-AA, PP-g-AA-cysteine, optimized PP-g-AA-cysteine and cysteine powder

Concerning PP-g-AA-tyrosine, the presence of acrylic acid is evidenced by the peak of asymmetric elongation of the carboxylic group at 1722 cm^{-1}. The presence of tyrosine was shown by the following peaks: elongation of the aromatic ring at 1595, 1581 and 1510 cm^{-1}; elongation of the C-O bond in the phenol group at 1329 and 1242 cm^{-1}; and elongation of the O-H bond in the phenolic group at 3192 cm^{-1}. A very small peak at 1560 cm^{-1} could correspond to the elongation of the amide group formed during the chemical coupling of acrylic acid and tyrosine, confirming the grafting, but this peak is not very pronounced.

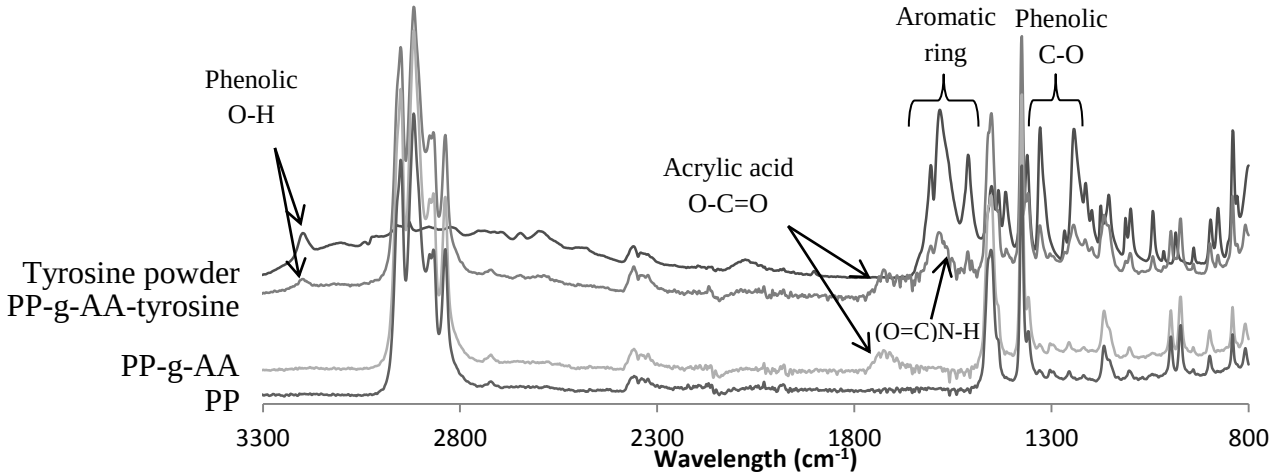

Figure 29: FTIR-ATR spectra of the virgin PP, PP-g-AA, PP-g-AA-tyrosine and tyrosine powder

Due to the uncertainty of FTIR-ATR observations, XPS analyses were carried out on cysteine and tyrosine powders, and also on optimized PP-g-AA-cysteine and PP-g-AA-tyrosine samples. Evolution of the atomic percentage of carbon, oxygen, nitrogen and sulfur is described in table 9. Evidence of the presence of tyrosine or cysteine is given by the presence of nitrogen at the surface of PP-g-AA-tyrosine and both nitrogen and sulfur at the surface of PP-g-AA-cysteine.

Table 9: Atomic quantification by XPS of cysteine powder, PP-g-AA-cysteine, tyrosine powder and PP-g-AA-tyrosine

Samples	C1s	O1s	N1s	S2p	(O1s)/(C1s)	(N1s)/(C1s)	(S2p)/(C1s)
PP-g-AA	82.1%	17.9%	0%	0%	21.8	0	0
Cysteine powder	48.3%	26.4%	14.0%	11.3%	54.7	29.0	23.4
PP-g-AA-cysteine	68.9%	25.1%	3.7%	2.3%	36.4	5.4	3.3
Tyrosine powder	70.3%	22.0%	7.7%	0%	31.3	11.0	0
PP-g-AA-tyrosine	75.2%	19.3%	5.5%	0%	25.7	7.3	0

First, the decomposition of cysteine C1s peak was necessary to identify the binding energy for each chemical group. Figure 30a shows that the C1s peak obtained for cysteine can be decomposed into 3 peaks: one peak at 285.4 eV (fwhm = 1.3), corresponding to C-S bonds; one peak at 286.2 eV (fwhm = 1.3), corresponding to C-N bonds; and another peak at 288.2 eV (fwhm = 1.3), corresponding to the O=C-O bonds. The C1s peak of PP-g-AA-cysteine (figure 30b) can be then decomposed into 4 peaks: an important peak at 285.0 eV (fwhm = 1.3) is observed, corresponding to C-C bonds. Evidence of the grafting of acrylic acid is given by the peak at 286.4 eV (fwhm = 1.3), which corresponds to the ether group formed between PP and acrylic acid, and can also correspond to the C-N bond in cysteine. Two other peaks can be observed: one at 288.3 eV (fwhm = 1.3), corresponding to the contribution of acrylic acid, polyacrylic acid and cysteine (O-C=O), and also corresponding to the amide group (N-C=O) formed during the grafting of cysteine on PP-g-AA, and the other one a peak at 285.2 eV (fwhm = 1.3), corresponding to the thiol group of cysteine (C-SH).

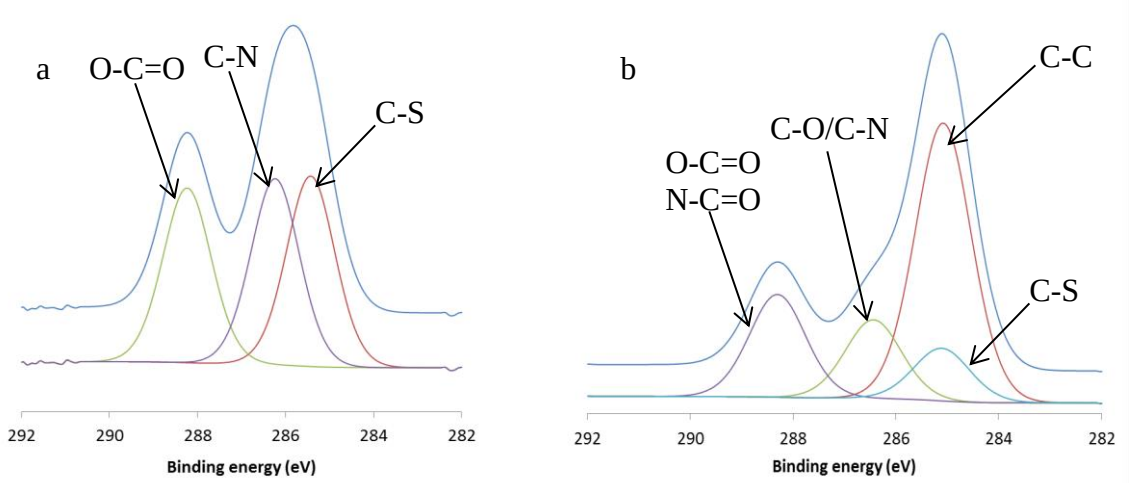

Figure 30: XPS high resolution C1s spectra of (a) cysteine powder and (b) PP-g-AA-cysteine.

In comparison, the C1s peak of tyrosine (figure 31a) can be decomposed into 5 peaks: one peak at 283.9 eV (fwhm = 1.2), for aromatic C-C bonds; one peak at 285.0 eV (fwhm = 1.2), for aliphatic C-C bonds; another peak at 285.9 eV (fwhm = 1.2), corresponding to the C-O and C-N bonds; one peak at 288.1 eV (fwhm = 1.2), corresponding to O-C=O bonds; and a smaller peak at 290.8 eV (fwhm = 1.2), for the satellite peak of C=C. Then, the C1s peak of PP-g-AA-tyrosine can be decomposed into 5 peaks (figure 31b): an important peak at 284.0 eV (fwhm = 1.1) is observed, corresponding to aromatic C-C bonds. The peak at 285.0 eV (fwhm = 1.1) corresponds to aliphatic C-C bonds. Three other peaks are observed: one peak at 285.8 eV (fwhm = 1.1), for C-O and C-N bonds from tyrosine; one peak at 287.2 eV (fwhm = 1.1), corresponding to the N-C=O bonds due to the immobilization

of tyrosine on acrylic acid; and another peak at 288.2 eV (fwhm = 1.1), for the carboxylic acid of tyrosine.

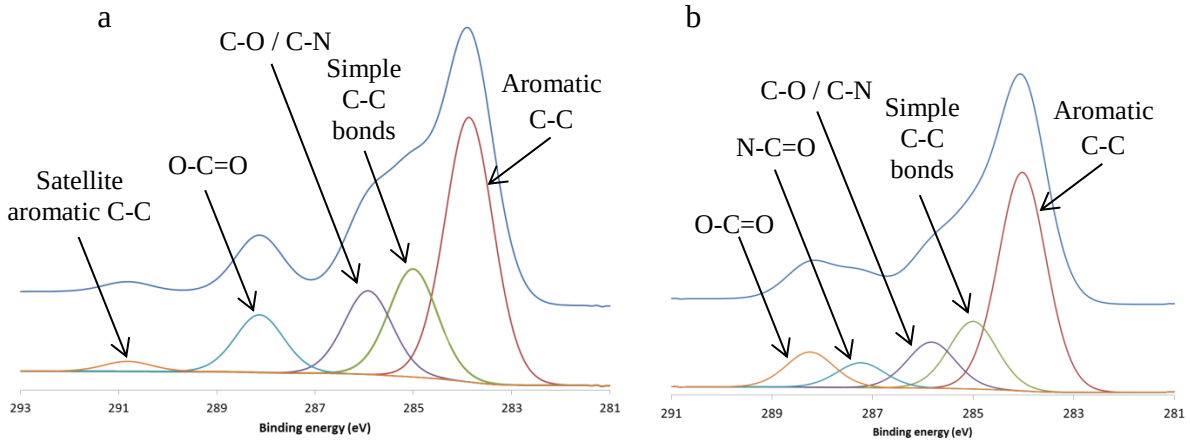

Figure 31: XPS high resolution C1s spectra of (a) tyrosine powder and (b) PP-g-AA-tyrosine.

Thus, according to FTIR and XPS results, cysteine and tyrosine are proven to be covalently grafted on PP-g-AA. The amide groups formed are due to the chemical coupling between the acid groups of acrylic/polyacrylic acid and the amine groups of the amino acid. It was thus necessary to determine the sorption efficiency of these two functionalized materials in prepared solutions containing trace metals.

III.3. Sorption efficiency of PP-g-AA-cysteine and PP-g-AA-tyrosine

III.3.1. Development of the protocol

The efficiency of the functionalized materials for the removal of copper from aqueous polluted media was then evaluated (appendix 2). First, sorption studies were carried out using solutions containing copper, which is the most abundant heavy metal in the sediments from Dunkirk. Thus, samples of virgin and functionalized fabrics were immersed in 100 mL of a solution containing copper (1000 mg/L) at pH 4.5 and 20°C for 24 h. Then, samples were washed in 50 mL of ultrapure water, in order to remove copper ions that are not really sequestered by the textile. Then, the sample was digested with sulfuric acid (purity of 95%, VWR) and hydrochloric acid (purity of 37%, VWR) in order to release the copper in a solution, diluted afterwards with ultrapure water to reach a constant volume of 100 mL. At last, this final solution was titrated using flame atomic absorption spectrometry (Thermo Solaar S4 AA Spectrometer, Thermo S Series, Multi-elements combined coded hollow-cathode lamp for Cr Cu Mn Ni, Thermo Scientific).

The influence of several experimental parameters on the adsorption process was evaluated: different initial copper concentrations (0 to 5000 mg/L), different contact times (0

to 24 hours), different pH conditions (pH 4.0 to 8.0), and different NaCl (Sodium chloride for analysis EMSURE® ACS, ISO, Reag. Ph. Eur., Merck) concentrations (0 to 30 g/L NaCl) were used to determine the experimental conditions allowing to sequester the highest amount of copper from the solution.

III.3.2. Determination of the sorption isotherm

The sorption efficiency of PP-g-AA-cysteine and PP-g-AA-tyrosine was evaluated using single metal solutions (copper, chromium or lead). Figure 32 and 33 show the evolution of the amount of trace metal ions sequestered (mmol/g PP) as a function of the equilibrium concentration of metals in the polluted solution. Functionalized textiles were observed to chelate trace metal ions increasingly with the equilibrium concentration of metals in the solution until a certain concentration where it reaches a plateau: at this moment, the textile is saturated with trace metals. In the case of PP-g-AA-cysteine, the maximum amount of metal adsorbed (Fig. 32) is 0.40 mmol Cr^{3+} /g PP, 0.66 mmol Pb^{2+}/g PP, 1.5 mmol Cu^{2+}/g PP ($CuSO_4$ solution), and 1.6 mmol Cu^{2+}/g PP ($Cu(NO_3)_2$ solution). Moreover, virgin PP did not adsorb any metal and PP-g-AA was able to adsorb 0.21 mmol Cr^{3+}/g PP, 0.23 mmol Pb^{2+}/g PP, 0.27 mmol Cu^{2+}/g PP ($CuSO_4$ solution), and 0.28 mmol Cu^{2+}/g PP ($Cu(NO_3)_2$ solution). These results show that functionalization is a strong asset to obtain an efficient material for trace metals sequestering. Moreover, the presence of cysteine (PP-g-AA-cysteine) allows obtaining a material that is 2 to 5 times more efficient than the one containing only acrylic/polyacrylic acid (PP-g-AA), depending on the trace metal.

At a concentration of 1000 mg/L, the textile is saturated with the four trace metals used (whatever the counter-ion). Two physical models have been used in order to determine the behavior of the surface: Langmuir and Freundlich isotherms. As it can be observed in figure 32, the Langmuir model fits better the experimental results than the Freundlich model. The associated correlation coefficients (R^2), presented in table 10, are in accordance with this observation. Then, as Langmuir isotherm is the most adequate model, it is possible to determine the theoretical maximum capacity of sorption q_m and the Langmuir constant b (Table 10). This constant gives information on the adsorption and desorption mechanisms of trace metals as $b=k_{ads}/k_{des}$. High values of b are obtained which means that the adsorption process is predominant over desorption. Moreover, chromium (b = 40.57 L/mmol) is much more difficult to desorb than the other trace metals tested.

Finally, because the sorption process fits well the Langmuir model, the Gibbs free energy ΔG^0 can also be calculated (Table 10). The same value is obtained for $CuSO_4$ and

$Cu(NO_3)_2$, proving that there is no influence of the counter-ion. The Gibbs free energy is more important for lead and above all for chromium: adsorption means strong interactions between the surface and the trace metals. Thus, it can be concluded that trace metals (i.e. copper (II), lead (II), and chromium (III)) sorption on PP-g-AA-cysteine is a spontaneous adsorption mechanism according to the thermodynamics of the system but that desorption is not spontaneous. To summarize, Cu(II), Pb(II) and Cr(III) adsorption on PP-g-AA-cysteine is favored energetically.

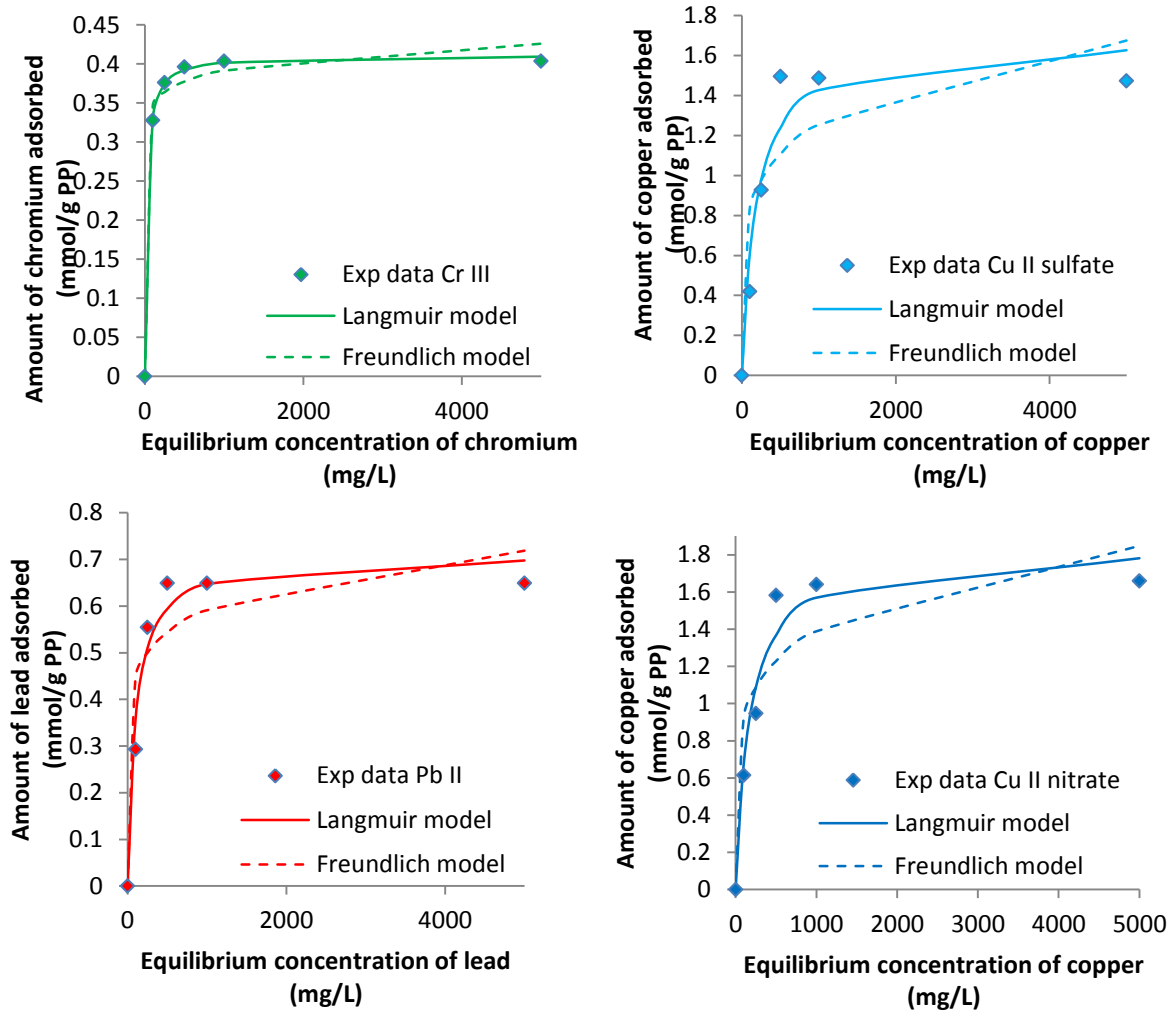

Figure 32: Amount of heavy metals trapped by the PP-g-AA-cysteine (at 20°C and pH 4.5 for 24h) as a function of the concentration in the solutions

Concerning the evolution of the amount of copper adsorbed as a function of the equilibrium concentration of trace metal, the same trend is observed for PP-g-AA-tyrosine than for PP-g-AA-cysteine. For low copper concentrations, PP-g-AA-tyrosine can chelate copper increasingly with the equilibrium concentration of $CuSO_4$. Then, from 1000 mg/L, the amount of copper adsorbed (0.75 mmol Cu^{2+}/gPP) remains stable whatever the equilibrium copper concentration (figure 33): the textile is saturated with copper.

Table 10: Data related to Langmuir isotherm in the trapping of copper, lead and chromium by PP-g-AA-cysteine at 20°C and pH 4.5

		Cu (II)	Cu (II)	Pb (II)	Cr (III)
	Counter-ion	SO_4^{2-}	NO_3^-	NO_3^-	NO_3^-
Langmuir	**R^2**	0.94	0.96	0.97	0.9995
	q_m (mg/gPP)	107 ± 6	117 ± 7	147 ± 10	21.3 ± 0.3
	q_m (mmol/gPP)	1.68 ± 0.09	1.8 ±0.1	0.71 ± 0.04	0.410 ± 0.006
	b (L/mmol)	5.51	5.71	10.07	40.57
	ΔG^0 (kJ/mol)	-12.7	-12.6	-11.2	-7.8
Freundlich	**R^2**	0.7	0.8	0.8	0.98
	K_f	22.9	25.8	52.9	14.2
	n	5.5	5.6	8.2	19.0

Some physical models can be used to describe the copper sorption on the textile surface: Langmuir, Freundlich, Redlich-Peterson, and Toth isotherms have been considered (figure 33). Except for Freundlich isotherm, these models fit well the experimental results (table 11). However, as Redlich-Peterson and Toth isotherms correspond to heterogeneous adsorption systems, they fit better the experimental results than Langmuir isotherm. According to figure 33, Toth isotherm seems slightly better than Redlich-Peterson model, especially as q_e value obtained by Toth model (0.75 mmol Cu/g PP) is closer to the experimental value (0.75 mmol Cu/g PP) than q_e value obtained by Redlich-Peterson model (0.76 mmol Cu/g PP). Thus, specific sites responsible for the sorption of copper were proven to exist at the surface of the fibers. These specific sites are not only the acidic groups of acrylic acid, but also the acidic and phenolic groups of tyrosine.

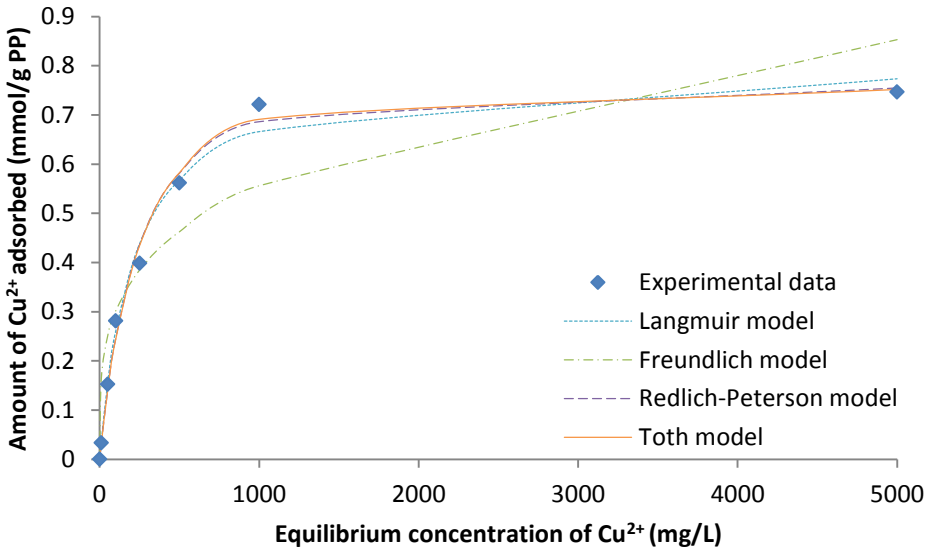

Figure 33: Amount of copper trapped by the PP-g-AA-tyrosine as a function of the equilibrium copper concentration in the artificially polluted solution (pH 4.5, 20°C)

Table 11: Obtained Parameters and R^2 value for Langmuir, Freundlich, Redlich-Peterson and Toth isotherm models

Models	Equations	Parameters	Results
Langmuir	$q=q_m*b*C/(1+b*C)$	q_m	51.21 (0.81 mmol/g PP)
		b	0.0048
		R^2	0.98
Freundlich	$q=K_f*C^{1/n}$	K_f	5.63
		n	3.76
		R^2	0.8
Redlich-Peterson	$q=K_R*C/(1+a_R*C^g)$	K_R	0.21
		a_R	0.0025
		g	1.06
		R^2	0.992
		q_e	48.0 (0.76 mmol/g PP)
Toth	$q=K_T*C/(a_T+C)^{1/\tau}$	K_T	112.15
		a_T	315.7
		τ	0.92
		R^2	0.992
		q_e	47.8 (0.75 mmol/g PP)

with q ($mg.g^{-1}$) the sorption capacity, C ($mg.L^{-1}$) the copper concentration, q_m ($mg.g^{-1}$) the maximum sorption capacity, q_e ($mg.g^{-1}$) the sorption capacity at equilibrium, b ($L.mg^{-1}$) the Langmuir isotherm constant, K_f ($mg.g^{-1}.(L.g^{-1})^n$) the Freundlich isotherm constant, K_R ($L.g^{-1}$) and a_R (mg^{-1}) the Redlich-Peterson isotherm constants, K_T ($mg.g^{-1}$) and a_T ($mg.L^{-1}$) the Toth isotherm constants, and n the adsorption intensity, g the Redlich-Peterson isotherm exponent and t another Toth isotherm constant.

III.3.3. Kinetic studies

Heavy metals are continuously adsorbed until saturation of the textile. For instance, copper is continuously adsorbed by PP-g-AA-tyrosine for 1 h, whereas it is continuously adsorbed by PP-g-AA-cysteine for 3 h. From the experimental results, it is possible to determine the kinetic law of metal ions adsorption on the grafted surface using several kinetic models [119]:

- intraparticle homogeneous solid diffusion model (HSDM) and intraparticle linear driving force (LDF) for the mass transfer modeling (MTM) where the intrinsic sorption reaction is considered to be fast ;

- pseudo-first-order (PFO) model and pseudo-second-order (PSO) model for surface reaction modeling (SRM) where the mass transfer is assumed to be fast.

Mass transfer models are not the best models to fit the experimental data as it can be observed in table 12, whereas surface reaction models are most appropriate to explain the sorption mechanism. Thus, the mass transfer step is quicker than the adsorption of copper at the surface of the textile. The copper sorption kinetics for PP-g-AA-cysteine and PP-g-AA-tyrosine can be explained using the same kinetic law: the PSO model fits very well the experimental data. Concerning the adsorption of chromium by PP-g-AA-cysteine, the PSO

model is also the most adapted. As PSO model is verified in these cases, the adsorption of metal ions onto the functionalized surface is the rate-controlling step of the mechanism, and thus, this step is the slowest [120]. Concerning the adsorption of lead by PP-g-AA-cysteine, the PFO model fits better the experimental data. Thus, the adsorption of lead is reversible: lead can be adsorbed and released from the specific sites.

As shown in table 12, copper adsorption takes place more rapidly with PP-g-AA-tyrosine than with PP-g-AA-cysteine. Moreover, within 5 s, a slight blue coloration appears, but only on PP-g-AA-tyrosine, and this coloration, due to the sequestration of copper, greatly and quickly deepens. Thus, PP-g-AA-tyrosine may also be used in trace metal ions detection.

Table 12: k and R^2 values for the Cu and Na adsorption kinetic models at 20°C

		PP-g-AA-cysteine				PP-g-AA-tyrosine	
Models	**Parameters**	**Cr^{3+}**	**Pb^{2+}**	**$Cu^{2+}(NO_3^-)$**	**$Cu^{2+}(SO_4^{2-})$**	**$Cu^{2+}(SO_4^{2-})$**	**Na^+**
PFO	**k_1**	0.066	0.059	0.087	0.086	0.145	0.078
	q_{e1}	0.37	0.67	1.62	1.46	0.69	0.55
	R^2	0.94	0.96	0.996	0.991	0.96	0.97
PSO	**k_2**	0.282	0.115	0.086	0.087	0.254	0.209
	q_{e2}	0.38	0.73	1.71	1.71	0.76	0.60
	R^2	0.98	0.92	0.995	0.995	0.996	0.97
HSDM	**q_{e3}**	0.35	0.62	1.56	1.41	0.68	0.52
	R^2	0.7	0.7	0.8	0.8	0.8	0.7
LDF	**q_{e4}**	0.35	0.67	1.62	1.46	0.69	0.57
	R^2	0.95	0.91	0.996	0.991	0.96	0.8
Exp. data	**q_e**	0.4	0.66	1.6	1.5	0.75	0.56

with t (min^{-1}) the time, q_e ($mmol.g^{-1}$) the sorption capacity at equilibrium, k_1 (min^{-1}) is the rate constant of the pseudo-first-order sorption, k_2 ($g.mmol^{-1}.min^{-1}$) is the rate constant of the pseudo-second-order sorption.

III.3.4. Influence of the pH

pH is one of the most important parameters as the sorption efficiency of the functionalized fabrics towards trace metal ions greatly depends on the pH conditions (figure 34). The first explanation is the change of the metal speciation. For instance, at 1000 mg/L of Cu^{2+}, copper starts to precipitate from pH 5.25, whereas for the same concentration, chromium and lead start to precipitate from pH 6 and pH 8 respectively. As the adsorption seems to be mainly due to electrostatic interactions, the functionalized surface will not be able to adsorb precipitated copper. The second phenomenon is the modification of the functionalized surface which can be more or less protonated, and thus, more or less anionic or cationic depending on the pH of the solution.

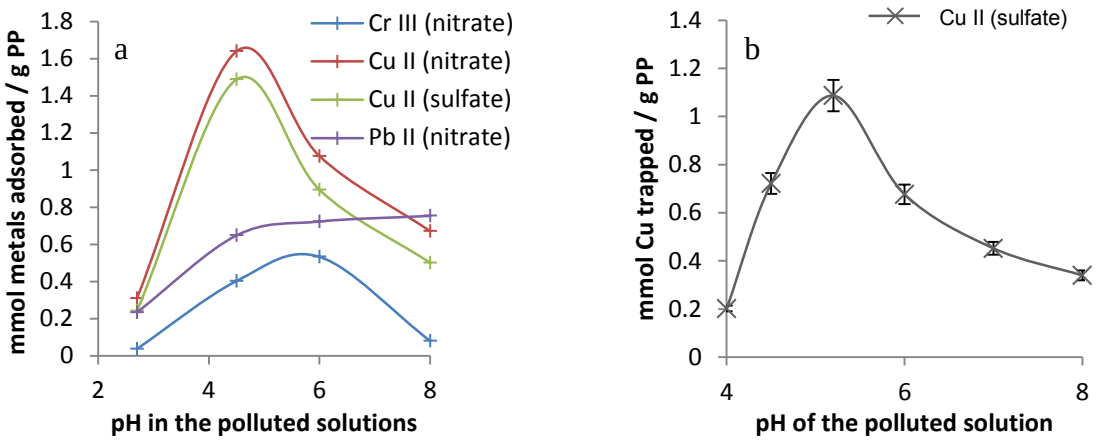

Figure 34: Amount of metals adsorbed by (a) PP-g-AA-cysteine and (b) PP-g-AA-tyrosine (at 20°C, 1000 mg/L metal, for 24h) versus the pH of the solutions

The pH value corresponding to the maximum amount of heavy metals adsorbed is located just before the beginning of the precipitation: in this study, around pH 5-5.2 for copper and around 6 for chromium. However, lead does not precipitate in the studied range of pH, and thus, a progressive increase of the sorption efficiency was observed from pH 2.7 to pH 8. In the optimized conditions, the amount of trace metals adsorbed by the grafted nonwoven is around 0.54 mmol for Cr, 1.51 mmol for Cu ($CuSO_4$) and 1.65 mmol for Cu ($Cu(NO_3)_2$) per gram of PP.

Above pH 5.2, copper precipitates into $Cu(OH)_2$, leading to a decrease of the copper concentration in the solution. Thus, as the copper ions concentration is lower, less copper ions can be adsorbed by the functionalized fabrics. Concerning chromium, various chromium forms can be observed above pH 6: $Cr_2(OH)_2^{4+}$, $Cr_3(OH)_4^{5+}$, $Cr(OH)_2^{+}$, $Cr(OH)_3$ and $Cr(OH)^{4-}$ [121]. It is assumed that chromium cannot be adsorbed if too many hydroxyl groups are present: hydrogen bonds may be created but they do not withstand the washing step and trace metals are then released.

Below pH=4.5, whatever the trace metal, the amount of protons in the solution is not negligible. Indeed, the concentration of protons is higher at lower pH, and consequently, a competition between metal ions and protons can be observed: if the pH is lower, the continuous regeneration of the surface by protons is more important, and thus, the adsorption efficiency is lower.

Moreover, as lead does not precipitate from pH 2.7 to 8, the amount of metal adsorbed by the PP-g-AA-cysteine is continuously increasing with a maximum amount of 156 mg/g PP (0.75 mmol/g PP) at pH 8. This result proves that the surface becomes more and more anionic, favoring the electronic attraction with trace metal cations. Moreover, this result is

very interesting as the usual pH values of seawater and sediments are respectively around 8.2 and 7.8.

III.3.5. Influence of the ionic strength

Presence of sodium in wastewater can have a non-negligible impact on the sorption efficiency of the functionalized material. Generally, studies show that the higher is the NaCl concentration, the lower is the amount of complexed trace metals [122-124]. This trend is observed in the case of PP-g-AA-cysteine (figure 35a): adsorption capacity of metal ions decreases quite linearly as a function of the NaCl concentration. Indeed, chromium adsorption decreases from 0.40 mmol/g to 0.12 mmol/g of PP, i.e. a reduction of 71%; lead adsorption decreases from 0.65 mmol/g to 0.36 mmol/g of PP, i.e. a reduction of 45%; and copper adsorption decreases from 1.5 to 0.74 mmol/g of PP and from 1.6 to 0.83 mmol/g of PP for $CuSO_4$ and $Cu(NO_3)_2$ solutions respectively, i.e. a reduction of 50%. Thus, in presence of NaCl, the grafted textile is twice less efficient to decontaminate copper, and 3.5 times less efficient to decontaminate chromium. This phenomenon evidences the electrostatic interactions between the anionic surface and the metal cations during adsorption, and can be explained by a competition between sodium and the metal ions at the textile surface [125].

Contrary to PP-g-AA-cysteine, the sorption capacity of PP-g-AA-tyrosine is surprisingly not affected by the presence of NaCl (figure 35b). Some hypotheses were made to explain this phenomenon: first, the complexation of the aromatic ring with sodium is considered unlikely according to the HSAB theory, whereas it is favored in the case of copper. Then, as some carboxylic acid groups are present at the surface of the fibers, the interaction between these functional groups and sodium is possible. Thus, complementary experiments were carried out, consisting in the sorption of sodium by the functionalized materials in the absence of trace metals. The evolution of the amount of sodium retained on PP-g-AA-tyrosine was determined as a function of the immersion time: two MT models and two SR models were considered, and the SRM fit better the experimental data than the MTM. Moreover, the same value of R^2 was observed for PFO and PSO models (table 12). However, the equilibrium sorption capacity was better fitting the experimental results using the PFO model (q_e = 0.55 mmol Na/g PP whereas for PSO q_e = 0.60 mmol Na/g PP, and experimentally, q_e = 0.56 mmol Na/g PP), and the PFO curve fits better the trend of sodium sorption. As observed in figure 36, the tyrosine-grafted textile favors the sorption of copper compared to sodium when it is immersed in a 1000 mg/L copper solution in presence of 30 g/L NaCl. Thus, when copper and sodium are simultaneously present in the solution, there

is a competition between them to be adsorbed at the surface of the functionalized sample: copper is adsorbed faster than sodium, and when sodium is near the specific sites, these ones are already occupied by copper.

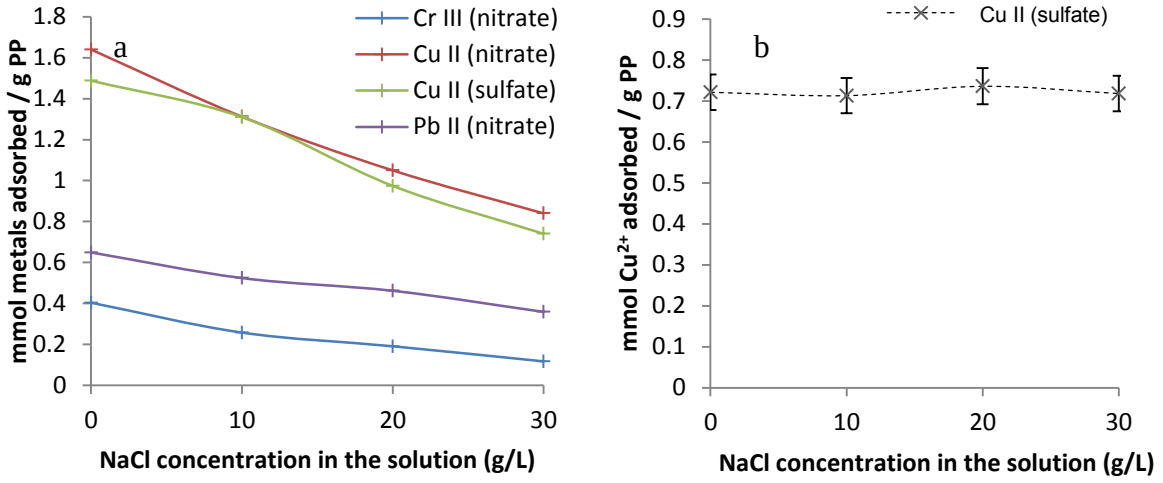

Figure 35: Amount of metals adsorbed by (a) PP-g-AA-cysteine and (b) PP-g-AA-tyrosine (at 20°C, 1000 mg/L for 24h) as a function of the NaCl concentration in the solutions

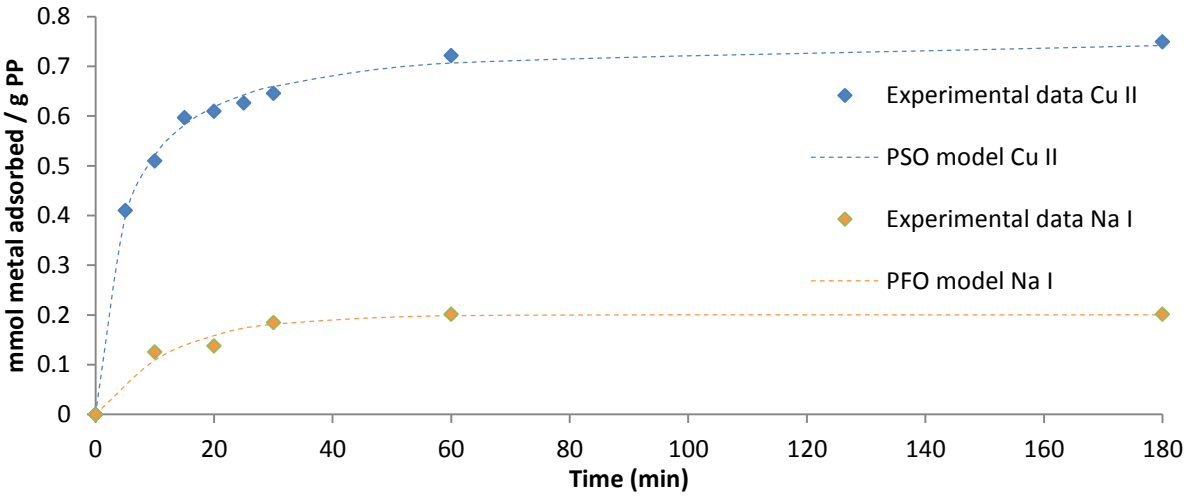

Figure 36: Comparison between the amount of copper and sodium trapped by PP-g-AA-tyrosine as a function of time in a 30 g/L NaCl solution (pH 4.5, 20°C)

III.3.6. Influence of the presence of other metals

The sorption efficiency of PP-g-AA-cysteine was determined for three metal ions in single metal solutions, i.e. chromium, copper and lead. However, as sediments leachate contain various heavy metals, the sorption behavior of the PP-g-AA-cysteine in contact with a solution containing a mixture of trace metals is necessary. Indeed, there is a competition between copper, chromium and lead due to the limited adsorption sites number, and also to

the size and the speciation of the trace metals. Thus, sorption kinetics, pH and ionic strength have an impact on the amount of trace metals adsorbed, and this effect is more pronounced for a mixture of metals. Figure 37 shows that in a solution containing a mixture of trace metals, the amount of ions adsorbed at the surface of the sample for each trace metal is inferior to the amount trapped with the solution containing only the considered trace metal. A maximum of copper can be sequestered at pH 4.5 (0.52 mmol of Cu per gram of PP in the solution without sodium), and a maximum of chromium is adsorbed at pH 6.0 (0.25 mmol of Cr per gram of PP in the solution without sodium). At higher pH, the chromium concentration on PP-g-AA-cysteine is too low to be detected by the atomic absorption spectrometer.

Copper and chromium precipitate at high pH (higher than 5 and 6 respectively). Thus, the concentration of these metal ions in the solution decreases when the pH increases. Then, less copper and chromium can be sequestered by the functionalized textile and thus more and more free sites at the surface of the PP-g-AA-cysteine can adsorb lead. A maximum sorption capacity is observed at pH 8.0, with 0.3 mmol of Pb per gram of PP without sodium, which is much less important than the results obtained for the sorption of lead in a single metal containing solution.

Presence of sodium decreases the sorption efficiency of the PP-g-AA-cysteine toward copper and lead whereas the amounts of chromium adsorbed at pH 4.5 and 6.0 are quite equivalent whatever the sodium concentration. In the case of a mixture of metals, chromium adsorption is not affected by the presence of sodium, but is much more affected by the presence of other metals such as copper and lead. Concerning lead and copper, presence of sodium has an important effect on the sorption capacity: at pH 4.5, only 0.20 mmol of Cu^{2+}/g of PP is adsorbed instead of 0.52 mmol of Cu^{2+}/g of PP without sodium. Moreover, as all the metals are under cationic form, the small amount of lead adsorbed at pH 4.5 can be explained by the fact that the sorption of lead is reversible due to the kinetic model obtained in the case of lead.

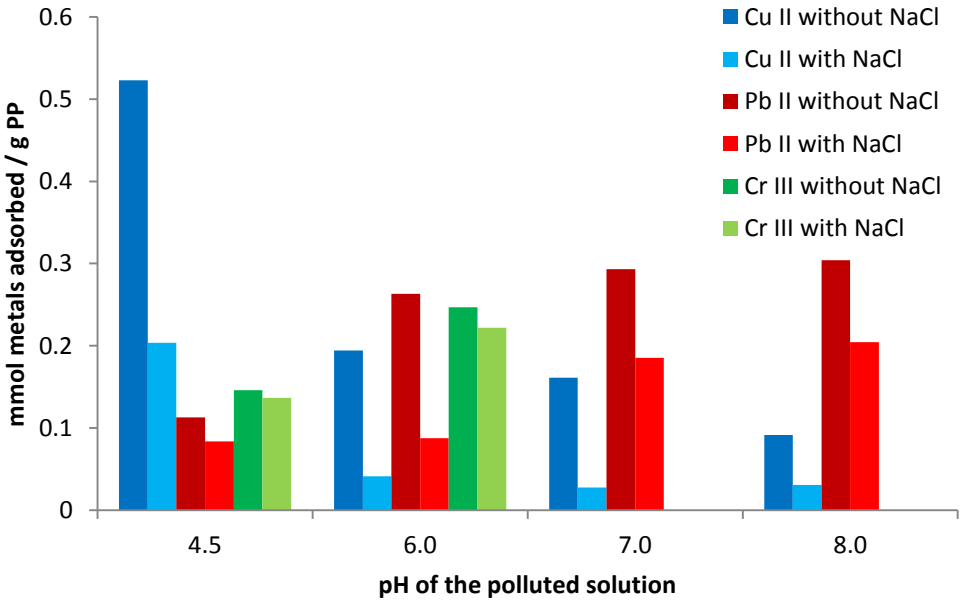

Figure 37: Amount of heavy metals adsorbed (mmol/g PP) by PP-g-AA-cysteine in the solution containing a mixture of heavy metals with and without NaCl

III.3.7. Tests on Dunkirk sediments leachate

According to the results obtained previously, PP-g-AA-tyrosine was selected for the investigation on Dunkirk sediments leachate (from the 6th inner harbor basin). Even if the adsorption efficiency towards copper of the PP-g-AA-tyrosine is inferior to that of PP-g-AA-cysteine (for a 1000 mg/L copper concentration at pH 4.5 and 20°C for 24 h), PP-g-AA-tyrosine presents some important advantages: the sorption kinetics is faster; and this material is more adapted to marine sediments as it adsorbs preferentially copper even if sodium is present in the medium.

In this study, the sediment leachate did not contain a sufficient amount of trace metals. Consequently, the leachate was doped with copper, lead, zinc, cadmium and chromium. Then, in order to remove trace metals from the doped leachate, the selected protocol was the following one: (i) the leachate was first filtrated with a syringe filter at 0.45 µm cellulose acetate with a diameter of 25 mm; (ii) one functionalized sample was then immersed in 100 mL of the filtrated leachate at 20°C for 2 h; (iii) the sample was removed from the solution; and finally, (iv) the solution was analyzed using inductively-coupled plasma with optical emission spectrometry (ICP-OES) in order to determine the trace metal concentration. To assess the efficiency of the functionalized textile, the filtrated leachate was first analyzed in order to know the trace metal concentration before carrying the adsorption experiments.

Concerning cadmium and lead, PP-g-AA-tyrosine gives interesting results (figure 38). Indeed, in the leachate there was about 15 µmol of Cd/kg and 47 µmol of Pb/kg. The virgin

PP does not take away a lot of trace metal: the leachate contains 14.9 ± 0.2 µmol Cd/kg and 46.0 ± 0.4 µmol Pb/kg. Finally, after the treatment of the leachate with PP-g-AA-tyrosine, the leachate contains 12.1 ± 0.1 µmol Cd/kg and 40 ± 1 µmol Pb/kg corresponding to a decrease of the amount of trace metals in the doped leachate of 19% and 15% for cadmium and lead respectively.

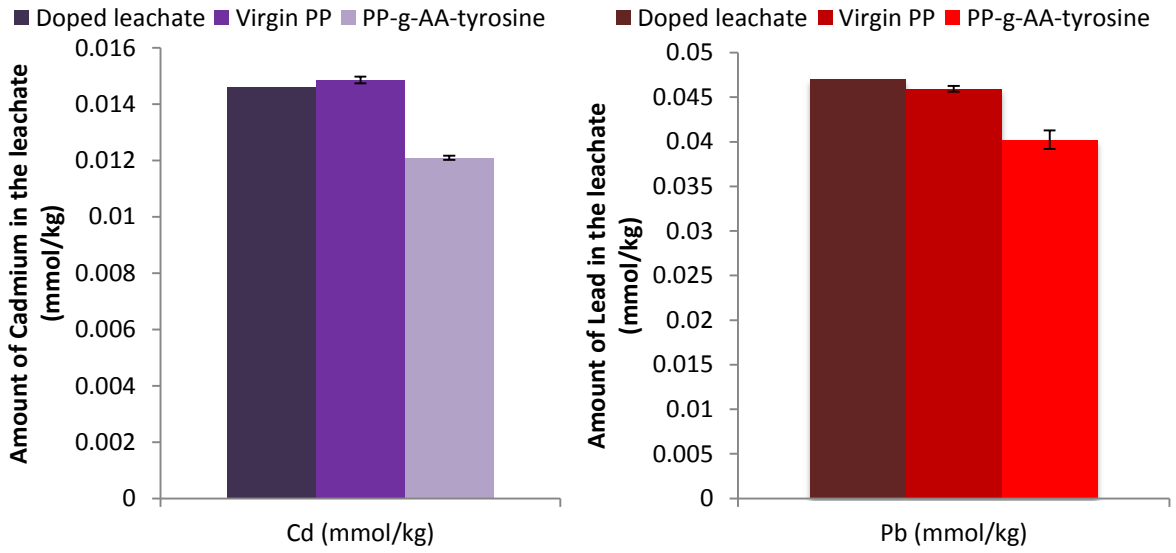

Figure 38: Amount of cadmium and lead present in the filtrated doped leachate, in the filtrated doped leachate after a treatment with virgin PP, and in the filtrated doped leachate after the treatment with PP-g-AA-tyrosine.

Concerning the amount of copper removed from the solution, the results seem promising, but the uncertainty is important (figure 39). Indeed, at the beginning, there was 155 µmol of Cu/kg, and after virgin PP treatment, only 146 ± 1 µmol of Cu/kg remained in the solution (thus, ~6% of the total amount of copper was removed from the doped leachate). Thus, about 10 µmol Cu/kg seem being taken away by the virgin PP. Moreover, after PP-g-AA-tyrosine treatment, only 143 ± 4 µmol of Cu/kg are still present in the solution (and consequently, ~8% of the total amount of copper was adsorbed by the tyrosine-functionalized-material). The amount of copper is decreasing in the leachate as a function of the treatment. However, as the uncertainty is quite important, it is not possible to conclude on the efficiency of PP-g-AA-tyrosine toward copper.

Finally, results concerning chromium and zinc are not relevant and cannot be used to explain the efficiency of the functionalized material. Indeed, in the doped leachate 3 µmol Cr/kg and 390 µmol Zn/kg. After immersion and removing of virgin PP, there were only 1 µmol Cr/kg and 310 ± 20 µmol Zn/kg were present. The immersion of the PP-g-AA-tyrosine does not change a lot the amount of chromium and zinc removed from the leachate,

as still 1 µmol Cr/kg and 327 ± 3 µmol Zn/kg were retrieved. Thus, it is not possible to conclude on the efficiency of PP-g-AA-tyrosine toward chromium and zinc in this case.

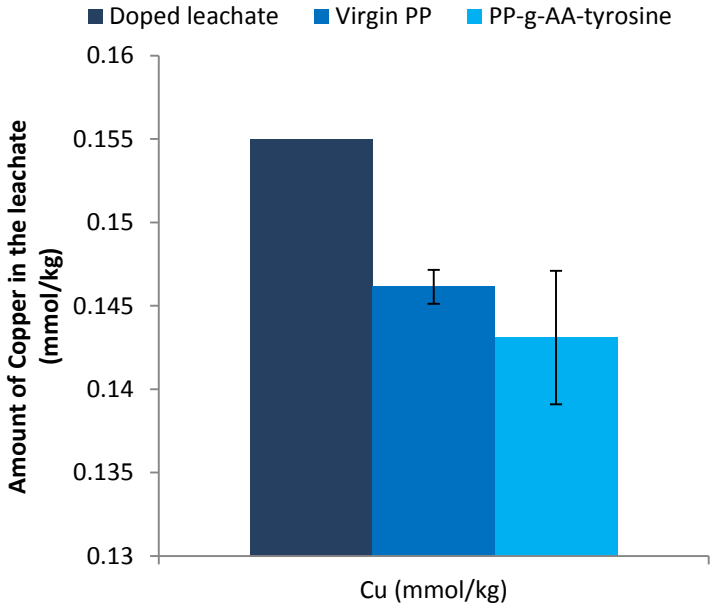

Figure 39: Amount of copper present in the filtrated doped leachate, in the filtrated doped leachate after a treatment with virgin PP, and in the filtrated doped leachate after the treatment with PP-g-AA-tyrosine.

III.4. Conclusion

In this chapter, the optimization of the cysteine/tyrosine immobilization step was carried out. Evidence of a covalent grafting of cysteine and tyrosine was given using some analytical techniques: SEM, FTIR/ATR and XPS. Then, the sorption efficiency of these two materials was evaluated. The use of amino acids gives promising results as the maximum sorption capacities are about 1.6 mmol Cu^{2+}/g PP and 0.76 mmol Cu^{2+}/g PP for PP-g-AA-cysteine and PP-g-AA-tyrosine respectively, instead of 0.49 mmol Cu^{2+}/g PP for chitosan. The sorption kinetics show that PP-g-AA-tyrosine adsorbs copper faster than PP-g-AA-cysteine: PP-g-AA-tyrosine is saturated after 1 h instead of 3 h for PP-g-AA-cysteine. Moreover, the blue coloration due to the adsorption of copper at the surface of the textile can be observed after 5s contact time between the copper solution (from 50 mg/L) and PP-g-AA-tyrosine. The influence of pH is mainly explained by the metal speciation as the functionalized textiles can adsorb trace metals under cationic form. The ionic strength effect was used to select the functionalized material for further studies at industrial scale. Indeed, presence of NaCl strongly decreases the copper sorption efficiency of PP-g-AA-cysteine whereas it does not have any effect on the copper sorption efficiency of PP-g-AA-tyrosine. Then, some studies were carried out using PP-g-AA-tyrosine to treat doped leachate from

Dunkirk harbor sediments. As the initial concentration in metal ions is too low, the total amount of metal adsorbed seems less important. This result can be explained by: (i) the kinetics, as the amount of metal in the solution is lower, the transfer or diffusion to the fiber surface is probably slower and thus two hours might not be sufficient to allow the saturation of PP-g-AA-tyrosine samples; and (ii) the equilibrium between the metal adsorbed and the metal ions in the solution: as there are less metal ions, the maximum amount of metals adsorbed can be lower than the amount adsorbed in highly concentrated solutions.

The surface cheracterizations of the functionalized materials and particularly the XPS analyses allowed determining the different types of bindings at the surface of the fibers. Thus, it can be possible to simulate the fibers in order to better understand the copper/amino acids complexes formed during the adsorption step. The next chapter describes the calculations carried out using quantum chemistry in order to determine the copper/amino acids complexes.

Chapter IV

Sorption mechanisms and computational chemistry

IV.1. Introduction

In this chapter, the interactions occuring between the amino acid and the considered metal, copper in this part, were investigated using computational chemistry tools. Thus, theoretical calculations were carried out in order to determine the most favorable optimized structures as a function of the stabilization energy. Different levels of theory were used to optimize the geometries and to calculate the potential energies of the metal/amino acid complexes. The results presented in this part concern the copper sequestration with one amino acid: cysteine or tyrosine. This preliminary work was carried out in order to identify the potential coordination sites for copper.

To determine the optimized geometries, density functional theory method (DFT) coupled with Dunning style basis sets [126-130] was considered. Calculations considering Cu^{2+}/cysteine and Cu^{2+}/tyrosine complexes were first carried out to determine conformers using B3LYP/cc-pVDZ (correlation consistent-polarized valence double zeta, for preliminary calculations consisting in the pre-optimization of the structures in order to save time), B3LYP/cc-pVTZ (correlation consistent-polarized valence triple zeta) and B3LYP/aug-cc-pVTZ (aug for augmented). Finally, the Dual-Level methodology, consisting in using two levels of theory (in this work CCSD(T)//B3LYP level of theory), was used in order to ensure accurate stabilization energy values.

On the other hand, preliminary studies were carried out using quantum chemistry to simulate the functionalized fibers. First of all, the aim is to build the structure at the surface of the fibers thanks to information obtained with XPS analyses. All potential configurations and conformations of the surface must be taken into account. Then, it would be possible to observe the new complexes formed between the functionalized surface and copper ions.

IV.2. Theoretical calculation methods

IV.2.1. Resolution of the Schrödinger equation

Any system composed of *N* particles can be totally described by the wave function Ψ which depends on the coordinates of each particle. The wave function does not have any physical significance. However, $|\Psi|^2$ can be used to identify the probability of presence of particles in a determined volume at a precise moment. Moreover, each measurable physical variable in a system is linked to a linear mathematical operator. The Hamiltonian operator is associated with the energy *E*. Thus, the Schrödinger equation is the following one:

$$\hat{H}\,\Psi = E\,\Psi \qquad \text{Eq. (4)}$$

This equation can be solved for a one-electron system. For any molecule composed of *K* nucleus and *j* electrons, the Hamiltonian operator can be written as follows:

$$\hat{\mathrm{H}} = -\frac{1}{2}\sum_K \frac{\Delta_K}{M_K} - \frac{1}{2}\sum_j \Delta_j - \sum_j \sum_K \frac{Z_K}{r_{jK}} + \sum_i \sum_{j>i} \frac{1}{r_{ij}} + \sum_K \sum_{L>K} \frac{Z_K Z_L}{R_{KL}} \qquad \text{Eq. (5)}$$

with Z_K the atomic number of the nucleus *K*, M_K the mass of the nucleus *K*, R_{KL} the distance between the two nuclei *K* and *L*, r_{jK} the distance between the nucleus *K* and the electron *j*, and r_{ij} the distance between two electrons *i* and *j*. The Hamiltonian operator can be written more simply:

$$\hat{\mathrm{H}} = \hat{T}_N + \hat{T}_e + \hat{V}_{eN} + \hat{V}_{ee} + \hat{V}_{NN} \qquad \text{Eq. (6)}$$

With $\hat{T}_N$ he kinetic energy operator for nucleus, $\hat{T}_e$ the kinetic energy operator for electrons, $\hat{V}_{eN}$ the electron-nucleus interaction potential, $\hat{V}_{ee}$ the electron-electron interaction potential and $\hat{V}_{NN}$ the nucleus-nucleus interaction potential.

In order to solve Schrödinger equation considering a multi-electronic system, iterative resolutions with some approximations have to be carried out. The first one is the Born-Oppenheimer approximation: as the nucleus is very big compared to the electrons, the nucleus is considered fixed in space leading to $\hat{T}_N = 0$ and $\hat{V}_{NN} = E_{II}$, with E_{II} being a constant.

IV.2.2. Hartree-Fock and Post Hartree-Fock methods

The direct resolution of the Schrödinger equation is not analytically possible in the case of multi-electronic systems. Some approximations have to be carried out in order to modify the equation so as to obtain the Hartree-Fock equations.

Hartree-Fock method is in fact one of the basic methods used in quantum chemistry. This method is based on two approximations: the Born-Oppenheimer approximation and also the orbital approximation, allowing to describe the multi-electronic wave function using a Slater determinant. Generally, molecular orbitals used for the construction of the Slater determinant are developed thanks to linear combination of atomic orbitals. However, the Hartree-Fock wave function does not take into account the existing electronic correlation. Thus, the calculated stabilization energy is higher than the exact value. The difference between the exact value and the value obtained by the Hartree-Fock method is called the correlation energy.

In order to estimate the correlation energy, post Hartree-Fock methods were developed. Two methods are well-known: the Møller-Plesset method, consisting in the use of the perturbation method in the Hartree-Fock wave function; and the Coupled-Cluster, one of the "configuration interaction" methods. Hartree-Fock method is necessary to calculate the wave function, then allowing the calculations using a level of theory like CCSD(T) for instance.

IV.2.3. Density Functional Theory

DFT method is a computational quantum mechanical modeling used for the investigation of the electronic structure of atoms, molecules of condensed phases from small molecular systems (a few atoms) to higher molecular systems (about hundred atoms). The properties of multi-electron systems can be determined using functionals, which spatially depend on the electron density in the case of DFT. The use of this method in the field of quantum chemistry is developing since the beginning of the 21st century.

In 1964, P. Hohenberg and W. Kohn stated that the external potential "is a unique functional of" the electronic density in the ground state, "apart from a trivial additive constant" [131]. Thus, compared to other methods, the multi-electronic wave function is replaced by the electronic density in the ground state, reducing the quantic problem of N electrons from $3N$ to 3 spatial coordinates. The most frequently used DFT potential is the Becke 3 parameters Lee-Yang-Parr or B3LYP [132, 133].

The DFT method presents some advantages: the possibility to work with a lot of atoms in the systems; the optimized geometries allowing the energy calculations; and the faster speed of calculations compared to Møller-Plesset method. In this work, the DFT method is appropriate to simulate the interaction between copper and amino acids in the ground state.

IV.2.4 Choice of the level of theory

Many basis sets exist, and it is necessary to select the appropriate basis set. In this PhD thesis, the correlation consistent polarized basis set was used as a good yield for the total correlation energy can be obtained (from 94 to 97% for the atoms from boron to neon) [134].

The preliminary calculations were carried out using the cc-pVDZ basis set, considering one metal for one amino acid. In order to improve the results, the cc-pVTZ was used as it increases the number of considered atomic orbitals. Finally, cc-pVTZ can be augmented with diffusion functions (aug-cc-pVTZ), leading to a more significant result.

IV.3. Potential energy surface

IV.3.1. Definition of the potential energy surface

Due to the Born-Oppenheimer approximation, electrons are considered to immediately adjust to the position change of each nuclei. Moreover, the potential energy surface of a molecule can be considered as a function depending only on the nuclear coordinate for a known electronic state (because the electron weight is less important than the nuclei weight ($m_{electrons}/m_{nuclei}$ = 1/1800)). For each nuclear position, a potential energy (electronic energy + nuclear repulsion energy) of the molecule exists, which is also called representative point. All the representative points, for a known electronic state, are also called the potential energy surface.

Considering a system with *N* atoms, the molecular system is defined with 3*N* cartesian coordinates. Some modifications of these coordinates can lead to the same energy of the energy surface. When all the atoms move in the same direction or when they turn around the same axis, no change concerning the potential energy is observed. Thus, the potential energy surface is represented with (3*N*-6) degrees of freedom and (3*N*-5) degrees of freedom in the case of non-linear and linear systems, respectively.

The calculations of all the representative points of the potential energy surface, considering a system containing a large number of degrees of freedom, is not currently possible due to the limited power of computers (processor output, storage capacity of the hard drive). Fortunately, in most cases, only few representative points have a "chemical" meaning, and thus, only these points have to be determined.

Exploring of the potential energy surface gives information on the molecular structure, as well as on the reactivity of different molecules.

IV.3.2. Stationary points on the potential energy surface

On the potential energy surface, some representative points are particular as they have a first derivative (the gradient (*g*)) of the potential energy (*E*) as a function of the degrees of freedom (*x*) of the molecular system equal to zero.

$$g(x) = \partial E / \partial x = 0 \qquad \text{Eq. (7)}$$

These representative points are called "stationary points". In order to find the chemical meaning of these points, the second derivative (the Hessian (*H*)) of the potential energy (*E*) is required.

$$H(x,y) = \partial^2 E / \partial x \partial y \qquad \text{Eq. (8)}$$

After the diagonalization of the Hessian matrix, the eigenvalue of the system can be determined. The number of negative eigenvalues allows identifying the chemical meaning of the stationary point:

- if there is not any negative eigenvalue: the stationary point is a minimum on the potential energy surface, corresponding to a reactant, a final product, a complex or a reaction intermediate.
- if there is one negative eigenvalue: the stationary point is a first order saddle point corresponding to the transition state. This point joins two minima on the potential energy surface and is really important for studying the reactivity of the involved molecules.
- if there are more than one negative eigenvalues: the stationary point is a superior order saddle point (these points do not have any chemical signification).

IV.3.3. Calculation of the vibration frequencies

The calculation of the vibration frequencies (ν_i) can be carried out with the harmonic approximation, and uses the eigenvalues of the Hessian matrix. At 0K, the atoms of a molecule do not remain completely static because they oscillate around the lowest oscillation level. The calculation of the vibration frequencies give the value of this point, also named the zero-point-energy, or *ZPE*.

$$ZPE = \tfrac{1}{2} \sum_i^{normal\ vibration\ modes} h\nu_i \qquad \text{Eq. (9)}$$

IV.4. Dual-level methodology

The Gaussian09 software was used to carry out the calculations. It was observed that the calculation results depend strongly on the level of calculation. As the Dual-Level methodology reduces the dependence to the calculation level by considering two levels of theory, this methodology is commonly used to estimate the relative stability of chemical compounds. One of the most well-known Dual-Level methodology used in quantum chemistry is the coupling between B3LYP for the DFT method and CCSD(T) for the coupled cluster method [135, 136]: first, the optimized geometries on the potential energy surface were obtained using DFT level of theory, and then, the optimized geometry parameters were used in order to calculate the CCSD(T) potential energies.

In this work, B3LYP and CCSD(T) coupled with different basis sets were used in order to determine the optimized geometry and the potential energies of copper/amino acid complexes.

IV.5. Theoretical study of amino acid/metal complexes

IV.5.1. Computational methods

Ab initio and DFT calculations were performed using the Gaussian09 software. Metal/amino acid complexes were optimized with the hybrid density functional theory (B3LYP) using the following Dunning style basis sets: cc-pVDZ, cc-pVTZ and aug-cc-pVTZ.

First, amino acids were considered in gas phase in order to find the optimized geometries without taking into account the presence of a solvent. Then, when the optimized geometry was obtained, it was possible to calculate the new optimized geometry considering amino acids in water. The polarizable continuum model (PCM) [137, 138] has been used to simulate the water solvent. Finally, copper cation can be added in order to observe the interaction between amino acids and the trace metal in aqueous solution.

Thanks to the calculation, it is possible to calculate the potential energy (*U*p, kJ/mol) of the molecule, and also the residual vibrational energy (*ZPE*, kJ/mol) at 0K. For each stationary point, the enthalpy at 0K (H_{0K}, kJ/mol) can be calculated using the following equation:

$$H_{0K,\ biomolecule} = U_{p\ biomolecule} + ZPE_{biomolecule} \qquad \text{Eq. (10)}$$

In order to find the most stable copper/amino acid complex, the stabilization energy has to be calculated for each conformer, according to the following equation:

$$\Delta E_{stabilisation} = H_{0K,\ complex} - H_{0K,\ Cu} - H_{0K,\ biomolecule} \qquad \text{Eq. (11)}$$

Finally, the geometric parameters optimized at the B3LYP/aug-cc-pVTZ level of theory have been used to calculate the potential energies at the CCSD(T)/aug-cc-pVTZ level of theory (Dual-level methodology).

All these calculations were carried out *via* the *centre de ressources informatiques* of the Lille1 University (CRI-Lille1).

IV.5.2. Results and discussion

First of all, it was necessary to find the more stable conformation for each amino acid. Then, the amino acid and the divalent copper were brought together. The different structures obtained can be compared thanks to the value of the enthalpy at 0K. Cysteine is the first amino acid considered in this study. Two conformational structures, optimized considering water as solvent, have been found on the potential energy surface and have been reported in Figure 40. According to the calculated potential energies for both structures, Cys-I structure

is sligthly stable than Cys-II structure due to the enthalpy at 0K, i. e. -719,4477796 ha and -719,4470288 ha (hartree) for Cys-I and Cys-II respectively, leading to a difference of 1.97 kJ/mol between these two conformers.

Cys-I Cys-II

Figure 40: Conformational structures proposed for cysteine in water using the CCSD(T)/aug-cc-pVTZ//B3LYP/aug-cc-pVTZ level of theory

Then, as there are three different binding sites in cysteine, i. e. amine, carboxylic acid and thiol groups, various conformational structures have to be considered. Moreover, Shimazaki reported that cysteine can be efficient to interact with copper at different pH conditions, because of the presence of these three functional groups [89]. Indeed, compared to other amino acids that can chelate metals by N,O-chelation, cysteine can also chelate metals by other types of chelation: according to Palackova studies, between pH = 2 and pH = 4.5, an oxygen-sulfur chelation (O,S-chelation) is mainly observed whereas between pH = 6 and pH = 9 a nitrogen-sulfur chelation (N,S-chelation) is predominant [139]. Thus, these three possibilities were considered for the calculations, and also the tridentate chelate consisting in N,O,S-chelation. The following diagram (figure 41) was thus obtained.

According to figure 41, the most stable structures is the N,O,S-chelate, and then, the N,S-chelate. The N,O-chelate and the O,S-chelate seem having less stable structures. However, these results have to be taken with caution because amino acids are normally under zwitterionic forms. Considering the N,S-chelate from figure 41, the nitrogen possesses a free lone pair as for the nitrogen of cysteine in basic medium. Thus, the result obtained in this case is in accordance with Palackova observations [139]. However, in the O,S-chelate from figure 41, the carboxylate group is protonated which is possible for pH below 2, and consequently, the result obtained in that case cannot be compared to Palackova observations. Thus, these preliminary results give some tendencies concerning the sequestration of copper by cysteine, but it would be interesting for the calculations to consider the zwitterion form and then to vary the pH to be closer to real conditions.

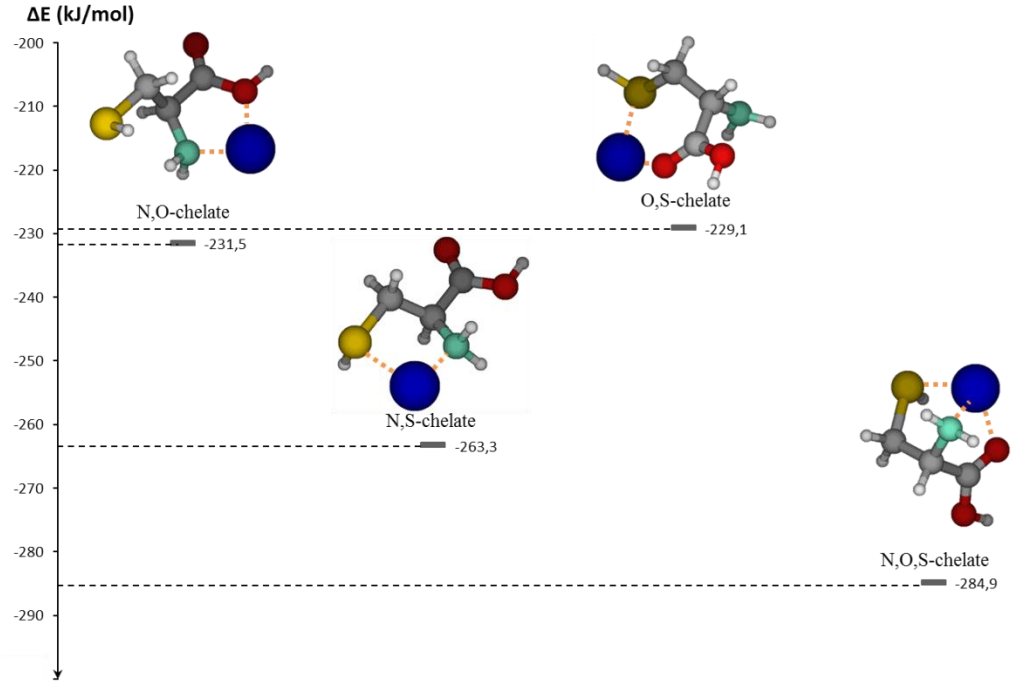

Figure 41: Comparison of the stabilization energy (kJ/mol) of the different chelates obtained by calculations using the CCSD(T)/aug-cc-pVTZ//B3LYP/aug-cc-pVTZ level of theory with the ZPE correction.

If the bond lengths between copper and heteroatoms are compared for the 4 different chelates (Table 13), it can be seen that the Cu-N bond length is the shortest for the N,O-chelate corresponding to the strongest Cu-N bond. On the contrary, the strongest Cu-O and Cu-S bond lengths are obtained in the O,S-chelate. However, these two complexes, i. e. N,O-chelate and O,S-chelate, are less stable than N,S-chelate and N,O,S-chelate. As the longest Cu-N, Cu-O and Cu-S bonds lengths are observed in the N,O,S-chelate, it can be supposed that the addition of a third heteroatom around the copper ion increases the bond lengths between the metal ion and the three heteroatoms. This result could be due to the repulsive interaction between all these heteroatoms.

Table 13: Bond lengths (in Å) between copper and heteroatoms in the different complexes obtained

	Cu-N	Cu-O	Cu-S
N,O-chelate	1.959	1.981	-
N,S-chelate	1.963	-	2.288
O,S-chelate	-	1.894	2.268
N,O,S-chelate	1.973	2.185	2.355

These results (Table 13) are similar to those described in the literature. In fact, some EXAFS studies were carried out onto Cu/amino acids complexes in order to determine the distance between copper and heteroatoms. Glycine is considered as a model for N,O-chelate

because glycine possesses only one amine and one carboxylic acid groups. It was observed that in the Cu/glycine complex, the Cu-N and Cu-O bonds are respectively 2.000 Å long and 1.955 Å long [101], which is in good agreement with the results obtained by computational chemistry. However, from our calculations, the Cu-O bond length is longer than the Cu-N bond length for the N,O-chelate whereas Carrera [101] observed the opposite trend. Moreover, a ranking was established for the bonds between metal and heteroatoms: Metal-O < Metal-N < Metal-S [55] and our results are not in accordance this ranking. This observation can be explained by the fact that in the N,O-chelate considered in figure 41, the oxygen interacting with copper is bonded to an hydrogen atom: thus, an repulsive interaction may be expected between hygrogen and copper leading to a less stable complex. Another calculation has to be carried out with the conformer of this copper/L-cysteine complex in order to be closer to the experimental part.

Several studies were carried out on tyrosine. It was observed that tyrosine can interact with metals such as copper thanks to the carboxylic acid and amine groups, like all the other amino acids. But tyrosine can also interact with metals thanks to the phenol group either through the aromatic ring or through the oxygen atom [46, 89, 98]. However, as the aromatic ring of tyrosine is very large and cannot move, less metal/biomolecule complex conformations than in the case of cysteine can be obtained. Thus, as only one tyrosine molecule is considered for metal chelation, only two conformations are available: N,O-chelation, which is common to all amino acids, and the N,O,Ar-chelation (with Ar = aromatic ring) (figure 42). It was observed that the tridentate gives a more stable complex than the bidentate, as the potential energy was respectively -2270.54537253 and -2270.543585 ha using the B3LYP/aug-cc-pVTZ level of theory, corresponding to a difference of 4.69 kJ/mol between these two conformers. However, these results have to be improved using other basis sets.

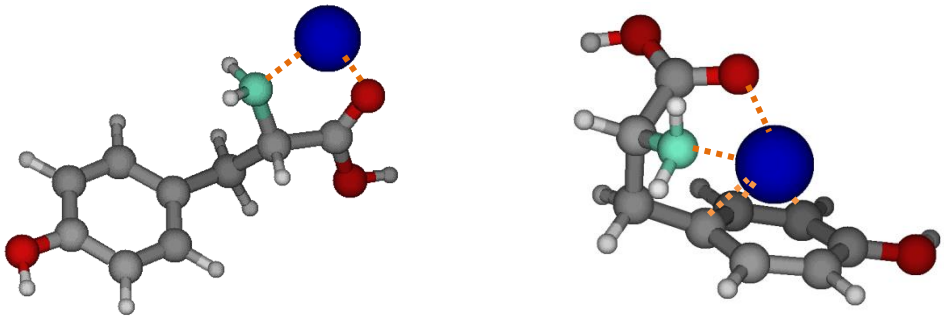

N,O-chelate N,O,Ar-chelate

Figure 42: Conformations of the N,O-chelate and the N,O,Ar-chelate obtained by calculations using the B3LYP/aug-cc-pVTZ level of theory

These results give a first idea of the most stable copper/amino acids complexes. However, they are not really representative as amino acids are: (i) under zwitterionic form, and thus, some negatively charged atoms will attract the metal cations, and (ii) immobilized onto PP-g-AA through amino groups, and thus, the amine group cannot interact as easily as that of free amino acids. Moreover, as several amino acid molecules are grafted all along the fibers, copper can be chelated by chemical groups from different amino acids and not necessarily from a single amino acid. Thus, the presence of the fiber has an influence on the sequestration of copper and on the complexes formed. Therefore, the fiber structure has to be taken into account in the calculations.

IV.6. Theoretical study including the functionalized fibers

Preliminary studies were carried out on the complexes formed between one metal and one amino acid. But, other complexes can exist at the surface of the fibers due to the close distance between the chemical groups from the different amino acids. Thus, the simulation of the functionalized fiber is needed to determine the potential complexes that can be formed with copper.

In this section, only a part of the PP-g-AA-cysteine fiber was simulated. Surface characterizations made previously (chapters 2 and 3), and mainly XPS analyses, allowed determining the most probable structure at the fiber surface (figure 43): first, the activation step leads mainly to the formation of hydroperoxide and proxide groups; then acrylic and polyacrylic acids are grafted onto these chemical groups leading to the formation of ether groups; finally, due to steric hindrance issues, the grafting of the cysteine molecules at the fiber surface will occur preferably through a chemical coupling.

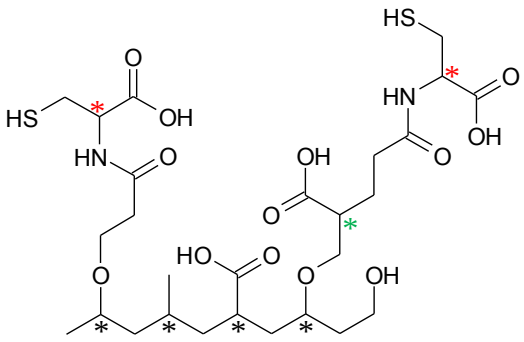

Figure 43: Potential structure of a part of functionalized fiber

It is necessary to verify that the proposed functionalized surface is in accordance with the experimental results. From Figure 43, the atomic percentages of carbon, oxygen, nitrogen and sulfur were calculated and compared to the experimental values from XPS (Table 14). In

the proposed structure, the proportion of carbon atoms is lower than on the real functionalized fibers leading to a slight overestimation of the amount of heteroatoms.

Table 14: Comparison between the atomic percentage at the surface of PP-g-AA-cysteine (XPS data) and in the proposed structure

	C1s	O1s	N1s	S2p
XPS data	68.9%	25.1%	3.7%	2.3%
Hypothetical structure	62.3%	28.9%	4.4%	4.4%

Asymmetric carbons (identified by an asterisk in figure 43) can be found all along the PP chain and also in the functionalized layer. The carbons identified by a red asterisk correspond to the asymmetric carbon of cysteine: as L-cysteine was used in this work, the configuration of this carbon is defined and cannot change. On the contrary, the carbon identified by a green asterisk is not defined before the functionalization step and corresponds to bond created during the plasma process. Two configurations are possible and have to be considered for the calculations. Moreover, many conformations also exist for this structure, and thus, many calculations are required in order to find the most stable structure.

First calculations were carried out in order to build the functionalized fiber. As there is a high number of atoms, the B3LYP level of theory was coupled with the 3-21G* Pople basis set. This optimized structure (figure 44) presents a weak bond between a carboxylic acid and an amide group leading to a more stable conformation. This part of the molecules presents a folded structure forming a cavity in which the copper ion can be sequestered, especially because of the presence of several heteroatoms.

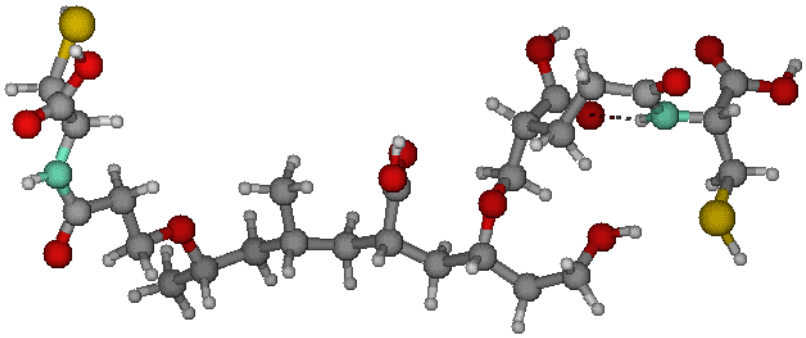

Figure 44: Hypothetical structure of a part of functionalized fiber obtained using B3LYP/3-21G*

IV.7. Conclusion

Preliminary studies were carried out in order to determine the most favored conformations for copper/cysteine and copper/tyrosine complexes. However, these results

have to be improves considering the zwitterionic form (figure 45) and setting a pH value in order to ensure consistent results compared to experimental data. Moreover, the analysis of metal/amino acid complex is not sufficient to explain the structure formed at the surface of the fibers after immersion of the functionalized fabrics into the copper solution. Thus, it is necessary to simulate the functionalized fiber in order to determine more precisely the new complexes formed.

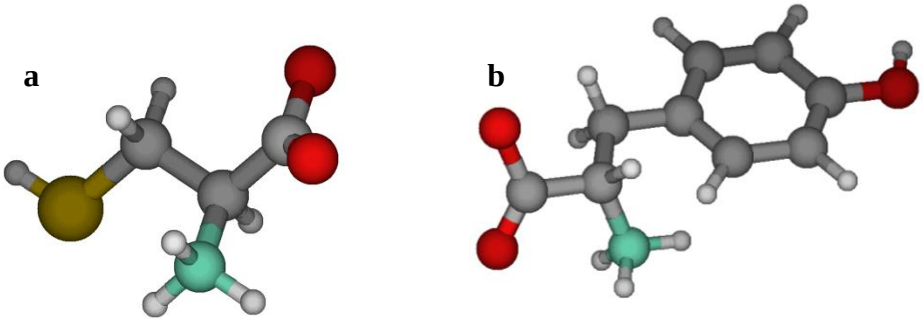

Figure 45: Zwitterionic structure of (a) cysteine and (b) tyrosine

A part of the functionalized fiber, i. e. PP-g-AA-cysteine, was built taking into account the surface characterization results (presented in chapters 2 and 3). Two main configurations can be considered, and the most stable conformation for each of these structures must be used for further calculations adding copper ions. The preliminary calculations allowed to observe that the grafting of biomolecules may lead to the formation of some cavities at the surface, in which some copper ions may be sequestered. Further investigations have to be carried out using elaborated levels of theory.

This preliminary work is helpful to understand the complexes formed between copper and amino acids, even if further calculations have to be done considering the zwitterionic form and a specific pH value. Then, the complexes formed between copper ions and the functionalized fiber will be determined and compared to the complexes formed between copper ions and amino acids. Finally, it would be interesting to explain the selectivity of the functionalized fibers (favorable adsorption of copper compared to chromium and lead) or the ionic strength effect.

General Conclusion

The treatment of polluted sediments is a serious subject and many studies have been dedicated to this issue. In this PhD thesis, geotextiles were considered due to their filtration and drainage properties. However, synthetic textiles do not have the ability to sequester heavy metals from wastewater or sediments leachate. Thus, it was necessary to graft molecules onto the synthetic fibers in order to bring a remediation property to the textiles.

Biomolecules were particularly considered as interesting complexing agents. Indeed, polysaccharides, such as cellulose, alginate or chitosan, are often used to remove trace metals from wastewater. Moreover, in the detoxification system of some cells, other biomolecules, such as polypeptides or amino acids, are known to sequester trace metals. The structure of these molecules was analyzed, and it was noticed that some chemical groups present in these biomolecules are responsible for the heavy metals sequestration. Moreover, these chemical groups contained at least one of these heteroatoms: oxygen, nitrogen or sulfur; except for the aromatic ring.

Finally, considering the HSAB theory, cysteine and tyrosine were selected as they contain respectively a thiol and a phenol group, and these two functional groups favor the sequestration of Cu^{+}, Cd^{2+}, Hg^{2+}, RHg^{+}, Hg_2^{2+} but also the complexation of Fe^{2+}, Co^{2+}, Ni^{2+}, Cu^{2+}, Zn^{2+}, Pb^{2+}. Then, these two molecules were compared in order to determine which one is the most appropriate to be used for further remediation tests at industrial scale.

First of all, the selected amino acids have to be immobilized onto the fibers. This work was divided into two steps: first, the grafting of acrylic acid, and then, the chemical coupling of the biomolecules onto the free carboxylic acid groups. The grafting of acrylic acid was carried out using physical methods (low pressure cold plasma and excimer laser processes) leading to very clearly different results: by plasma method, a thin and regular coating can be observed all around the fibers (2 wt.-%) whereas, by laser method, a new morphology is created at the surface of the irradiated part of the fibers (3 wt.-%). However, in the case of the laser process, some recombination reactions seem to occur, leading to a loss of free carboxylic acid groups, and thus, to a less important amount of immobilized biomolecules. This is why the plasma treatment was selected for the grafting of acrylic acid onto synthetic fibers.

Immobilization of biomolecules was carried out by chemical coupling using a carbodiimide: 0.033 mmol of cysteine or 0.039 mmol of tyrosine were immobilized. The efficiency of the grafted materials was then analyzed. It was observed that PP-g-AA-cysteine can sequester an important amount of copper (~100 mg/g PP) compared to PP-g-AA-tyrosine

(~50 mg/g PP). However, PP-g-AA-tyrosine is an interesting material because of the fast sorption kinetics and also the unchanged efficiency whatever the amount of sodium chloride in the solution. Thus, PP-g-AA-tyrosine was selected for further tests with doped leachate from Dunkirk harbor sediments.

Using this leachate, it was observed that the total amount of metal ions adsorbed is less important. This fact can be explained by the lower initial concentration of metals in the leachate compared to the amount in the artificially contaminated model solutions. As a result of the difference in the concentrations, the kinetics may be changed leading to a slower transfer or diffusion step, and thus, two hours might not be sufficient to allow the saturation of PP-g-AA-tyrosine. Moreover, as the solution contains less metal ions than the model solution, and due to the equilibrium between the metal adsorbed and the metal in the solution, the maximum amount of adsorbed metal can be lower than the amount adsorbed in highly concentrated solution.

Preliminary theoretical studies were carried out in order to determine the amino acids/metal complexes that can be formed. Some structures were observed but are not relevant enough because: (i) it could be better to use zwitterionic forms for further calculations, thus including new partial charges depending on the considered pH, and (ii) it is necessary to take into account the presence of the fiber because amino acids are grafted onto fibers leading to other possible structures for complexes.

As a conclusion, this work highlights the great potential of amino acids in remediation processes, even if these biomolecules cannot be used directly in the contaminated effluents, but rather grafted onto materials. Physical methods, such as plasma and laser, were used to allow a good grafting of these amino acids through the use of a spacer: acrylic acid. These tests were carried out at a laboratory scale, but larger textile surfaces have to be treated in order to scale up the remediation process. As the treatment with our radiofrequency plasma does not allow online process at industrial scale, the grafting of molecules onto textile using atmospheric plasma was considered. Some preliminary tests were carried out and are presented in the outlooks.

Outlooks

Acrylic acid grafting using atmospheric plasma

1. Introduction

It was observed that radiofrequency cold plasma process is a very efficient method to functionalize geotextiles. Indeed, fibers are totally covered with a film of acrylic and polyacrylic acids, allowing the immobilization of chelating biomolecules. However, due to the vacuum constraint, this functionalization method can hardly be scaled up, and above all, in an online process. The idea was thus to develop a protocol easy to transfer at industrial scale in an online process, based on the use of another kind of plasma process, the atmospheric ultra-light discharge (ULD) developed by AcXys Technologies. This technique presents some advantages compared to cold plasma process as each side of the textile structure can be functionalized separately, with one given molecule, leading to a bifunctional material.

The best conditions to activate the surface of the fabrics were first determined. Then, some preliminary experiments were conducted in order to select series of parameters allowing the grafting of acrylic acid. These first results are presented in the following part as well as some outlooks concerning the optimization of the acrylic acid grafting. Finally, the planned remediation device, in which the functionalized textiles will be used, is described at the end of this chapter.

2. Acrylic acid grafting onto PP and PET by atmospheric plasma process

The atmospheric ultra-light discharge (ULD) cold plasma process (appendix 1) is a method transferable at industrial scale that can potentially be used for the functionalization of fabrics. The UMET laboratory purchased this equipment from AcXys Technologies in Grenoble. The device was fully operational from the beginning of 2014 but before, I had the opportunity to make some preliminary tests at AcXys Technologies. In fact, only few studies were previously done on textile supports and it was necessary to determine the experimental conditions to activate and functionalize the geotextiles. With the ULD source, the plasma is generated at atmospheric pressure allowing the online treatment. The protocol used to treat fabrics is the same as the protocol used with radiofrequency cold plasma process: (i) activation of the fabric with plasma; (ii) impregnation of the activated PET or PP in acrylic acid using a roll-padder; (iii) grafting and polymerization of acrylic acid using atmospheric plasma process; (iv) washing and drying. However, only nitrogen and air can be used as plasmagene gas for the treatments. Thus, it is necessary to determine and optimize the conditions for the activation step and the graft-polymerization of acrylic acid onto the fabrics.

2.1. Development and optimization of the grafting of acrylic acid

2.1.1. Activation step

To determine the suitable conditions for the activation of textiles, the influence of three parameters has to be evaluated: the power of the plasma (from 1400 to 2000 W), the speed of the conveyor (from 1 to 10 m/min), and the number of successive treatments (from 1 to 99). Some parameters remain constant: the plasmagene gas is nitrogen, the plasmagene gas flow is fixed at 120 L/min, and the distance between the sample and the source is maintained at 5 mm. In order to ensure a homogeneous activation with good wettability properties for the whole sample, water contact angle measurements must be carried out not only on the treated surface but also on the opposite side of the treated sample (figure 46).

PET fabrics can be activated directly and the optimal conditions were determined: a nitrogen plasma, with a nitrogen flow of 120 L/min, at 2000W, to ensure a sufficient modification at the surface of the fibers; and a conveyor speed of 10 m/min in order to avoid the fibers degradation due to temperature. The influence of the number of successive treatments on the hydrophilization of PET was evaluated (0 to 40 successive treatments).

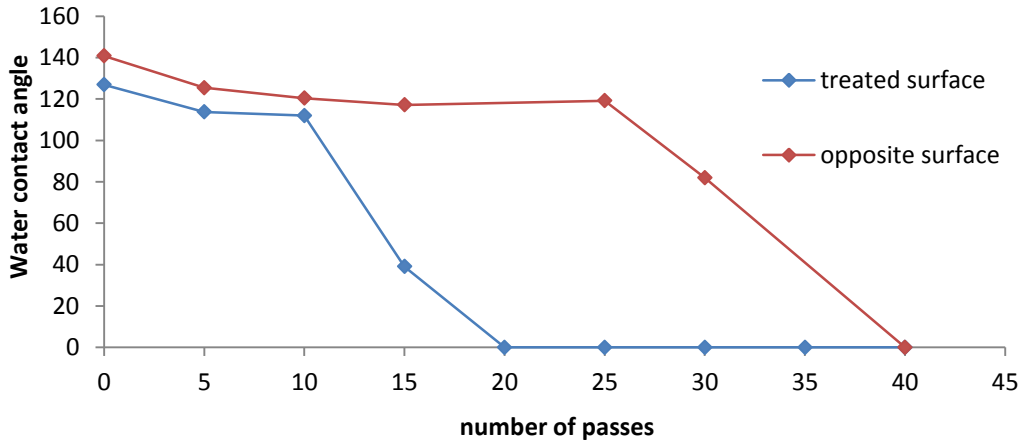

Figure 46: Water contact angle values at the surface of nonwoven PET fabrics as a function of the number of treatments through atmospheric ULD plasma (2000W, N_2, 120L/min, 10m/min)

As it it can be observed in figure 46, the treated surface becomes hydrophilic after 15 successive treatments using the ULD plasma, leading to a water contact angle of 39°. From 20 successive treatments, the water contact angle is equal to 0°, corresponding to high wettability properties. On the opposite side of the treated surface, some modifications can be observed after more than 25 treatments, and a water contact angle of 0° is obtained from 40 treatments. These results might be explained by the fact that reactive particles from the plasma have to go through the whole texile thickness to modify the opposite surface.

Regarding the PP fabrics, it was necessary to use CO_2 as a doping gas in addition to nitrogen because the experimental conditions previously used for PET fabrics did not allow the activation of PP. Indeed, studies carried out at AcXys Technologies in Grenoble showed the positive influence of this gas mixture on the hydrophilization of PP surfaces. After varying the different parameters, the following conditions were used to treat the samples: 2000 W, 125 L/min of N_2 with 0.95 L/min of CO_2, a conveyor speed of 10 m/min, and 10 successive treatments with a sample/source distance of 5 mm. Treated PP samples were then able to absorb distilled water.

2.1.2. Preliminary grafting tests

Some preliminary studies were carried out in order to graft acrylic acid onto the previously activated nonwoven fabrics. First the evaluation of the temperature inside the plasma was necessary as both textiles and acrylic acid are sensitive to the temperature conditions. Thus, thermocouples were placed along the curtain of plasma so as to measure the temperature inside the plasma according to the plasma power and as a function of the time of treatment (figure 47). The maximum temperature reached inside the plasma at 2000 W and 1700 W are respectively equal to 147°C and 132°C. As the boiling point of acrylic aicd is 141C, a plasma power higher than 1700 W cannot be used. In parallel, a minimum of 1400 W is necessary to obtain a homogeneous plasma. Finally, the plasma power was maintained at 1400W during the acrylic acid grafting step. The influence of the conveyor speed on the acrylic acid grafting rate was then studied.

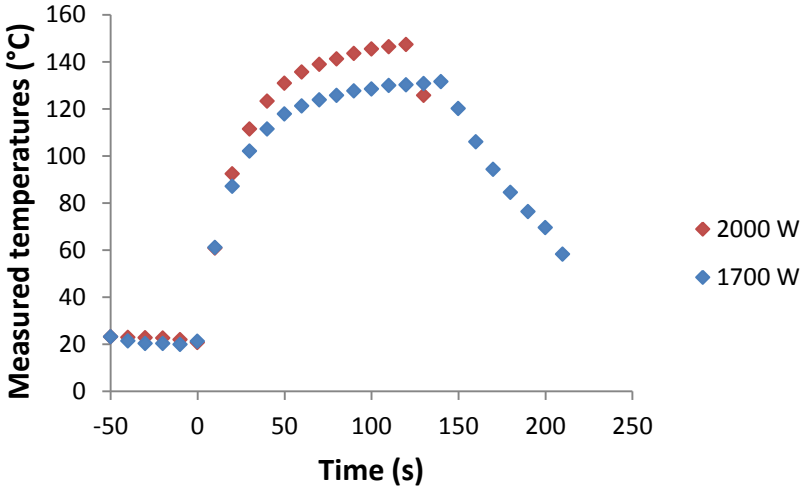

Figure 47: Temperature measured using a graphtech (midi LOGGER GL220) inside the plasma at 2000 W and at 1700 W

This study was mainly carried out onto PP samples as the experiments with cold plasma were also done with PP samples. To activate the PP samples without using CO_2, this step was carried out using the radiofrequency cold plasma device (protocol described § II.2.1). The number of treatments was fixed at 60, and the plasma was generated in a nitrogen flow of 120 L/min, at 1400 W. Figure 48 shows the influence of the conveyor speed on the acrylic acid grafting rate. When the conveyor speed is high (for example at 10 m/min), the grafting rate is less important than for slower conveyor speeds. An optimum grafting rate of 2.4 wt.-% obtained at 6 m/min.

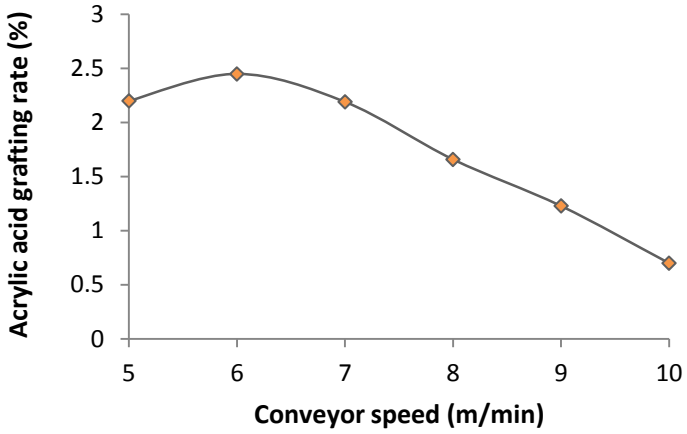

Figure 48: Acrylic acid grafting rate as a function of the conveyor speed

2.2. Characterization of grafted fabrics

Some FTIR/ATR analyses were carried out in order to identify the chemical groups of acrylic acid, and thus, to prove the presence of acrylic acid at the surface of the fibers (figure 49). Presence of acrylic acid was evidenced by a peak at 1723 cm^{-1} corresponding to the carboxylic acid groups. Moreover, the amount of grafted acrylic acid is not the same on both sides of the fabric, being much more important on the irradiated side. Thus, the plasma can diffuse through the textile during the treatment, and due to the density and the porosity of the textile, less reactive particles from the plasma might reach the other side of the material leading to a gradient of acrylic acid grafting rate through the whole thickness of the textiles.

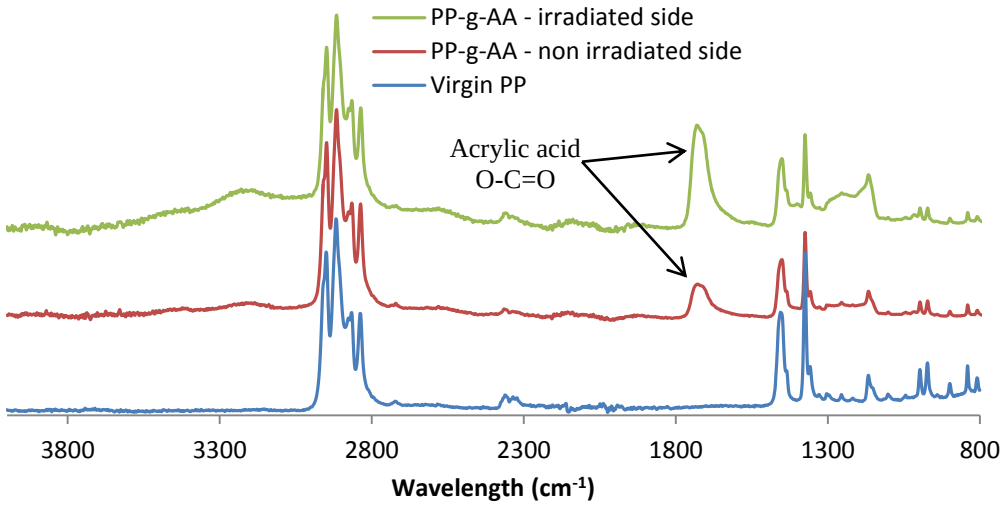

Figure 49: FTIR-ATR spectra of the virgin PP and PP-g-AA on the irradiated and non irradiated sides after the atmospheric plasma treatment (at 1400 W, N_2 120 L/min, 3 m/min and 60 passes)

The functionalized textiles can thus be used to sequester trace metals from model solutions. An example of the efficiency of this material to sequester copper is given in figure 50. The color of the virgin PP does not change after immersion in a copper solution whereas some changes can be observed in the case of the functionalized PP samples. PP-g-AA-tyrosine prepared only with the cold plasma device was immersed in a copper sulfate solution leading to the appearance of blue color on the textile surface which proves the presence of divalent copper ions. Finally, concerning the PP-g-AA prepared by atmospheric plasma, a quite homogeneous change of color is observed: the green-blue color corresponds to Cu^+ ions as in that case, the sample was immersed in a CuCl solution.

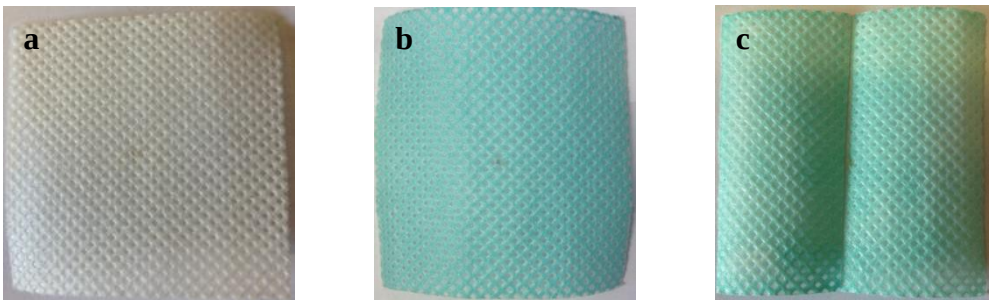

Figure 50: Images of (a) virgin PP, (b) PP-g-AA-tyrosine prepared by cold plasma and (c) PP-g-AA prepared by atmospheric plasma after immersion into a copper solution

3. Development of the remediation process

Before testing the functionalized materials at industrial scale, trace metals sequestration will be studied at pilot scale in a storage site of Baudelet Environnement company (figure 51), one of the industrial partners of the project.

Figure 51: Storage site in Baudelet Environnement, Blaringhem, France

This site will first be covered with a specific system developed by Afitex, another industrial partner of the DEPOLTEX project. This system (scheme 6) is composed of a Geomembrane combined with a functionalized needlepunched geotextile. Between these two materials, some drains are regularly inserted in order to ensure good drainage and filtration properties. This structure has to be placed under sand and the sediments to be treated. Then, mobile pollutants will move through the sediments and the sand layer by percolation, due to sediments exposure to the rain. Thus, the mobile trace metals will reach the functionalized textiles and will be sequestered, allowing the decontaminated water to be evacuated by the drains. When pollution levels reached after the treatment correspond to class III, sediments can be removed from the site in order to be re-used in civil engineering. The functionalized textiles can also be removed, and if possible, be regenerated in order to be used again for the remediation of sediments.

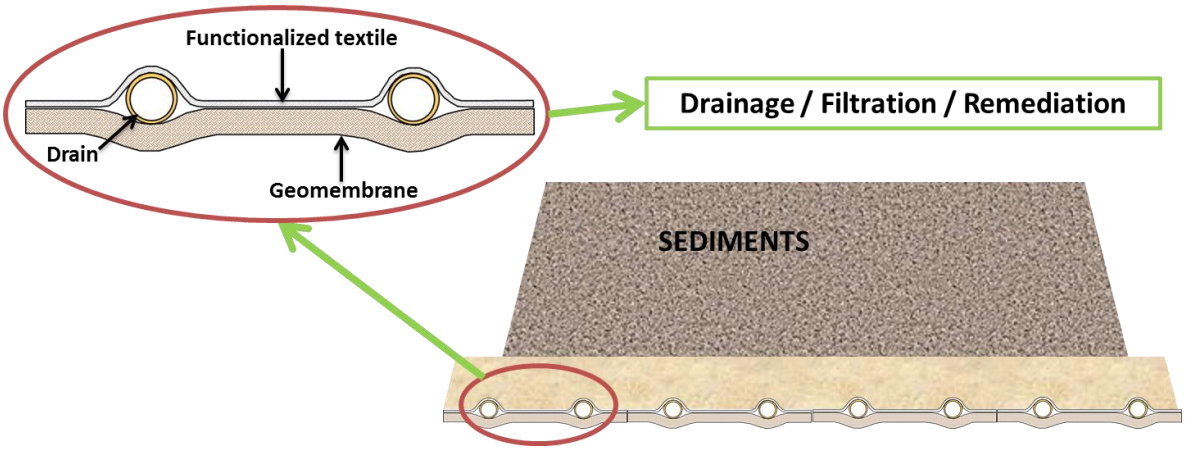

Scheme 6: Remediation process proposed in the DEPOLTEX project by AFITEX [140]

4. Conclusion

As a conclusion, preliminary tests with atmospheric plasma treatment give promising results concerning the acrylic acid grafting. The activation of PET fabrics was easily carried out using nitrogen as plasmagene gas. However, concerning PP, it would be necessary to use a doping gas, such as CO_2, in order to improve the wettability of the fabrics. Then, for the grafting step, the conditions were adapted in order to avoid the degradation of acrylic acid and/or textiles. The highest grafting rate (2.45 w.-%) was obtained under the following conditions: 1400 W, N_2 120 L/min, 60 successive treatments and 6 m/min. The amount of acrylic acid grafted onto the fabrics can be optimized using an experimental design. Moreover, it may be necessary to optimize the process in order to obtain a high grafting rate in a short time.

References

1. Chassin, P., D. Baize, P. Cambier, and T. Sterckeman, Les éléments traces métalliques et la qualité des sols - Impact à moyen et à long terme. *Forum « Le sol, un patrimoine menacé ? »*, **1996**.
2. Michel, L., Arrêté du 28 octobre 2010 relatif aux installations de stockage de déchets inertes, version consolidée au 19 août 2013, in *NOR: DEVP1022585A*, d.l.é. Ministère de l'écologie, du développement durable et de la mer, Editor.
3. Fischer Boel, M., Decision n°2003/33/CE du 19/12/02 établissant des critères et des procédures d'admission des déchets dans les décharges, conformément à l'article 16 et à l'annexe II de la directive 1999/31/CE. *Journal Officiel des Communautés européennes*, **2003**. L 182.
4. Peng, J.-f., Y.-h. Song, P. Yuan, X.-y. Cui, and G.-l. Qiu, The remediation of heavy metals contaminated sediment. *Journal of Hazardous Materials*, **2009**. 161(2–3): p. 633-640.
5. Anirudhan, T.S., C.D. Bringle, and P.G. Radhakrishnan, Heavy metal interactions with phosphatic clay: Kinetic and equilibrium studies. *Chemical Engineering Journal*, **2012**. 200–202(0): p. 149-157.
6. Malandrino, M., O. Abollino, S. Buoso, A. Giacomino, C. La Gioia, and E. Mentasti, Accumulation of heavy metals from contaminated soil to plants and evaluation of soil remediation by vermiculite. *Chemosphere*, **2011**. 82(2): p. 169-178.
7. Tessier, A., P.G.C. Campbell, and M. Blsson, Sequential extraction procedure for the speciation of particulate trace metals. *Analytical Chemistry*, **1979**. 51(7): p. 844-851.
8. Kalina, M., M. Klučáková, and P. Sedláček, Utilization of fractional extraction for characterization of the interactions between humic acids and metals. *Geoderma*, **2013**. 207–208(0): p. 92-98.
9. Lishtvan, I.I., Y.G. Yanuta, A.M. Abramets', G.S. Monich, N.S. Glukhova, and V.N. Aleinikova, Interaction of humic acids with metal ions in the water medium. *Journal of Water Chemistry and Technology*, **2012**. 34(5): p. 211-217.
10. Dinu, M.I., Comparison of complexing ability of fulvic and humic acids in the aquatic environment with iron and zinc ions. *Water Resources*, **2010**. 37(1): p. 65-69.
11. Ducoroy, L., B. Martel, M. Bacquet, and M. Morcellet, Cation exchange finishing of nonwoven polyester with polycarboxylic acids and cyclodextrins. *Journal of Applied Polymer Science*, **2007**. 103(6): p. 3730-3738.
12. Alongi, J., F. Carosio, A. Frache, and G. Malucelli, Layer by Layer coatings assembled through dipping, vertical or horizontal spray for cotton flame retardancy. *Carbohydrate Polymers*, **2013**. 92(1): p. 114-119.
13. Gomes, A.P., J.F. Mano, J.A. Queiroz, and I.C. Gouveia, New biomaterial based on cotton with incorporated Biomolecules. *Journal of Applied Polymer Science*, **2014**.
14. Lin, J., S. Qiu, K. Lewis, and A.M. Klibanov, Mechanism of bactericidal and fungicidal activities of textiles covalently modified with alkylated polyethylenimine. *Biotechnology and Bioengineering*, **2003**. 83(2): p. 168-172.
15. Ducoroy, L., M. Bacquet, B. Martel, and M. Morcellet, Removal of heavy metals from aqueous media by cation exchange nonwoven PET coated with β-cyclodextrin-polycarboxylic moities. *Reactive and Functional Polymers*, **2008**. 68: p. 594-600.
16. Le Thuaut, P., B. Martel, G. Crini, U. Maschke, X. Coqueret, and M. Morcellet, Grafting of cyclodextrins onto polypropylene nonwoven fabrics for the manufacture of reactive filters. I. Synthesis parameters. *Journal of Applied Polymer Science*, **2000**. 77(10): p. 2118-2125.
17. Decker, C., Polymerisation sous rayonnement UV. *Techniques de l'ingénieur, traité Plastiques et Composites*, **2000**. référence AM3044: p. 1-34.

18. Zheng, Y., H. Liu, P.V. Gurgel, and R.G. Carbonell, Polypropylene nonwoven fabrics with conformal grafting of poly(glycidyl methacrylate) for bioseparations. *Journal of Membrane Science*, **2010**. 364: p. 362-371.
19. Niino, H., J. Krüger, and W. Kautek, Biomaterial immobilization on polyurethane films by XeCl excimer laser processing. *Applied Physics A: Materials Science & Processing*, **2001**. 72(1): p. 53-57.
20. Degoutin, S., M. Jimenez, M. Casetta, S. Bellayer, F. Chai, N. Blanchemain, C. Neut, I. Kacem, M. Traisnel, and B. Martel, Anticoagulant and antimicrobial finishing of non-woven polypropylene textiles. *Biomedical Materials*, **2012**. 7(3): p. 1-13.
21. Saxena, S., A.R. Ray, and B. Gupta, Chitosan immobilization on polyacrylic acid grafted polypropylene monofilament. *Carbohydrate Polymers*, **2010**. 82(4): p. 1315-1322.
22. Bessada, R., G. Silva, M.C. Paiva, and A.V. Machado, Functionalization of PET and PA6.6 woven fabrics. *Applied Surface Science*, **2011**. 257(18): p. 7944-7951.
23. Behary, N., A. Perwuelz, C. Campagne, D. Lecouturier, P. Dhulster, and A.S. Mamede, Adsorption of surfactin produced from Bacillus subtilis using nonwoven PET (polyethylene terephthalate) fibrous membranes functionalized with chitosan. *Colloids and Surfaces B: Biointerfaces*, **2012**. 90(0): p. 137-143.
24. Tseng, H.-J., S.-h. Hsu, M.-W. Wu, T.-H. Hsueh, and P.-C. Tu, Nylon textiles grafted with chitosan by open air plasma and their antimicrobial effect. *Fibers and Polymers*, **2009**. 10(1): p. 53-59.
25. Kalia, S., K. Thakur, A. Celli, M.A. Kiechel, and C.L. Schauer, Surface modification of plant fibers using environment friendly methods for their application in polymer composites, textile industry and antimicrobial activities: A review. *Journal of Environmental Chemical Engineering*, **2013**. 1(3): p. 97-112.
26. Höcker, H., Plasma treatment of textile fibers. *Pure and Applied Chemistry*, **2002**. 74(3): p. 423-427.
27. Shishoo, R., Plasma technologies for textiles, ed. R. Shishoo**2007**: Woodhead Publishing Limited. 360.
28. Hegemann, D., Plasma polymerization and its applications in textiles. *Indian Journal of Fibre and Textile Research*, **2006**. 31(1): p. 99-115.
29. Morent, R., N. De Geyter, J. Verschuren, K. De Clerck, P. Kiekens, and C. Leys, Non-thermal plasma treatment of textiles. *Surface and Coatings Technology*, **2008**. 202(14): p. 3427-3449.
30. Muraviev, D., J. Noguerol, and M. Valiente, Seawater as Auxiliary Reagent in Dual-Temperature Ion-Exchange Processing of Acidic Mine Waters. *Environmental Science & Technology*, **1997**. 31(2): p. 379-383.
31. Karakışla, M., The adsorption of Cu(II) ion from aqueous solution upon acrylic acid grafted poly(ethylene terephthalate) fibers. *Journal of Applied Polymer Science*, **2003**. 87(8): p. 1216-1220.
32. Hu, J., C. Yin, H.Q. Mao, K. Tamada, and W. Knoll, Functionalization of poly(ethylene terephthalate) film by pulsed plasma deposition of maleic anhydride. *Advanced Functional Materials*, **2003**. 13(9): p. 692-697.
33. Mostafa, K.M., A.R. Samarkandy, and A.A. El-Sanabary, Preparation of poly(DMAEM)-cross linked pregelled starch graft copolymer and its application in waste water treatments. *Carbohydrate Polymers*, **2011**. 86: p. 491-498.
34. Tekin, K., L. Uzun, C.A. Sahin, S. Bektas, and A. Denizli, Preparation and characterization of composite cryogels containing imidazole group and use in heavy metal removal. *Reactive & Functional Polymers*, **2011**. 71: p. 985-993.

35. Lai, Y.-L., M. Thirumavalavan, and J.-F. Lee, Effective adsorption of heavy metal ions (Cu2+, Pb2+, Zn2+) from aqueous solution by immobilization of adsorbents on Ca-alginate beads. *Toxicological & Environmental Chemistry*, **2010**. 92(4): p. 697-705.
36. Crini, G., Non-conventional low-cost adsorbents for dye removal: A review. *Bioresource Technology*, **2006**. 97(9): p. 1061-1085.
37. Misra, V., A review on the use of biopolymers for the removal of toxic metals from liquid industrial effluents. *International Journal of Environment and Waste Management*, **2009**. 3: p. 393-410.
38. Delalande, O., H. Desvaux, E. Godat, A. Valleix, C. Junot, J. Labarre, and Y. Boulard, Cadmium-glutathione solution structures provide new keys for understanding the detoxification process. *FEBS Journal*, **2010**. 277: p. 5086-5096.
39. Zenk, M.H., Heavy metal detoxification in higher plants - a review. *Gene*, **1996**. 179(1): p. 21-30.
40. Cobbett, C.S., Phytochelatins and Their Roles in Heavy Metal Detoxification. *Plant Physiology*, **2000**. 123(3): p. 825-832.
41. Maret, W., K.S. Larsen, and B.L. Vallee, Coordination dynamics of biological zinc "clusters" in metallothioneins and in the DNA-binding domain of the transcription factor Gal4. *Proceedings of the National Academy of Sciences*, **1997**. 94(6): p. 2233-2237.
42. Klaassen, C.D., J. Liu, and S. Choudhuri, METALLOTHIONEIN: An Intracellular Protein to Protect Against Cadmium Toxicity. *Annual Review of Pharmacology and Toxicology*, **1999**. 39: p. 267-294.
43. Rauser, W.E., Structure and function of metal chelators produced by plants: The case for organic acids, amino acids, phytin, and metallothioneins. *Cell Biochemistry and Biophysics*, **1999**. 31(1): p. 19-48.
44. Van Der Helm, D. and C.E. Tatsch, The Crystal Structure of Bis-(L-tyrosinato)copper(II). *Acta Crystallographica*, **1971**. B28(8): p. 2307-2312.
45. Ma, J.C. and D.A. Dougherty, The cation-π interaction. *Chemical Reviews*, **1997**. 97(5): p. 1303-1324.
46. Hu, P., C. Sorensen, and M. Gross, Influences of peptide side chains on the metal ion binding site in metal ion-cationized peptides: Participation of aromatic rings in metal chelation. *Journal of the American Society for Mass Spectrometry*, **1995**. 6(11): p. 1079-1085.
47. Ryzhov, V. and R.C. Dunbar, Interactions of Phenol and Indole with Metal Ions in the Gas Phase: Models For Tyr and Trp Side-Chain Binding. *J. Am. Chem. Soc.*, **1999**. 121(10): p. 2259-2268.
48. Erdem, E., N. Karapinar, and R. Donat, The removal of heavy metal cations by natural zeolites. *Journal of Colloid and Interface Science*, **2004**. 280(2): p. 309-314.
49. Tejowulan, R.S. and W.H. Hendershot, Removal of trace metals from contaminated soils using EDTA incorporating resin trapping techniques. *Environmental Pollution*, **1998**. 103(1): p. 135-142.
50. Witus, L.S. and M.B. Francis, Using Synthetically Modified Proteins to Make New Materials. *Accounts of Chemical Research*, **2011**. 4(9): p. 774-783.
51. Malachowski, L., J.L. Stair, and J.A. Holcombe, Immobilized peptides/amino acids on solid supports for metal remediation. *Pure and Applied Chemistry*, **2004**. 76(4): p. 777-787.
52. Pearson, R.G., Hard and Soft Acids and Bases. *Journal of The American Chemical Society*, **1963**. 85(22): p. 3533-3539.

53. Parr, R.G. and R.G. Pearson, Absolute hardness: companion parameter to absolute electronegativity. *Journal of The American Chemical Society*, **1983**. 105(26): p. 7512-7516.
54. Sigel, H. and D.B. McCormick, Discriminating behavior of metal ions and ligands with regard to their biological significance. *Accounts of Chemical Research*, **1970**. 3(6): p. 201-208.
55. Martin, R.B., A stability ruler for metal ion complexes. *Journal of Chemical Education*, **1987**. 64(5): p. 402.
56. Rulíšek, L. and Z. Havlas, Theoretical Studies of Metal Ion Selectivity. 1. DFT Calculations of Interaction Energies of Amino Acid Side Chains with Selected Transition Metal Ions (Co2+, Ni2+, Cu2+, Zn2+, Cd2+, and Hg2+). *Journal of The American Chemical Society*, **2000**. 122(42): p. 10428-10439.
57. Dong, D., Y.M. Nelson, L.W. Lion, M.L. Shuler, and W.C. Ghiorse, Adsorption of Pb and Cd onto metal oxides and organic material in natural surface coatings as determined by selective extractions: New evidence for the importance of Mn and Fe oxides. *Water Research*, **2000**. 34(2): p. 427-436.
58. Perrono, P., Les micropolluants métalliques des boues des stations d'épuration urbaine et l'épandage agricole, **1999**, Université de Picardie, Amien.
59. Serpaud, B., R. Al-Shukry, M. Casteignau, and G. Matejka, Heavy metal adsorption (Cu, Zn, Cd and Pb), by superficial stream sediments: effects of pH, temperature and sediment composition. *Revue des Sciences de l'Eau*, **1994**. 7(4): p. 343-365.
60. Templeton, D.M., F. Ariese, R. Cornelis, L.G. Danielsson, H. Muntau, H.P. Van Leeuwen, and R. Łobiński, Guidelines for terms related to chemical speciation and fractionation of elements. Definitions, structural aspects, and methodological approaches (IUPAC recommendations 2000). *Pure and Applied Chemistry*, **2000**. 72(8): p. 1453-1470.
61. Uzu, G., S. Sobanska, Y. Aliouane, P. Pradere, and C. Dumat, Study of lead phytoavailability for atmospheric industrial micronic and sub-micronic particles in relation with lead speciation. *Environmental Pollution*, **2009**. 157(4): p. 1178-1185.
62. Uzu, G., S. Sobanska, G. Sarret, J.J. Sauvain, P. Pradère, and C. Dumat, Characterization of lead-recycling facility emissions at various workplaces: Major insights for sanitary risks assessment. *Journal of Hazardous Materials*, **2011**. 186(2–3): p. 1018-1027.
63. Meers, E., R. Samson, F.M.G. Tack, A. Ruttens, M. Vandegehuchte, J. Vangronsveld, and M.G. Verloo, Phytoavailability assessment of heavy metals in soils by single extractions and accumulation by Phaseolus vulgaris. *Environmental and Experimental Botany*, **2007**. 60(3): p. 385-396.
64. Burnol, A., L. Duro, and M. Grive, Eléments traces métalliques, Guide méthodologique, Recommandations pour la modélisation des transferts des éléments traces métalliques dans les sols et les eaux souterraines, in *Rapport d'étude INERIS-DRC-06-66246/DESP-R01a***2006**.
65. Wang, Q.-Y., D.-M. Zhou, and L. Cang, Bioavailability of Soil Copper from Different Sources: Integrating Chemical Approaches with Biological Indicators. *Pedosphere*, **2014**. 24(1): p. 145-152.
66. Peroza, E.A., R. Schmucki, P. Güntert, E. Freisinger, and O. Zerbe, The β_E-Domain of Wheat E_c-1 Metallothionein: A Metal-Binding Domain with a Distinctive Structure. *Journal of Molecular Biology*, **2009**. 387(1): p. 207-218.
67. Blindauer, C.A., Lessons on the critical interplay between zinc binding and protein structure and dynamics. *Journal of Inorganic Biochemistry*, **2013**. 121: p. 145-155.

68. Armentrout, P.B., E.I. Armentrout, A.A. Clark, T.E. Cooper, E.M.S. Stennett, and D.R. Carl, An experimental and theoretical study of alkali metal cation interactions with cysteine. *Journal of Physical Chemistry B*, **2010**. 114(11): p. 3927-3937.
69. Citir, M., E.M.S. Stennett, J. Oomens, J.D. Steill, M.T. Rodgers, and P.B. Armentrout, Infrared multiple photon dissociation spectroscopy of cationized cysteine: Effects of metal cation size on gas-phase conformation. *International Journal of Mass Spectrometry*, **2010**. 297(1-3): p. 9-17.
70. Maret, W. and Y. Li, Coordination dynamics of zinc in proteins. *Chemical Reviews*, **2009**. 109(10): p. 4682-4707.
71. Howard, M., H. A. Jurbergs, and J. A. Holcombe, Comparison of silica-immobilized poly(L-cysteine) and 8-hydroxyquinoline for trace metal extraction and recovery. *Journal of Analytical Atomic Spectrometry*, **1999**. 14(8): p. 1209-1214.
72. Johnson, A.M. and J.A. Holcombe, Poly(l-cysteine) as an Electrochemically Modifiable Ligand for Trace Metal Chelation. *Analytical Chemistry*, **2004**. 77(1): p. 30-35.
73. Jurbergs, H.A. and J.A. Holcombe, Characterization of Immobilized Poly(l-cysteine) for Cadmium Chelation and Preconcentration. *Analytical Chemistry*, **1997**. 69(10): p. 1893-1898.
74. Ritchie, S.M.C., K.E. Kissick, L.G. Bachas, S.K. Sikdar, C. Parikh, and D. Bhattacharyya, Polycysteine and other polyamino acid functionalized microfiltration membranes for heavy metal capture. *Environmental Science and Technology*, **2001**. 35(15): p. 3252-3258.
75. Xiao, L., G.G. Wildgoose, A. Crossley, R. Knight, J.H. Jones, and R.G. Compton, Removal of Toxic Metal-Ion Pollutants from Water by Using Chemically Modified Carbon Powders. *Chemistry – An Asian Journal*, **2006**. 1(4): p. 614-622.
76. Sljukic, B., G.G. Wildgoose, A. Crossley, J.H. Jones, L. Jiang, T.G.J. Jones, and R.G. Compton, The thermodynamics of sequestration of toxic copper(ii) metal ion pollutants from aqueous media by l-cysteine methyl ester modified glassy carbon spheres. *Journal of Materials Chemistry*, **2006**. 16(10): p. 970-976.
77. Wildgoose, G.G., H.C. Leventis, I.J. Davies, A. Crossley, N.S. Lawrence, L. Jiang, T.G.J. Jones, and R.G. Compton, Graphite powder derivatised with poly-l-cysteine using "building-block" chemistry-a novel material for the extraction of heavy metal ions. *Journal of Materials Chemistry*, **2005**. 15(24): p. 2375-2382.
78. Faghihian, H. and M. Nejati-Yazdinejad, Sorption performance of cysteine-modified bentonite in heavy metals uptake. *Russian Source*, **2009**. 74(7): p. 833-843.
79. Merrifield, J.D., W.G. Davids, J.D. MacRae, and A. Amirbahman, Uptake of mercury by thiol-grafted chitosan gel beads. *Water Research*, **2004**. 38(13): p. 3132-3138.
80. Armentrout, P.B., B. Yang, and M.T. Rodgers, Metal cation dependence of interactions with amino acids: Bond energies of Rb+ and Cs+ to Met, Phe, Tyr, and Trp. *Journal of Physical Chemistry B*, **2013**. 117(14): p. 3771-3781.
81. Dunbar, R.C., J.D. Steill, and J. Oomens, Encapsulation of Metal Cations by the PhePhe Ligand: A Cation−π Ion Cage. *Journal of The American Chemical Society*, **2011**. 133(24): p. 9376-9386.
82. Remko, M., D. Fitz, R. Broer, and B. Rode, Effect of metal Ions (Ni2+, Cu2+ and Zn2+) and water coordination on the structure of L-phenylalanine, L-tyrosine, L-tryptophan and their zwitterionic forms. *Journal of Molecular Modeling*, **2011**. 17(12): p. 3117-3128.
83. Dennis, G.R. and G.L.D. Ritchie, Dilute-solution field gradient induced birefringence and molecular quadrupole moment of benzene. *Journal of Physical Chemistry*, **1991**. 95(2): p. 656-660.

84. Solomon, E.I., U.M. Sundaram, and T.E. Machonkin, Multicopper oxidases and oxygenases. *Chemical Reviews*, **1996**. 96(7): p. 2563-2605.
85. Severin, K., R. Bergs, and W. Beck, Bioorganometallic Chemistry - Transition Metal Complexes with α-Amino Acids and Peptides. *Angewandte Chemie International Edition*, **1998**. 37(12): p. 1634-1654.
86. Deschamps, P., P.P. Kulkarni, M. Gautam-Basak, and B. Sarkar, The saga of copper(II)-L-histidine. *Coordination Chemistry Reviews*, **2005**. 249(9-10): p. 895-909.
87. Khangarot, B.S. and R.S. Rathore, Protective action of 24 amino acids on the toxicity of copper to a freshwater tubificid worm Tubifex tubifex Muller. *Water, Air, and Soil Pollution*, **2004**. 157(1-4): p. 53-63.
88. Birlik, E., A. Ersöz, E. Açıkkalp, A. Denizli, and R. Say, Cr(III)-imprinted polymeric beads: Sorption and preconcentration studies. *Journal of Hazardous Materials*, **2007**. 140(1–2): p. 110-116.
89. Shimazaki, Y., M. Takani, and O. Yamauchi, Metal complexes of amino acids and amino acid side chain groups. Structures and properties. *Dalton Transactions*, **2009**(38): p. 7854-7869.
90. Volesky, B., Biosorption and me. *Water Research*, **2007**. 41(18): p. 4017-4029.
91. Guibal, E., Interactions of metal ions with chitosan-based sorbents: a review. *Separation and Purification Technology*, **2004**. 38(1): p. 43-74.
92. Abdel-Halim, E.S. and S.S. Al-Deyab, Removal of heavy metals from their aqueous solutions through adsorption onto natural polymers. *Carbohydrate Polymers*, **2011**. 84(1): p. 454-458.
93. Kolozsi, A., I. Vosekalna, T. Martinek, E. Larsen, and B. Gyurcsik, Copper(ii) and zinc(ii) ion binding properties of a MAP type branched ligand with histidines as surface functionalities. *Dalton Transactions*, **2009**(29): p. 5647-5654.
94. Mayr, H., M. Breugst, and A.R. Ofial, Farewell to the HSAB Treatment of Ambident Reactivity. *Angewandte Chemie International Edition*, **2011**. 50(29): p. 6470-6505.
95. Pearson, R.G., Hard and soft acids and bases, HSAB, part 1: Fundamental principles. *Journal of Chemical Education*, **1968**. 45(9): p. 581.
96. Rulíšek, L.r. and J. Vondrášek, Coordination geometries of selected transition metal ions (Co2+, Ni2+, Cu2+, Zn2+, Cd2+, and Hg2+) in metalloproteins. *Journal of Inorganic Biochemistry*, **1998**. 71(3–4): p. 115-127.
97. Waldron, K.J., J.C. Rutherford, D. Ford, and N.J. Robinson, Metalloproteins and metal sensing. *Nature*, **2009**. 460(7257): p. 823-830.
98. Yamauchi, O., A. Odani, and M. Takani, Metal-amino acid chemistry. Weak interactions and related functions of side chain groups. *Journal of the Chemical Society, Dalton Transactions*, **2002**(18): p. 3411-3421.
99. Ortega, R., A. Carmona, I. Llorens, and P.L. Solari, X-ray absorption spectroscopy of biological samples. A tutorial. *Journal of Analytical Atomic Spectrometry*, **2012**. 27(12): p. 2054-2065.
100. Faller, P., C. Hureau, P. Dorlet, P. Hellwig, Y. Coppel, F. Collin, and B. Alies, Methods and techniques to study the bioinorganic chemistry of metal-peptide complexes linked to neurodegenerative diseases. *Coordination Chemistry Reviews*, **2012**. 256(19-20): p. 2381-2396.
101. Carrera, F., E. Sánchez Marcos, P.J. Merkling, J. Chaboy, and A. Muñoz-Páez, Nature of metal binding sites in Cu(II) complexes with histidine and related N-coordinating ligands, as studied by EXAFS. *Inorganic Chemistry*, **2004**. 43(21): p. 6674-6683.
102. Nicolis, I., P. Deschamps, E. Curis, O. Corriol, V. Acar, N. Zerrouk, J.C. Chaumeil, F. Guyon, and S. Bénazeth, XAS applied to pharmaceuticals: Drug administration and bioavailability. *Journal of Synchrotron Radiation*, **2001**. 8(2): p. 984-986.

103. Jalilehvand, F., K. Parmar, and S. Zielke, Mercury(ii) complex formation with N-acetylcysteine. *Metallomics*, **2013**. 5(10): p. 1368-1376.
104. Jalilehvand, F., B.O. Leung, M. Izadifard, and E. Damian, Mercury(II) cysteine complexes in alkaline aqueous solution. *Inorganic Chemistry*, **2006**. 45(1): p. 66-73.
105. Mesu, J.G., T. Visser, F. Soulimani, E.E. Van Faassen, P. De Peinder, A.M. Beale, and B.M. Weckhuysen, New insights into the coordination chemistry and molecular structure of copper(II) histidine complexes in aqueous solutions. *Inorganic Chemistry*, **2006**. 45(5): p. 1960-1971.
106. Manceau, A., A. Simionovici, M. Lanson, J. Perrin, R. Tucoulou, S. Bohic, S.C. Fakra, M.A. Marcus, J.P. Bedell, and K.L. Nagy, Thlaspi arvense binds Cu(ii) as a bis-(l-histidinato) complex on root cell walls in an urban ecosystem. *Metallomics*, **2013**. 5(12): p. 1674-1684.
107. Yu, M., W. Chu, and Z. Wu, XAFS study of the configuration of L-histidine with Mn2+, Co2+, Ni2+, Cu2+, Zn2+ at pH 6.0. *Nuclear Instruments and Methods in Physics Research, Section A: Accelerators, Spectrometers, Detectors and Associated Equipment*, **2010**. 619(1-3): p. 408-410.
108. Louis Joseph Dogué, I., N. Mermilliod, and R. Foerch, Grafting of acrylic acid onto polypropylene -- comparison of two pretreatments: γ-irradiation and argon plasma. *Nuclear Instruments and Methods in Physics Research Section B: Beam Interactions with Materials and Atoms*, **1995**. 105(1-4): p. 164-167.
109. Massa, G., R. Mazzei, G. Garcia Bermudez, A. Filevich, and E. Smolko, Grafting of acrylic acid onto polypropylene films irradiated with argon ions. *Nuclear Instruments and Methods in Physics Research Section B: Beam Interactions with Materials and Atoms*, **2005**. 236(1-4): p. 272-276.
110. Sciarratta, V., U. Vohrer, D. Hegemann, M. Müller, and C. Oehr, Plasma functionalization of polypropylene with acrylic acid. *Surface and Coatings Technology*, **2003**. 174-175: p. 805-810.
111. Liu, Z.-M., Z.-K. Xu, L.-S. Wan, J. Wu, and M. Ulbricht, Surface modification of polypropylene microfiltration membranes by the immobilization of poly(N-vinyl-2-pyrrolidone): a facile plasma approach. *Journal of Membrane Science*, **2005**. 249(1-2): p. 21-31.
112. Gancarz, J., M. Pozniak, A. Bryjak, and Frankiewicz, Modification of polysulfone membranes. 2. Plasma grafting and plasma polymerization of acrylic acid. *Acta Polymerica*, **1999**. 50(9): p. 317-326.
113. Morent, R., N. De Geyter, S. Van Vlierberghe, A. Beaurain, P. Dubruel, and E. Payen, Influence of operating parameters on plasma polymerization of acrylic acid in a mesh-to-plate dielectric barrier discharge. *Progress in Organic Coatings*, **2011**. 70(4): p. 336-341.
114. Ursu, C., I. Bordianu, M. Dobromir, M. Drobota, C. Cotofana, M. Olaru, and C. Simionescu, Excimer laser-induced surface modification of poly(ethylene terephthalate). *Revue Roumaine de Chimie*, **2012**. 57(4-5): p. 501-506.
115. Wu, G., M.D. Paz, S. Chiussi, J. Serra, P. González, Y.J. Wang, and B. Leon, Excimer laser chemical ammonia patterning on PET film. *Journal of Materials Science: Materials in Medicine*, **2009**. 20(2): p. 597-606.
116. Yingling, Y.G. and B.J. Garrison, Coarse-grained model of the interaction of light with polymeric material: Onset of ablation. *Journal of Physical Chemistry B*, **2005**. 109(34): p. 16482-16489.
117. Wochnowski, C., M.A.S. Eldin, and S. Metev, UV-laser-assisted degradation of poly(methyl methacrylate). *Polymer Degradation and Stability*, **2005**. 89(2): p. 252-264.

118. Pawlukojc, A., J. Leciejewicz, A.J. Ramirez-Cuesta, and J. Nowicka-Scheibe, L-Cysteine: Neutron spectroscopy, Raman, IR and ab initio study. *Spectrochimica Acta Part A: Molecular and Biomolecular Spectroscopy*, **2005**. 61(11-12): p. 2474-2481.
119. Chatterjee, A. and S. Schiewer, Multi-resistance kinetic models for biosorption of Cd by raw and immobilized citrus peels in batch and packed-bed columns. *Chemical Engineering Journal*, **2014**. 244(0): p. 105-116.
120. Chiou, M.S. and H.Y. Li, Adsorption behavior of reactive dye in aqueous solution on chemical cross-linked chitosan beads. *Chemosphere*, **2003**. 50(8): p. 1095-1105.
121. Dos Santos, V.C.G., A.d.P.A. Salvado, D.C. Dragunski, D.N.C. Peraro, C.R.T. Tarley, and J. Caetano, Highly improved chromium (III) uptake capacity in modified sugarcane bagasse using different chemical treatments. *Química Nova*, **2012**. 35: p. 1606-1611.
122. Chen, W.B. and Z. Cao, Removal of lead(II) and copper(II) from hypersaline media with amorphous tin(IV) phosphate. *Asian Journal of Chemistry*, **2013**. 25(7): p. 3655-3659.
123. Yang, T., X.X. Zhang, M.L. Chen, and J.H. Wang, Highly selective preconcentration of ultra-trace cadmium by yeast surface engineering. *Analyst*, **2012**. 137(18): p. 4193-4199.
124. Zaitseva, N., V. Zaitsev, and A. Walcarius, Chromium(VI) removal via reduction–sorption on bi-functional silica adsorbents. *Journal of Hazardous Materials*, **2013**. 250–251(0): p. 454-461.
125. Liu, W., T. Wang, A.G.L. Borthwick, Y. Wang, X. Yin, X. Li, and J. Ni, Adsorption of Pb^{2+}, Cd^{2+}, Cu^{2+} and Cr^{3+} onto titanate nanotubes: Competition and effect of inorganic ions. *Science of The Total Environment*, **2013**. 456–457(0): p. 171-180.
126. Dunning Jr, T.H., Gaussian basis sets for use in correlated molecular calculations. I. The atoms boron through neon and hydrogen. *The Journal of Chemical Physics*, **1989**. 90(2): p. 1007-1023.
127. Kendall, R.A., T.H. Dunning Jr, and R.J. Harrison, Electron affinities of the first-row atoms revisited. Systematic basis sets and wave functions. *The Journal of Chemical Physics*, **1992**. 96(9): p. 6796-6806.
128. Woon, D.E. and T.H. Dunning Jr, Gaussian basis sets for use in correlated molecular calculations. III. The atoms aluminum through argon. *The Journal of Chemical Physics*, **1993**. 98(2): p. 1358-1371.
129. Peterson, K.A., D.E. Woon, and T.H. Dunning Jr, Benchmark calculations with correlated molecular wave functions. IV. The classical barrier height of the H+H2→H2+H reaction. *The Journal of Chemical Physics*, **1994**. 100(10): p. 7410-7415.
130. Wilson, A.K., T. Van Mourik, and T.H. Dunning Jr, Gaussian basis sets for use in correlated molecular calculations. VI. Sextuple zeta correlation consistent basis sets for boron through neon. *Journal of Molecular Structure: THEOCHEM*, **1996**. 388(1-3): p. 339-349.
131. Hohenberg, P. and W. Kohn, Inhomogeneous Electron Gas. *Physical Review*, **1964**. 136(3B): p. B864-B871.
132. Lee, C., W. Yang, and R.G. Parr, Development of the Colle-Salvetti correlation-energy formula into a functional of the electron density. *Physical Review B*, **1988**. 37(2): p. 785-789.
133. Becke, A.D., Density-functional thermochemistry. III. The role of exact exchange. *The Journal of Chemical Physics*, **1993**. 98(7): p. 5648-5652.

134. Dunning, T.H., Gaussian basis sets for use in correlated molecular calculations. I. The atoms boron through neon and hydrogen. *The Journal of Chemical Physics*, **1989**. 90(2): p. 1007-1023.
135. Canneaux, S., Etude théorique de processus atmosphérique : réaction du radical OH avec l'acétone et capture d'un composé organique volatil par une goutte d'eau, **2004**, Université de Reims Champagne-Ardenne.
136. Henon, E., Theoretical chemistry application: study of the mechanims and kinetics of some reactions of atmospheric interest., **2003**, Université de Reims Champagne-Ardenne.
137. Tomasi, J., B. Mennucci, and E. Cances, The IEF version of the PCM solvation method: An overview of a new method addressed to study molecular solutes at the QM ab initio level. *Journal of Molecular Structure*, **1999**. 464: p. 211-226.
138. Tomasi, J., B. Mennucci, and R. Cammi, Quantum mechanical continuum solvation models. *Chemical Reviews*, **2005**. 105: p. 2999-3093.
139. Palackova, H., J. Vinklarek, J. Holubova, I. Cisarova, and M. Erben, The interaction of antitumor active vanadocene dichloride with sulfur-containing amino acids. *Journal of Organometallic Chemistry*, **2007**. 692(17): p. 3758-3764.
140. Schoutteten, T. Projet DEPOLTEX - Système de dépollution. in *Réunion technique*. **2014**. Coudekerque-Branche.

Appendix 1: Material and experimental device

Appendix 1.1. Fabrics used in this work

Fabrics	INTN50	INTN100	INTNI150	E1931
Polymer	PP	PP	PET	PET
Type	Nonwoven	Nonwoven	Nonwoven	Knitted
Consolidation	Hot rolling or Calendering		Needlepunching	-
Basis weight (g/cm²)	50	100	150	150
Thickness (mm)	0.45	0.7	1.1	0.8-1
Air porosity (L/m²/s)	2700	1200	1750	-
Water porosity (L/m²/s)	530	-	-	-
Size of pores (µm)	64	57	37	-

Appendix 1.2. Physical processes used for functionalization

In this work, three physical processes were used: radiofrequency low pressure cold plasma, atmospheric ultra-light discharge and excimer laser processes (Figure 52). The plasma engines used belong to the UMET laboratory and the excimer laser belongs to PhLAM laboratory.

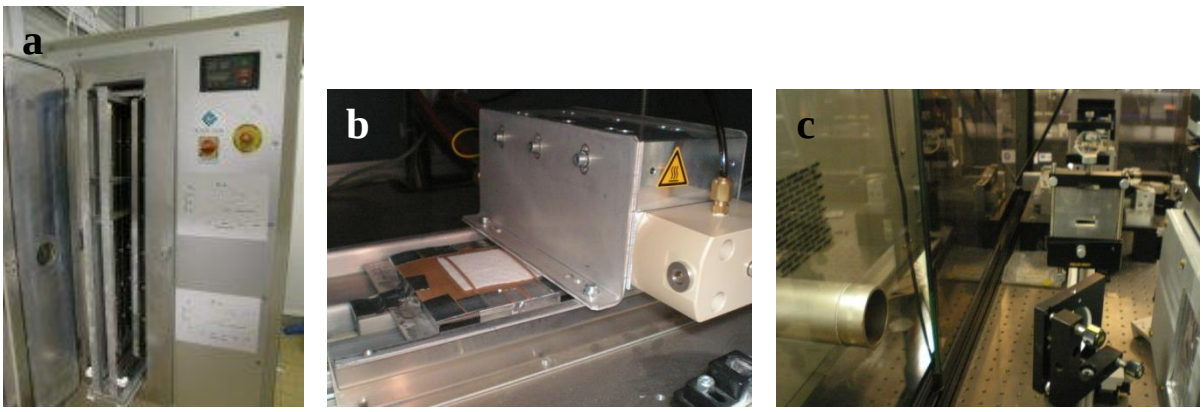

Figure 52: Photographies of a) RFplasma b) ULD source of the atmospheric plasma c) KrFexcimer laser with the optic bench.

a. Plasma processes

Plasma is the fourth state of matter considering the first three are solid, liquid and gas. Plasma is defined as a partially ionized gas but broadly neutral. By extension, plasma is also the machine used to create plasma for various purposes. Two kinds of plasma exist: hot plasma (or thermal plasma), which are at thermal equilibrium as the temperature of the electron is equal to the temperature of the ions and other neutral particles in the plasma; cold plasma (or non-thermal plasma), which are not at the thermal equilibrium as the temperature of the electron is very high compared to the temperature of the plasma particles (in this case,

other constituents of the plasma are at ambient temperature). In these present studies, the grafting of molecules is carried out onto synthetic textiles that are not tolerant to high temperatures. Thus, only cold plasma processes are considered.

a.i. Radiofrequency low pressure cold plasma process

Generally, three modules are common to existing low pressure plasma machines: excitation source, a pumping unit and a reaction chamber. Plasma can be generated with an electromagnetic wave or with an electric discharge. The pumping unit allows the decrease of the pressure in the reaction chamber until obtaining a primary vacuum (from 100 Pa to 10^{-4}Pa according to the machine). The radiofrequency plasma used was an Europlasma apparatus CD1200-400 COMBI MC, Radio Frequency generator Dressler, 13.56 kHz. The main reactions occurring in plasma are given in scheme 7. This method is criticized because of the high consuming of electrical energy required to obtain the primary vacuum. Nevertheless, plasma processes avoid the use of toxic solvents and give homogeneous coating at the surface of the fibers.

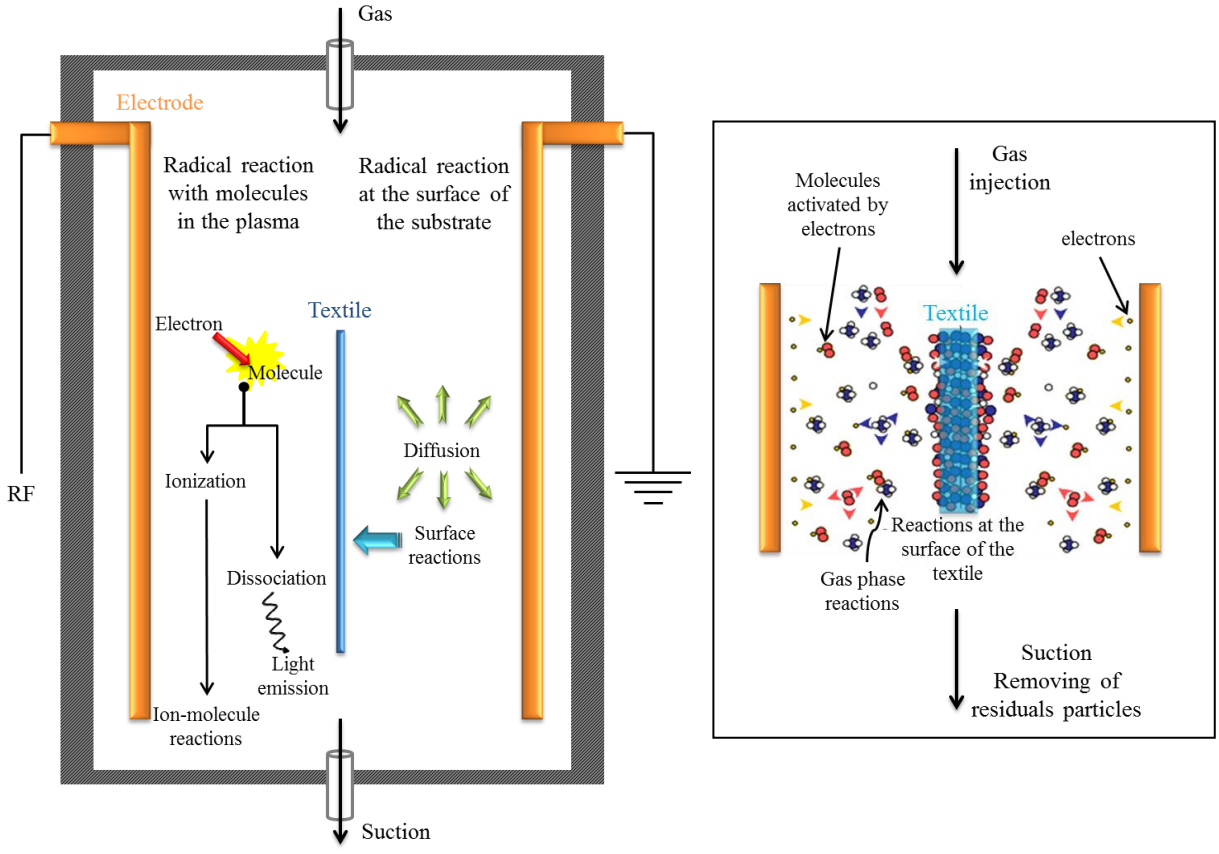

Scheme 7: Reactive processes during the deposition or the grafting of molecules onto textiles and mechanism details during the grafting of molecules onto textiles

a.ii. Atmospheric ultra-light discharge plasma process

The use of radiofrequency low pressure cold plasma process to graft molecules onto textiles is very interesting but is also considered hard to transfer at industrial scale, and more precisely, cannot be used in online processes. Thus, atmospheric plasma processes can be a solution to treat textiles in online process. However, most of the atmospheric plasmas are at high temperature leading to the degradation of the textile.

A recent technology was developed to allow the treatment of materials for temperature up to 120°C: the atmospheric ultra-light discharge plasma (Ultra Light Discharge, Activa 120, AcXys technologies). In this work, textiles made of PP or PET were used, and their melting point is 145 and 245°C respectively. In this case, the plasma is generated in the form of an homogeneous 120 mm curtain (Scheme 8).The generation of the plasma is allowed thanks to the passage a gas flow in a high electric field.

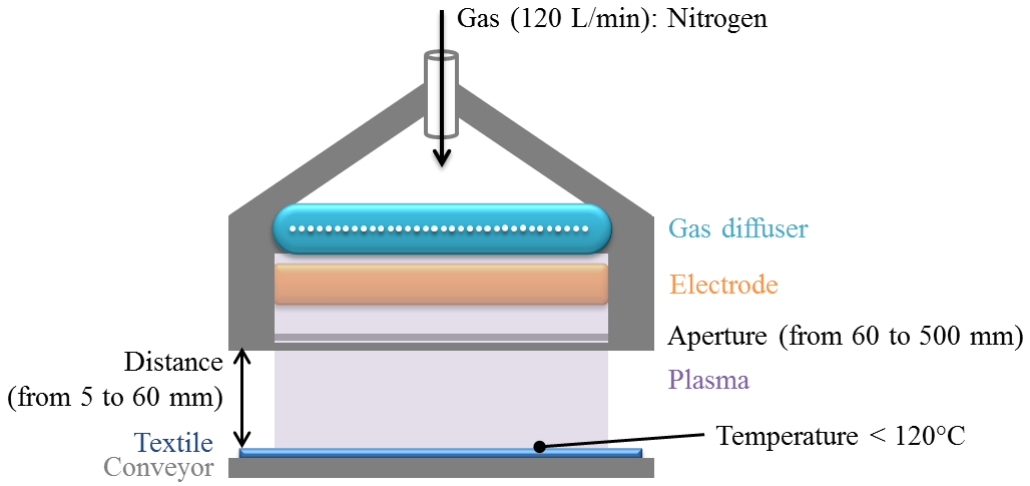

Scheme 8: Generation of a curtain plasma using ULD source

The distance between the ULD source and the surface of the material can be changed: when the distance is higher, there are more interactions between particles in the plasma, and consequently, more recombination is possible before the treatment of the surface.

Nitrogen is the only one gas that can be used as plasmagene gas in this system. However, it is possible to use other gas as doping gas (O_2, CO_2, N_2O or compressed air) allowing the improvement of the activation step or the grafting one. In this system, it is also possible to adjust the conveyor speed and the number of passages in the curtain plasma.

b. Excimer laser process

The excimer (**exci**ted d**imer**) laser is a laser with photochemical effect. Indeed, considering this kind of laser the chemical reactivity results from the disturbance of interatomic bonds following the excitation of the electrons due to the adsorption of a photon at least. Laser/matter interaction is more efficient in ultraviolet than in infrared because the creation of radicals is possible in ultraviolet leading to some radical reaction at the surface of the material.

Laser with photochemical effect have a lot of advantages compared to other lasers: important photon energy (several eV), very high spatial resolution (until 0.1 µm compared to laser with thermic effect which is limited at 1 µm), limitation of the thermic effect, and selective reactivity, according to the wavelength, at the irradiated surface of the material. The excimer laser that was used in this work was a Lambda Physik, model Compex 205. The experimental parameters for the laser treatment are given in table 15.

Table 15: Experimental parameters for the laser treatment

Model of excimer Laser	**Laser Lambda Physik, model Compex 205, KrF, 248 nm**
Voltage	33 kV
Fluency	10 to 70 mJ/cm²
Fluency uncertainty	± 5%
Number of pulses	100 to 900 pulses
Repetition rate	10 Hertz
Atmosphere	Ambient air
Irradiation mode	Scanning
Sample displacement speed	39 to 350 $\mu m.s^{-1}$
Surface irradiated per pulse	40 x 3.5 mm²

Appendix 2: Papers

Abstract

The treatment of dredged sediments contaminated with trace metals is an alternative to the current storage in accredited sites and could allow the reusability of sediments in civil engineering. The remediation process considered in this project consists in the deposition of polluted sediments onto geotextiles, structures possessing filtration properties. The leaching then favors the release of metals that can be sequestered by the geotextiles. However, these textile structures are mainly composed of synthetic polymers and thus cannot retain heavy metals. Therefore, they have to be functionalized with molecules able to adsorb metal ions present in aqueous media. The main objective of this PhD thesis was to develop functionalization processes using plasma and laser techniques, in order to immobilize biomolecules with chelating properties at the surface of the fabrics. These biomolecules were immobilized by chemical coupling onto –COOH groups obtained at the fabric surface by the grafting of a spacer, namely acrylic acid. The surface of the fibers was characterized at the different grafting steps by scanning electron microscopy, infrared spectrometry and X-ray photoelectron spectrometry: evidence of the covalent grafting of acrylic acid and then of biomolecules was given. Some remediation tests were then carried out in order to select the most interesting functionalized materials for further studies at pilot scale. In parallel, a computational study was initiated in order to determine the structure of the metal/biomolecule complexes.

Keywords: Textiles ; Plasma ; Laser ; Grafting ; Acrylic acid ; Amino acids ; Remediation ; Trace metals.

Résumé

Le traitement des sédiments de dragage pollués aux métaux lourds est une alternative à leur stockage sur sites homologués et pourrait permettre la réutilisation des sédiments en technique routière ou en butte paysagère. Le procédé de dépollution envisagé dans ce projet consiste à déposer les sédiments contaminés sur des géotextiles, matériaux présentant une structure poreuse idéale pour la filtration. La lixiviation permet ensuite de rendre mobile une partie des polluants métalliques afin qu'ils puissent être adsorbés par les géotextiles. Cependant, ces matériaux, généralement synthétiques, n'ont pas de capacité intrinsèque à retenir les métaux et doivent donc être fonctionnalisés avec des molécules capables de fixer les métaux lourds. Cette thèse est orientée vers le développement de procédés de fonctionnalisation par plasma et laser, l'objectif final étant d'immobiliser des biomolécules chélatantes à la surface des géotextiles. Ces biomolécules sont fixées par couplage chimique sur des fonctions –COOH obtenues préalablement par greffage d'un agent intermédiaire, l'acide acrylique. La surface des fibres a été analysée à chaque étape de traitement par microscopie électronique à balayage, spectrométrie infrarouge, et par spectrométrie photoélectronique à rayons X, prouvant le greffage covalent de l'acide acrylique puis des biomolécules. Enfin, des tests avec des solutions métalliques ont été effectués afin de pouvoir sélectionner le textile fonctionnalisé le plus efficace pour réaliser des essais à l'échelle pilote. Parallèlement, une étude de modélisation a été amorcée afin d'étudier plus précisément la structure des complexes métal/biomolécule obtenus.

Mots-clés: Textiles ; Plasma ; Laser ; Greffage ; Acide acrylique ; Acides aminés ; Dépollution ; Métaux lourds.